A Complete Analytic Theory for Structure and Dynamics of Populations and Communities Spanning Wide Ranges in Body Size

Axel G. Rossberg[*,†,1]

*Centre for Environment, Fisheries and Aquaculture Science (Cefas), Lowestoft Laboratory, Suffolk, United Kingdom
†Medical Biology Centre, School of Biological Sciences, Queen's University Belfast, Belfast, United Kingdom
[1]Corresponding author: e-mail address: axel.rossberg@cefas.co.uk

Contents

Advances in Ecological Research, Volume 46
ISSN 0065-2504
http://dx.doi.org/10.1016/B978-0-12-396992-7.00008-3

Abstract

The prediction and management of ecosystem responses to global environmental change would profit from a clearer understanding of the mechanisms determining the structure and dynamics of ecological communities. The analytic theory presented here develops a causally closed picture for the mechanisms controlling community and population size structure, in particular community size spectra, and their dynamic responses to perturbations, with emphasis on marine ecosystems. Important implications are summarised in non-technical form. These include the identification of three different responses of community size spectra to size-specific pressures (of which one is the

classical trophic cascade), an explanation for the observed slow recovery of fish communities from exploitation, and clarification of the mechanism controlling predation mortality rates. The theory builds on a community model that describes trophic interactions among size-structured populations and explicitly represents the full life cycles of species. An approximate time-dependent analytic solution of the model is obtained by coarse graining over maturation body sizes to obtain a simple description of the model steady state, linearising near the steady state, and then eliminating intraspecific size structure by means of the quasi-neutral approximation. The result is a convolution equation for trophic interactions among species of different maturation body sizes, which is solved analytically using a novel technique based on a multiscale expansion.

1. INTRODUCTION

1.1. Orientation on a changing planet

We have entered a period of rapid, global environmental change, in which anthropogenic climate change is one important factor (Solomon et al., 2007), which is complicated by additional drivers such as elevated nutrient discharge and the direct impacts of overexploitation on natural resources (Millennium Ecosystem Assessment, 2005). The planet's ecosystems may never before have experienced this type of environmental change. Knowing how they will respond could help us prepare for and, if possible, manage the consequences of these developments (Woodward et al., 2010a).

Experimental and comparative methods, the dominant modes of scientific enquiries in ecological research, have obvious limitations when addressing scenarios of unprecedented environmental change at global or even regional scales. The relevant temporal and spacial scales are too large to conduct experiments (O'Gorman et al., 2012), and the data required for direct comparative analyses are often simply not yet available (Twomey et al., 2012).

The natural response, therefore, is to resort to models. These models can, for example, be (i) experimental systems such as microcosms (Reiss et al., 2010) or mesocosms (Yvon-Durocher et al., 2011), (ii) statistical models to extrapolate ecological data to the environmental conditions expected in future, (iii) numerical models aimed at simulating the relevant aspects of future scenarios directly, or (iv) analytic models that seek to isolate the implications of general ecological and biological principles that are sufficiently fundamental not to be overruled by global change. Common to any such modelling is the expectation that some aspect of the scenarios one seeks to predict are sufficiently insensitive to ecological detail that such detail need not be reproduced in the models (Rossberg, 2007). These robust aspects are

those one can be predicted, for which one can prepare, and which one might attempt to manage. Those aspects of future system states that do depend on many details (Friberg et al., 2011), however, might simply be beyond control. Common to all modelling is the problem of knowing which aspects of future system states can be predicted and which system details are relevant for this.

A common approach to identifying aspects of complex systems amenable to modelling is to search for coherent patterns in data. Obviously, if clear patterns arise similarly in data from different systems, the mechanisms generating these patterns are unlikely to depend on many details (Riede et al., 2010). It is, therefore, natural for research addressing the large-scale ecological impacts of global change to concentrate on the major known macroecological patterns. The patterns at the focus of the present work are those found in the distributions of the biomasses of individuals or species over wide ranges in body size. The first step, before addressing specific problems in the face of global change, is to ask which ecological details are important for generating these patterns in reality and what the underlying mechanisms are; these will be the details that any type of model, for example (i)–(iv), would need to capture to be reliable. Answering these questions is the central aim of the present work.

Technically, this is done by deriving an approximate analytic solution of a detailed community model. In doing so, determining which approximations are feasible without much affecting the predicted body-size distributions means understanding which ecological details are unimportant for the outcome. The resulting, approximate descriptions of community structure and dynamics encapsulate the mechanisms by which those details that do matter bring about the dominating patterns and their responses to pressures. Therefore, judiciously applied approximations, rather than meaning loss of information, actually reveal what is important. This is why the route along which the approximate solution of the community model is derived is as important as the outcome. The step-by-step derivation, therefore, forms the main body of this chapter.

1.2. Size spectra

Much of the early empirical and theoretical work on size distributions related to plant communities (see Koyama and Kira, 1956). Regularities in size spectra have now been investigated, for example, for benthic communities (Duplisea, 2000; Gerlach et al., 1985), terrestrial soil (Mulder and Elser, 2009; Mulder et al., 2008; Reuman et al., 2008), and birds (Thibault et al., 2011). The most striking form of the phenomenon, however, is

found in pelagic communities. Sheldon et al. (1972) suggested, based on measurements and literature data, that pelagic biomass is approximately evenly distributed over the logarithmic body-size axis "from bacteria to whales", spanning up to 20 orders of magnitude in body mass. The core of this conclusion has remained unchallenged, although intensive human harvesting makes its validation for the largest size classes difficult (Gaedke, 1992b; Jennings and Blanchard, 2004; Sheldon et al., 1977). Over shorter size ranges, similar phenomena are observed for benthic communities (Duplisea, 2000; Gerlach et al., 1985) or in terrestrial soil ecosystems (Mulder and Elser, 2009; Mulder et al., 2008, 2011; Reuman et al., 2008).

The work of Sheldon et al. (1972) drew attention to the usefulness of characterising community structure through *size spectra*. In the form they used, size structure is represented irrespective of species identity, trophic level, or life-history stage. In a common, though by no means exclusive, protocol to determine size spectra in aquatic communities, individuals are assigned to logarithmic size classes by carbon content, for example, ..., 1–2 pgC, 2–4 pgC, ... using various optical and mechanical techniques. The density of biomass in each size class is then determined, for example, as a value averaged over a full year and a specific range of the water column.

Subsequent investigations revealed deviations from the hypothesis formulated by Sheldon et al. (1972) in the detail (Kerr and Dickie, 2001). As illustrated in Fig. 1, one often finds approximate power-law relationships between abundance and body mass as the basic pattern, that is, straight lines on double-logarithmic plots, with "slopes" (actually exponents) close to but different from the one corresponding to the Sheldon hypothesis (which is -2, -1, or 0, depending on the specific choices of dependent and independent variables; see Blanco et al., 1994). On top of this, size spectra often deviate from power laws by exhibiting several maxima (or "domes") spaced more or less evenly along the logarithmic body-size axis (see, e.g. Fig. 1, or Kerr and Dickie, 2001).

The idea that the size distribution of individuals can indicate the "health" of an ecological community (e.g. Castle et al., 2011; Jennings and Blanchard, 2004; Kerr and Dickie, 2001; Rice et al., 2011; Sheldon et al., 1977) has recently been inscribed in legal documents. Arguably, the simplest way of characterising a size distribution is to compare the relative proportions of biomass in two wide body-size classes. In a series of reports, reviewed by Greenstreet et al. (2011), the International Council for the Exploration of the Sea developed, as an indicator for community state, the Large Fish Indicator (LFI), defined as the proportion among all fish in a community of

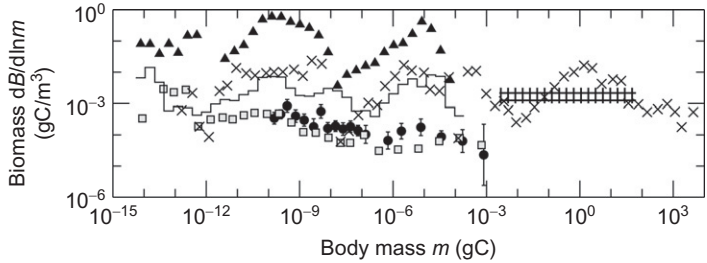

Figure 1 Five typical planktonic size spectra. Triangles represent data for the highly eutrophic lake Müggelsee averaged over 3 years, after Gaedke et al. (2004); stairs represent a seasonal average for Überlingersee, a division of the meso-eutrophic Lake Constance (Bodensee), after Gaedke (1992b), including an estimate for the contribution by fish (shaded area); crosses represent yearly averages for Lake Ontario, after Sprules and Goyke (1994), using a nominal depth of 50 m to convert to volume density; circles with 1 SD error bars represent the oligotrophic waters of the North Pacific Central Gyre averaged over 3 years of sampling by Rodriguez and Mullin (1986a), where measurements are compatible with a perfect power law; squares represent the oligotrophic open waters at a station near the Yakutat Seamount in the Northwest Atlantic, after Quiñones et al. (2003). For further examples, see Boudreau and Dickie (1992), among many others. The density of biomass along the logarithmic size axis dB/d ln m was estimated from the published data as $B_i m_i /(\Delta m_i)$, where B_i is the biomass of individuals in body-mass interval i (actually, their biomass per unit volume), m_i the midpoint of this body-mass interval on a logarithmic axis, and Δm_i is the linear width of the interval. This representation combines the advantage of Sheldon size spectra (Sheldon et al., 1972) of visualising structural details with the advantage of high intercomparability between empirical datasets (often highlighted for normalised spectra $B_i/\Delta m_i$), because $B_i m_i /(\Delta m_i)$ approximates the protocol-independent quantity dB/d ln m up to a relative error declining as fast as $(\Delta m_i/m_i)^2$ for small $\Delta m_i/m_i$. Axes are isometric to ease visual appreciation of the varying degrees of uniformity of the spectra.

individuals longer than a given length threshold. The Convention for the Protection of the Marine Environment of the North-East Atlantic proposed the LFI as a means to set an Ecological Quality Objective (OSPAR, 2006). EU legislation (European Commission, 2010) includes the LFI in a list of "Criteria to be used by the Member States to assess the extent to which good environmental status is being achieved". Among the important open issues in this context is, for example, the question of how fast the LFI will return to natural levels when fishing pressure is relaxed (OSPAR, 2006). Predictions appear to depend sensitively on the way communities are modelled (ICES, 2010; Shephard et al., 2012), and observed recovery is slower than was previously thought (Fung et al., 2012a). A better understanding of the underlying fundamental processes is thus required (Arim et al., 2011; Castle et al., 2011; Gilljam et al., 2011; Jacob et al., 2011; Melian et al., 2011).

In view of such current, practical questions regarding marine size spectra and their dynamics in response to anthropogenic pressures, the theory presented here is phrased with reference to marine communities and their perturbations by fishing. However, it should apply similarly to other cases of size-structured communities, for example, soil ecosystems, and partially also to communities of competing plants.

1.3. Mathematical size-spectrum models

As its starting point, any mathematical modelling requires a basic formal description of the system. This should be sufficiently detailed to contain or imply descriptions of the main phenomena of interest. Deciding how much detail one needs to start with is often a matter of trial and error. Typically, one will start with very simple basic descriptions and add model ingredients only upon the suspicion that this might lead to different conclusions. However, the implications of these more complete models can easily become difficult to understand. In particular, the application of formal analytic tools may become impossible. The history of the theory of community size spectra is no exception.

The earliest models developed to understand size spectra distinguished species by their trophic levels and considered the balance of energy flow through food chains (Kerr, 1974; Sheldon et al., 1977). Later theories, however, tended to follow the empirically successful paradigm of simplifying the description of community structure by disregarding species identity. This led to models in which individuals enter the community at a fixed lower cut-off size at constant rate, grow, consume other individuals, and eventually die through predation, fishing, or other causes (e.g. Benoît and Rochet, 2004; Blanchard et al., 2009; Camacho and Solé, 2001; Datta et al., 2010; Law et al., 2009; Platt and Denman, 1978; Silvert and Platt, 1978, 1980; Zhou and Huntley, 1997). In reality, the growth of individuals slows when they reach maturation, at a size dependent on their species identity, after which a large proportion of food intake is invested into reproductive efforts. To take interspecific variability in life histories into account, recent size-spectrum models often go back to distinguishing individuals by species (Hall et al., 2006) or maturation size class (Andersen and Beyer, 2006). To overcome another limitation of earlier theories, Arino et al. (2004) and Maury et al. (2007a,b) made the production of offspring dependent on available resources. Models such as those of Andersen and Ursin (1977), Shin and Cury (2004), Pope et al. (2006), and Hartvig et al. (2011) combine these lines of thought by resolving individuals by both body size

(or age) and species, and accounting for the full life cycle of each species separately. The complexity of these models, however, renders their mathematical analysis challenging (Hartvig et al., 2011).

The model analysed here was developed by Hartvig et al. (2011), building on the ideas of Andersen and Beyer (2006). The structure of the model is illustrated in Fig. 2: populations of different species (not necessarily fish) are coupled through feeding interactions. Some of the energy intake by feeding is used to cover maintenance costs, the rest invested into growth. After body mass reaches a maturation threshold, which depends on the species, increasingly larger proportions of surplus energy are invested into reproduction so that growth ultimately comes to a halt. Fecundity, therefore, depends on food availability, but not on the density of reproducing adults, as some models in fisheries science assume. Feeding interactions are particularly strong for predator individuals that are by a certain factor larger than their prey, but interaction strengths may in addition depend on species identities. Predation is the dominating cause of mortality. Each of these model components is represented by fairly simple submodels designed to keep the number of model parameters low. Where applicable, the size-dependence of biological and ecological rates is represented through allometric scaling laws. For a mathematical description of the model, see Section 4.

The model of Hartvig et al. (2011) represents, in simplified form, processes operating on a number of different levels of organisation: the short-term energy balance of individuals, the full life cycle including growth, maturation, and reproduction, the dynamics of intraspecific population structures, population dynamics driven by trophic interactions, and the resulting structure and dynamics of the community as a whole. The model is complete in that it contains, except for the energy input at the bottom of

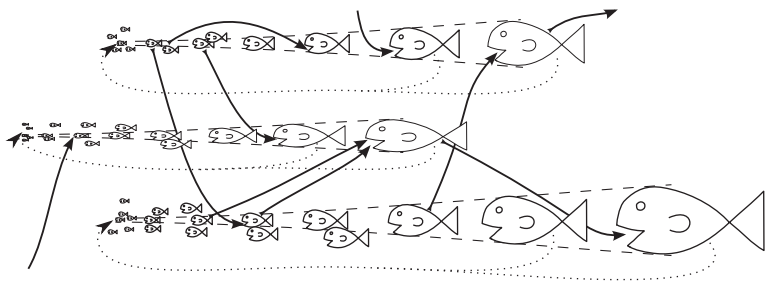

Figure 2 Schematic illustration of the model structure. Shown are three populations of species with different maturation body sizes that feed on and are fed on by other species and themselves. Dashed lines indicate growth of individuals, dotted lines reproduction, and thick arrows feeding interactions.

the food chain, no "loose ends;" the balance of biologically available energy within the system and the balance of individuals within each population are fully accounted for.

1.4. Approximations

Legitimate approximations of community models, here those that do not much affect predicted structure and dynamics of the size spectrum, inform one of those details of community dynamics of which community structure is largely independent. The approximation techniques used here will be discussed in detail when they are applied in the formal analysis. The following provides a non-technical overview.

The basic structure of the mathematical analysis follows from a standard technique used throughout the scientific literature: system dynamics is considered in a *linearised* form valid for small deviations from an equilibrium state. As a result, the analysis technically separates into three steps: (i) the derivation of the equilibrium state, (ii) linearization of system dynamics near this equilibrium state, and (iii) evaluation of this linearised description. Of course, approximations employed in one of the earlier steps remain in place at the later steps. The premise implied when applying this technique is that, although there will be corrections to system dynamics through non-linear effects, its semi-quantitative nature is captured already at the linear level. Whether this is indeed the case is not analysed here, although preliminary comparisons of results with empirical data such as in Fig. 1 are encouraging. What will be discussed in Section 9.6 is the question of whether the linearization is self-consistent in the sense that small deviations from equilibrium remain small in the future (and eventually die out).

An approximate analytic description of the model's equilibrium state becomes possible mainly by combining two standard techniques: *coarse graining* (Perry and Enright, 2006) along the maturation body-size axis and a *mean-field approximation* (Keitt, 1997; Wilson et al., 2003) of trophic interaction strengths. As explained in Section 5.1, these two approximations combined lead to a picture in which species are distinguished only by their characteristic size, for example, maturation body size, and individuals by body size and maturation size, where the community is described by a continuum of species of different maturation sizes, and where trophic interaction strengths depend only on the body sizes of predator and prey individuals. The validity of these approximations supports studies of model systems that focus on the body sizes of species

and individuals (Belgrano and Reiss, 2011). Although formal derivation of these approximations for the present model is conceivable, their justification here comes only from their frequent successful application in other contexts. One must therefore be mindful of possible artefacts. Indeed, as discussed in Sections 2.8 and 6.4, while the intricacies of real community food webs appear negligible for size-spectrum dynamics, the stabilising effect resulting from their structure with distinct species linked through a sparse network of feeding interactions cannot be ignored entirely.

Even with these two approximations, the direct mathematical analysis of linearised system dynamics would still be challenging. To simplify the problem further, the *Quasi-Neutral Approximation* (QNA; Rossberg and Farnsworth, 2011) of population dynamics is employed. The QNA assumes that variations through time in density-dependent life-history parameters, and the resulting modifications of intraspecific population structures, are rather small. Common mathematical techniques exploiting small parameters can then be applied. This allows direct calculation of the effective growth (or decay) rates of entire populations, which result from interactions between individuals of different populations at different life stages, without having to take the changes in population structures involved in these processes explicitly into account. When the QNA is valid, it justifies the use of community models that do not resolve different life stages within populations. The common concern that broad intraspecific size structure complicates community dynamics (Gilljam et al., 2011) should therefore not lead to outright dismissal of such models.

A last step required to bring linearised community dynamics into a form simple enough to derive analytic time-dependent solutions is to recognise that, when the offspring of a species are much smaller than the adults, its actual body size has little influence on dynamics under the approximations used here. Offspring may just as well be considered "infinitely small". The resulting, highly simplified description of community dynamics is called the Species Size-Spectrum Model. The approximation is verified by performing QNA and model linearization initially in a formulation where offspring size does depend on maturation body size and carefully analysing the implications of letting the ratio of offspring to adult size go to zero. Incompatibility of unicellular organisms with this condition is one of the reasons why microcosm experiments using such taxa (Reiss et al., 2010) are unsuitable for modelling marine size spectra.

An approximate analytic description of the response of the Species Size-Spectrum Model to external pressures (e.g. fishing) is then derived using a novel technique, related to a *singular perturbation expansion* (Kevorkian and Cole, 1996) of special solutions of the model. These special solutions correspond to the trophic cascades and the bending of size

spectra described in Section 2. The validity of the approximation (verified numerically) highlights the centrality of these phenomena for community dynamics.

This analytic theory for size spectrum structure and dynamics is complete to the degree that the underlying model of Hartvig et al. (2011) is complete. It explicitly specifies conditions for jointly attaining and maintaining equilibrium of all essential feedback loops that link individual physiology with community structure. These are the metabolic equilibrium of individuals, the demographic equilibrium of population structures, population-dynamical equilibrium, and the ecological balance of community size spectra.

1.5. Structure of the paper

After briefly reviewing relevant mathematical methods (Section 3) and providing a formal description of the model (Section 4), the approximate steady-state solution of the model is derived in Section 5. Using this solution, the QNA is applied to the model and linearised near the equilibrium in Section 6, leading to the Species Size-Spectrum Model. Novel mathematical techniques are then used to find approximate analytic solutions of that model (Section 7) and verified by comparison with simulations of the same model (Section 8). Section 9 provides technical discussion of further implications of the results and points to questions and research problems arising. Non-technical summaries of a number of noteworthy aspects of the theory are provided in Section 2.

2. SOME ASPECTS OF THE ANALYTIC THEORY EXPLAINED IN NON-MATHEMATICAL LANGUAGE

The formal mathematical analysis of the model by Hartvig et al. (2011) leads to several novel insights into structure and dynamics of size-structured communities and the underlying mechanisms. This section summarises and discusses some of these findings in a non-mathematical language. To avert the risk of misunderstanding inherent in such undertakings, consultation of the referenced parts of the theory for details and specifics is encouraged. Table 1 summarises the crucial mechanisms succinctly.

2.1. Two different scenarios generate power-law community size spectra

The analysis reveals two different scenarios that lead to formation of power-law size spectra (Section 5.2). In the first scenario, primary producers are sufficiently abundant for all grazers and all species higher up in the food chain to feed *ad libitum*. The second scenario corresponds to communities in which

Table 1 Summary of major regulating constraints controlling the model community's steady state

	Regulating constraint	
Phenomenon	**Eutrophic regime**	**Oligotrophic regime**
Size-spectrum exponent (slope)	Physiological mortality rate	Constant satiation
Mortality	Growth and physiological mortality rates	
Individual growth rate	Satiation	
Satiation	Maximal	Size-spectrum coefficient and search/attack rate
Size-spectrum coefficient (intercept)	Producer abundance	Physiological mortality rate
Physiological mortality rate	Intraspecific size structure	
Intraspecific size structure	Population-dynamic equilibrium	
Search/attack rate	Unknown (see Section 9.6)	

typical individuals at all sizes find enough food so as not to die of starvation but if more food was available they could grow faster and generate more offspring. (The crossover between the two scenarios is not considered.)

Figure 1 illustrates that biomass densities of individuals in all size classes can be much higher in eutrophic systems than they are in oligotrophic systems, so situations in which consumers effectively feed *ad libitum* are more likely. The first scenario is therefore here called the *eutrophic regime* here and the second the *oligotrophic regime*. Of course, this nomenclature is not meant to imply that trophic status is defined by consumer satiation. The labelling just hints at the fact that, the more eutrophic a system is, the more likely the regime with *ad libitum* feeding will be encountered.[1]

Perfect oligotrophic power-law size spectra require the "right" abundance of primary producers or a corresponding tuning of other biological or ecological parameters. One conceivable mechanism for this is the evolutionary adaptation of attack (or search) rates to avoid overexploitation of resources (Rossberg et al., 2008). The size-spectrum is determined solely

[1] Bolt labelling of mathematically distinct regimes is common scientific practice. Solid-state physicists, for example, refer to scenarios unfolding at the temperature of liquid nitrogen (-196°C) as the "high-temperature regime" Pratap et al., 1999).

by the allometric exponents for metabolic and attack rates (Andersen and Beyer, 2006 and Section 5.2), typically leading to slopes close to the value suggested by Sheldon et al. (1972). With somewhat over-abundant producers, size spectra will bend upward on double-logarithmic scales, and *vice versa* (Section 9.6).

Eutrophic power-law size spectra appear to impose fewer constraints on parameters. In the eutrophic regime, the size-spectrum slope depends on the efficiency of energy transfer from smaller to larger species. Depending on ecological parameters, the slope can become larger or smaller than in the oligotrophic case, and for real systems, it can vary along the size axis. Absolute abundances scale with the abundances of primary producers.

As the oligotrophic regime is characterised by *ad libitum*, and therefore density-independent, feeding, model populations in this regime are regulated entirely through density-dependent mortality, so it might be a surprise that, despite this pure "top-down control", the abundance of primary producers can determine population abundances at higher trophic levels. This becomes possible because overabundance of species in any given size class releases the early life stages of larger species from predation mortality. As a result, the populations of larger species grow and deplete smaller species through increased mortality—until a new equilibrium is reached (Section 8.4.5).

This new, differentiated picture of the controlling mechanisms might help to understand the role of trophic status in shaping observed size spectra. A general empirical pattern seems to be (Marquet et al., 2005) that in oligotrophic systems, size spectra closely follow power laws with slopes (i.e. exponents) in line with Sheldon's hypothesis Sprules and Munawar (1986), Rodriguez and Mullin (1986a), Gaedke (1992b), Quiñones et al. (2003), and that with increasing nutrient load, size spectra become more irregular, exhibiting weak trends in the best-fitting slopes, which vary between studies (Ahrens and Peters, 1991; Bays and Crisman, 1983; Bourassa and Morin, 1995; Dortch and Packard, 1989; Gaedke et al., 2004; Jeppesen et al., 2000; Pace, 1986; Sprules and Munawar, 1986), with some tendency to favouring higher relative abundance of larger individuals at high nutrient loads (Ahrens and Peters, 1991; Sprules and Munawar, 1986, see also Fig. 1) as expected from the present theory. Mulder and Elser (2009) and Mulder et al. (2009) found the same trend in soil communities. Indeed, such patterns are suggested already by comparisons of the size spectra recorded by Sheldon et al. (1972) around the American continent with corresponding maps of nutrient loading (Garcia et al., 2006). Related

to this may be the observation by Yvon-Durocher et al. (2011) that warming increases size-spectrum slopes in aquatic mesocosms.

2.2. Feeding alone couples size classes

An intermediate result of the analytic calculations is the Species Size-Spectrum Model, Eq. (78), a balance equation for the biomasses pertaining to species in different size classes, which are coupled through feeding interactions. The Species Size-Spectrum Model only accounts implicitly for intraspecific size structure. By showing that such a model can describe community dynamics and, by extension, the dynamics of the classical individual size spectrum, the present analysis differs from some earlier approaches. It implies that somatic growth does not essentially contribute to the ecological coupling along the size axis, notwithstanding its important contributions in controlling biomasses and population structures of species. This result provides firm foundations to related criticism by Kerr and Dickie (2001), who argue that the "*characteristics [of size spectra] form an inexorable consequence of mathematical relations between size-dependent allometries of the acquisition and transmission of energy through predation processes and the attendant metabolic dissipation*." (p. 138). They consider that "mechanisms operating at the physiological level" enter just by determining the "scaling of the efficiency coefficients" (p. 139) in this process. Indeed, the observed deep gaps between domes that Kerr and Dickie (2001) highlight would become tight bottlenecks were size classes primarily coupled through somatic growth. This insight parallels a corresponding observation that, despite the wide body-size ranges species span during growth, the individual size spectrum is highly correlated with the species size spectrum (Shephard et al., 2012).

2.3. Population-level predator–prey size-ratio windows are wide

Most verbal models and qualitative models of trophic interactions in aquatic communities[2] operate at the population or species level, as do many quantitative models. Understanding the general size-dependence of trophic interactions at the population level is therefore important not only for size-spectrum theory.

[2] Such models abound in the literature. Two randomly chosen examples are the statement "*Norway lobster, while not quite as an important part of the cod diet as whiting, is a slow-growing species and consequently more sensitive to the predation release produced by the removal of cod*" made by Speirs et al. (2010) or the graphs of food-web topologies by Yodzis (1998).

Under the simplifying assumption that the size-dependence of trophic interactions is controlled, apart from allometric scaling laws, only by relative sizes, it can be characterised by a predator–prey size-ratio window. This gives, for each ratio of predator to prey size, the probability or intensity of trophic interactions. The window can be defined either for interactions between individuals, with the relative sizes given, for example, in terms of the individuals' body masses, or for interactions between populations of species, with size then measured, for example, in terms of maturation body mass.

It is shown in Section 9.3 that the structure of (average) population-level predator–prey size-ratio windows is mostly determined by the intraspecific size structures of prey and predator. The individual-level predator–prey size-ratio window plays only a minor role. The predicted population-level predator–prey size-ratio window (Fig. 9) is wide, in line with empirical analyses by Neubert et al. (2000) and Woodward and Warren (2007). Under the idealisations invoked in the analytic theory, it decays with an exponent near zero (≈ -0.05) with increasing maturation body mass ratio (Fig. 9). In reality, the windows will, of course, be truncated above maturation size ratios where the newborns or hatchlings of one species are so large that they feed on the adults of the other.

2.4. Simple mass-balance models explain only equilibrium

It turns out (Section 9.2) that predicted equilibrium size spectra of communities perturbed by size-selective fishing can consistently be interpreted by verbal arguments or simplified, static mass-balance models (Christensen and Pauly, 1992) where "large species eat small species" without regard to the broad population-level predator–prey size-ratio windows resulting from somatic growth. However, when such simplified models would be used to predict dynamics (akin to the Ecopath with Ecosim approach; Pauly et al., 2000), this would lead to very different results from when size structure was, at least implicitly, included (Section 9.2, Fig. 10).

2.5. Both upward and downward cascades form in response to size-specific perturbations

The dynamics of complex systems can often efficiently be analysed and described in terms of their responses to controlled perturbations of system states. Adapting this idea to the ecological context, Bender et al. (1984) distinguish between short *pulse perturbations* and long-lasting *press perturbations* of

constant intensity. Here, press perturbations will be considered, if not stated otherwise. An example of such a perturbation is sustained fishing with a constant effort.

Trophic cascades, in which a perturbation of abundance at a higher trophic level leads through trophic top-down effects to alternating increases and decreases of abundances towards lower trophic levels, are a well understood phenomenon. They naturally arise in size-spectrum models (Benoît and Rochet, 2004). Andersen and Pedersen (2010) demonstrated in simulations of a size spectrum perturbed by fishing that, together with these "downward" cascades, another type of cascade can emerge, with alternating abundance increase and decrease towards higher trophic levels. The cascades found by Andersen and Pedersen (2010) were always damped, that is, the relative change in abundances became smaller with increasing distance from the externally perturbed size class. Periodic maxima ("domes") in size spectra, as observed, for example, by Schwinghammer (1981), Sprules et al. (1983), and Sprules and Goyke (1994), and documented in Fig. 1, are likely to correspond either to upward or to downward trophic cascades.

The Species Size-Spectrum Model accounts for both types of cascades (Section 8.4.1). Its analysis reveals that upward and downward cascades are mathematically independent phenomena (Section 7.4), and that both can be damped or not (i.e. amplifying), sensitively depending on model parameters (Sections 8.4.4 and 8.4.5). The intuitive mechanism underlying upward cascades is the more-or-less pronounced formation of a trophic ladder, with the steps corresponding to the cascade's local maxima and the space between steps to the minima. In simple variants of the Species Size-Spectrum Model with narrow individual-level predator–prey size-ratio windows (not analysed here), therefore one finds that in upward cascades subsequent abundance maxima are separated by the predator–prey size ratio, whereas for downward cascades subsequent maxima are separated by the square of the predator–prey size ratio (two steps down ladder). In the more realistic model variants considered in Section 8.4, this situation is realised for some parameter choices (e.g. Fig. 7A and B). However, for the standard parameter set used here (Section 8.1), which builds on that proposed by Hartvig et al. (2011), the distinction of upward and downward cascades by characteristic size ratios is blurred (Figs. 4 and 6).

The separation of subsequent local maxima for standard parameters corresponds in both directions to a factor $\approx 10^5$ in body mass (Fig. 4). Perhaps fortuitously, this agrees well with the separation of subsequent "domes" or

maxima in empirical size spectra (Fig. 1; Sprules and Goyke, 1994; Sprules et al., 1983). To classify cascades empirically, it might therefore be necessary to determine the direction of motion of perturbation responses in temporally resolved size spectra (Rodriguez and Mullin, 1986b; Rodriguez et al., 1987; Vasseur and Gaedke, 2007).

In the light of the observations in Section 2.4, it is conceivable, though by no means established, that the theoretical interpretation of "domes" in size spectra by Thiebaux and Dickie (1993) through equilibrium mass–balance equations is compatible with formation of these structures by one of the two mechanisms leading to periodic modulations in the present theory. The difference would be that, whereas Thiebaux and Dickie (1993) address the fully developed non-linear form of the domes, the present theory describes their dynamic emergence in the linear response to perturbations. The relationship between the two theories would then be similar to that encountered for water waves (Johnson, 1997), where linear and weakly non-linear theories describe low-amplitude waves, which are necessarily sinusoidal, whereas high-amplitude waves, which, as we know from experience, can assume entirely different shapes, are described by a different, non-linear theory.

The observation that different phyla are often associated with different domes (Gaedke, 1992a) does not necessarily stand in opposition to explanations of these structures in terms of general principles. In fact, evolution might naturally lead to this kind of specialisation within uneven size spectra.

2.6. Trophic cascades form slowly

Upward and downward trophic cascades in communities with broad intrapopulation size distributions will emerge slower than would be expected from models that do not account for intrapopulation size structure (Section 9.4). The reason is that pairs of species for which the adults are in a clear predator–prey relation to each other might interact as prey–predator or as competitors at other life-history stages. Figure 4, for example, documents formation of a downward cascade in the model with a delay corresponding to the threefold maturation age of the main size class targeted by fishing. Lags of 6–12 years between time-series of size-spectrum characteristics and of exploitation rates, which Daan et al. (2005) observed in the North Sea but found "*hard to account for*", might be explained by this observation. The slow recovery of the LFI shown by Fung et al. (2012a,b) in data and simulations is likely to reflect this phenomenon too.

2.7. Depletion of species higher up in the food chain is fast

For the scenario labelled as the oligotrophic regime, the Species Size-Spectrum Model predicts that upward trophic cascades are superimposed with an overall decline of species larger than the size class targeted by size-selective harvesting (Sections 8.4.1 and 8.4.4) and that this effect is the stronger the larger species are relative to the targeted size class (Section 9.4). The underlying mechanism is the same as that operating in simple food-chain models: insufficient supply of energy. However, with broad intrapopulation size distributions, the effect can propagate faster to larger species than it would in simpler models, because the indirect responses of larger species propagating through the food chain are combined with direct responses of similar magnitude attributable to harvesting or starvation of their juveniles. The timescale for the population response of large species to size-selective harvesting of smaller species or individuals is therefore of the order of magnitude of their maturation times.

2.8. Food-web structure essentially affects size-spectrum structure and dynamics

The derivation of the Species Size-Spectrum Model depicts communities as if there was a continuum of interacting species of all sizes and assumes that life-history traits and feeding interactions are determined by maturation sizes and body sizes alone. An immediate consequence is that species of comparable size are also similar in all their ecological traits and therefore compete with each other. Without appropriate regularisation of the model, the resulting competitive exclusion dynamics lead to instabilities of size spectra in which increases in the abundances of some species are compensated by decreases in the abundances of other species of very similar size (when coarsening the resolution of size classes, the spectra are generally stable). In reality, stable size-structured communities can form because ecological traits differ even between species of equal maturation size (Jacob et al., 2011), and, perhaps most importantly, in general, feeding interactions do not depend only on the sizes of prey and predator (Naisbit et al., 2012). Species coexist by forming rather sparse food webs: for example, Rossberg et al. (2011) show that only about 10 species contribute more than 1% to the diet of the average fish species, independent of local species richness. This, it is argued in Section 6.4, modifies continuum size-spectrum dynamics at size resolutions corresponding to the maturation body-size ratios among species in the diets of typical predators.

Because, as a result of strongly overlapping intraspecific size distributions, size-spectrum dynamics rather slow, these food-web effects are

likely to be sufficiently strong to modify dynamics substantially, even on coarser scales. In the present analysis, food-web effects are derived, parametrised, and included in the model based on heuristic arguments rather than on first principles. The theory, while allowing many other insights, is therefore unsuitable for reliable quantitative predictions of community dynamics. This would require models that quantitatively account for food-web topology.

2.9. Body mass approximates reproductive value

Fisher (1930) defined the reproductive value of an individual as its expected contribution "*to the ancestry of future generations*". Recently, Rossberg and Farnsworth (2011) developed a method to extend this empirically useful concept from the density-independent (linear) dynamics of a single population to complex communities of interacting populations. They argued, with fisheries management in mind, that a quantification of the size of a population by the summed reproductive values of its members should allow better predictions of future population (or "stock") sizes than other measures of population size, for example, the commonly used spawning-stock biomass.

Remarkably, under a certain set of approximations, the present theory evaluates the reproductive value of individuals to be exactly equal to their body mass (Section 6.2). This result holds for both mature and immature individuals. The summed reproductive value of a population would then simply be its total biomass. Tests of this prediction by computing reproductive values from empirically determined life-history parameters of a population might lead to more reliable characterisations of stock sizes and help to resolve the question whether the smaller or the larger individuals of a stock should be harvested preferentially to maximise economic output under given constraints on ecological impact.

2.10. Physiological mortality is constrained by population dynamic equilibrium

Beyer (1989) recognised the importance of the specific physiological mortality rate, a dimensionless parameter defined as a cohort's mortality rate divided by its specific growth rate (i.e. the relative body mass increase per unit time). Physiological mortality as a function of body size determines a population's internal size structure. Here, it is shown that, under a certain set of approximations, specific physiological mortality must be exactly 1 for immature cohorts in population-dynamic equilibrium (Section 5.4). Greater mortality leads to the decline, less mortality to the growth of populations. Even under

relaxed assumptions, a value close to one can still be expected (Section 5.7). Indeed, the density dependence of physiological mortality alone essentially controls population dynamics (Section 6.3, Eqs. (61) and (63)). Real-world complications will modify these results, especially for species with rather small ratios of adult to newborn (or hatchling) body sizes, but overall a close relation between population-dynamic equilibrium and specific physiological mortality is expected. This insight might help fisheries managers interpreting the outcomes of virtual population analyses (Lassen and Medley, 2001) and relating them to stock dynamics.

To the extent that the specific physiological mortality of immature individuals attains a universal value, the results of Beyer (1989) imply that the size structure of the immature component of populations is universal, except for a truncation below the size of newborns or hatchlings (Section 6.2). An empirical test of this approximate universality of size distributions and a better understanding of the magnitude and the causes for deviations from it might lead to other generalisations regarding structure and dynamics of interacting size-structured populations (Houde, 2009).

2.11. Solutions of "size-spectrum" equations follow general characteristics

In Section 7, this chapter develops a general method to approximate the solutions of a wide class of equations that describe the dynamics of size-structure communities, subject to two general principles that are often invoked in ecological theory. The first principle is allometric scaling of ecological rates with a fixed power n of body size ($n = 3/4$ is often used), and the second principle posits that, apart from the allometric scaling of rates, interaction strengths between individuals depend only on their relative, but not their absolute, sizes.

The approximate general solution of this class of equations implies that, in response to press perturbations targeting a narrow range of size classes, fronts are emitted from the perturbed size range that travel at constant speed on a scale given by body mass raised to the power $(1 - n)$, either towards larger or towards smaller size classes. The fronts leave behind themselves either a static, modulated structure with a wavelength that is constant on the logarithm body mass axis (e.g. trophic cascades) or regions of either consistently raised or reduced abundances. The amplitude of the modulation or of the rise/decline can either increase away from the perturbed size class, or decrease. The effects of a pulse perturbation can be described by linear combinations of press perturbations (Section 9.6). A graphic method to

decide for a given system which of the various conceivable scenarios will be realised is introduced in Section 8.4.3.

3. METHODS

This section briefly recalls some standard concepts of functional analysis used in developments of the theory below. The text by Boccara (1990) covers most of these topics in mathematically rigorous yet accessible form.

For a real- or complex-valued function $f(x)$, define its Fourier transform $\hat{f}(\xi)$ such that

$$\hat{f}(\xi) = \int_{-\infty}^{\infty} e^{-i\xi x} f(x)\mathrm{d}x, \quad f(x) = \int_{-\infty}^{\infty} \frac{e^{i\xi x}}{2\pi} \hat{f}(\xi)\mathrm{d}\xi, \qquad [1]$$

where i is the imaginary unit ($i^2 = -1$). The convolution $f*g$ of two functions is defined as the function h given by

$$h(x) = [f*g](x) = \int_{-\infty}^{\infty} f(y-x)g(y)\mathrm{d}y. \qquad [2]$$

With normalisations as in Eq. (1), Fourier transformations directly carry convolutions over into multiplication, that is, for any two functions f, g, one has $\widehat{f*g} = \hat{f}\hat{g}$. This relation implies that $f*g = g*f$, $(f*g)*h = f*(g*h)$, and $f*(g+h) = f*g + f*h$.

Depending on the convergence of the defining integral, the value of a Fourier transform $\hat{f}(\xi)$ can be computed via Eq. (1) not only for any real ξ but also for some complex-valued ξ. Consider, for example, the Gaussian window

$$W_\sigma(y) = \exp\left(-\frac{y^2}{2\sigma^2}\right). \qquad [3]$$

Its Fourier integral evaluates for arbitrary complex ξ to

$$\hat{W}_\sigma(\xi) = \sqrt{2\pi}\sigma \exp(-\xi^2\sigma^2/2). \qquad [4]$$

As another example, the function defined by $f(x) = 0$ for $x < 0$ and $f(x) = e^{-2x}$ for $x \geq 0$ has, by Eq. (1), the Fourier transform $\hat{f}(\xi) = (2+i\xi)^{-1}$ for any complex ξ such that $\mathrm{Im}\{\xi\} < 2$. (Real and imaginary parts of complex numbers ξ are denoted by $\mathrm{Re}\{\xi\}$ and $\mathrm{Im}\{\xi\}$, respectively.) When $\mathrm{Im}\{\xi\} \geq 2$, the integral in Eq. (1) does not converge. However, the definition of $\hat{f}(\xi)$ is naturally extended to any

complex $\xi \neq 2i$ by analytic continuation. Then, the formula $\hat{f}(\xi) = (2 + i\xi)^{-1}$ is valid for all complex ξ except $\xi = 2i$. Such analytic continuations of Fourier transforms will play an important role below.

Dirac's delta function $\delta(x)$ symbolises the idealised case of a function that is zero for all x except $x = 0$, and so (infinitely) large at $x = 0$ that $\int_{-a}^{a} \delta(x)\mathrm{d}x = 1$ for any $a > 0$. It follows, for example, that $\int_{-a}^{a} f(x)\delta(x)\mathrm{d}x = f(0)$ for any $a > 0$.

A functional derivative $\delta F[g]/\delta g(y)$ is the generalisation of the notion of a gradient to vectors with continuous-valued indices y, that is, functions $g(y)$. Standard rules of differential calculus translate straightforwardly to functional derivatives, except that, because the dependence of an expression $F[g]$ in $g(x)$ on the single point of $g(x)$ where $x = y$ is generally tiny, functional derivatives contain an additional factor $\delta(y)$. For example, $\delta g(x)/\delta g(y) = \delta(x - y)$, and $\delta \int_{-\infty}^{\infty} f(g(z))\mathrm{d}z/\delta g(y) = \mathrm{d}f(u)/\mathrm{d}u$ evaluated at $u = g(y)$.

Define a scalar product for real-valued functions as

$$\langle f|g\rangle = \int_0^\infty f(x)g(x)\mathrm{d}x. \qquad [5]$$

The adjoint of a linear operator L (a linear mapping from functions $g(x)$ onto functions $[Lg](x)$) can then be defined as the linear operator L^+ that satisfies for all functions f and g (with some mathematical constraints):

$$\langle L^+ f|g\rangle = \langle f|Lg\rangle. \qquad [6]$$

It can be computed as

$$L^+ f(x) = \frac{\delta\langle f|Lg\rangle}{\delta g(x)}. \qquad [7]$$

4. MODEL

The model underlying this theory has been motivated and derived by Hartvig et al. (2011). Its major strengths are a consistent synthesis of dynamic descriptions of size-structured communities, populations, individual growth, and bioenergetics based on general biological principles; the model's small set of parameters, all of which are estimated from empirical data; and its demonstrated structural stability. This section provides only a technical summary and highlights minor deviations from the formulation of Hartvig et al. (2011). Table 2 lists symbols used throughout this work and their interpretation.

Table 2 List of important symbols

Symbol	Defined near equation	Interpretation
α	(11)	Assimilation efficiency
β		Preferred predator–prey size ratio
$\tilde{\beta}(w)$	(71)	Equilibrium population structure on log-scale
$\tilde{\beta}^{-}(w)$	(73)	$\tilde{\beta}(-w)$
$\tilde{\beta}_{\nu}^{-}(w)$	(126)	$e^{\nu w}\tilde{\beta}^{-}(w)$
γ	(10)	Coefficient of search/attack rate
ϵ	(12)	Efficiency of reproduction
η	(11)	Maturation- over asymptotic mass
$\kappa_0(w)$	(70)	Individual-level interaction kernel on log-scale
λ	(16)	Exponent of community size spectrum
$\mu_{\mathrm{p}}(m)$	(13)	Predation mortality
μ_0	(14)	Coefficient of natural mortality
$\tilde{\mu}$	(26)	Coefficient of predation mortality
ν	(73)	$3-\lambda-n$
σ_F	(77)	Width of harvested size range
$\phi(m)$	(19)	Density of prey available
$\tilde{\phi}$	(19)	Coefficient of $\phi(m)$
$\Phi(u)$	(79)	Fishing pressure on log-scale
$\psi(x)$	(11)	Reproduction selection function
$a_f(u, t)$	(93)	Delocalised response to fishing pressure
$a(m, m_*)$	(60)	Specific physiological mortality
$\tilde{a}$	(35)	Scale-free juvenile specific physiological mortality
$b(u)$	(75)	Perturbation of equilibrium biomass distribution over log-scale
$b_0(u)$	(89)	Fourier solution of Species Size-Spectrum model
$b_c(u)$	(93)	Core response to fishing pressure

Continued

Table 2 List of important symbols—cont'd

Symbol	Defined near equation	Interpretation
$B(m_*)$	(56)	Reduced dynamic variables of QNA
$B_{\mathrm{tot}}(m_*)$	(40)	Scale-invariant equilibrium biomass per maturation size class
$\tilde{B}_{\mathrm{tot}}$	(40)	Coefficient of $B_{\mathrm{tot}}(m_*)$
B_{m_*}	(49)	Equilibrium biomass per maturation size class
C_{m_*}	(53)	Normalisation constant of reproductive value
F	(77)	Maximal fishing mortality
$f(m)$	(10)	Degree of satiation
$\tilde{g}(x)$	(24)	Scale-free growth rate
$\tilde{g}_r(x)$	(24)	Scale-free fecundity
$g(m, m_*)$	(11)	Growth rate
$g_{\mathrm{r}}(m, m_*)$	(11)	Fecundity
$\tilde{g}_0$	(24)	Coefficient of growth rate/fecundity
h	(11)	Coefficient of maximal food intake
$J_{m_*}(m)$	(52)	Equilibrium flow of reproductive value
k	(11)	Coefficient of metabolic loss rate
$K_{\mathrm{tot}}(m_*)$	(42)	Metabolic losses per maturation size class
$\tilde{K}_{\mathrm{tot}}$	(42)	Coefficient of $K_{\mathrm{tot}}(m_*)$
$K(m_*, m'_*)$	(62)	Population-level interaction kernel on linear scales
$\tilde{K}(w)$	(74)	Population-level interaction kernel on log-scales
L_{m_*}	(47)	McKendrick–von Foerster operator
$L^+_{m_*}$	(51)	Adjoint McKendrick–von Foerster operator
m		Body size
M	(75)	Arbitrary unit mass
m_*		Body size at maturation
m_0, $m_0(m_*)$	(16)	Size of offspring

Table 2 List of important symbols—cont'd

Symbol	Defined near equation	Interpretation
m_F	(79)	Size class targeted by fishing
n	(10)	Exponent for physiological rates
$N(m, m_*)$	(16)	Distribution of individuals by body and maturation size
$N_i(m)$	(9)	Intraspecific size distribution
$\tilde{N}(x)$	(16)	Scale-free intraspecific size distribution
$\mathcal{N}(m)$	(17)	Community size spectrum
$\tilde{\mathcal{N}}$	(17)	Coefficient of community size spectrum
q	(10)	Exponent for search/attack rate
$s(x)$	(8)	Predator–prey size-ratio window
u_F	(108)	Logarithmic size class targeted by fishing
$V_{m_*}(m)$	(51)	Reproductive value
$W_\sigma(\gamma)$	(3)	Gaussian window
$W_{m_*}(m)$	(48)	Equilibrium population structure
x_0	(29)	Relative size of offspring

The model describes trophic interactions between reproductively isolated populations of heterotrophic species in large, size-structured aquatic communities. It distinguishes between individuals of different body mass m within each population j, and assumes all individuals of the same size and the same population to be equivalent. Each population is therefore characterised by a size distribution $N_j(m)$ of individuals. Specifically, following Hartvig et al. (2011), the number of individuals of population j within the infinitesimally small body mass interval $[m; m+dm]$ is given by $\mathcal{V}N_j(m)dm$, where $\mathcal{V}$ is the volume of the system considered (a formulation in terms of areal density would equally be possible). In general, $N_j(m)$ will be time-dependent.

Energy and biomass are thought to flow overwhelmingly from smaller to larger individuals (Gilljam et al., 2011; Woodward et al., 2010b). The demographics of the smallest species in the community are not modelled explicitly. Rather, the idealisation is invoked that all species are much larger than the smallest individuals in the community, so that the relevant

(log m)-axis stretches infinitely into both directions. This admits a description in which the prey species of every consumer are again consumers, and all species are consumed by some other, larger species so that, mathematically, there is an infinite hierarchy of species sizes in the community. The original model of Hartvig et al. (2011) instead summarises the density of individuals of small species by a *resource spectrum* $N_\mathrm{R}(m)$.

The biomass density of food available to an individual of species j with body mass m is given by

$$\phi_j(m) = \int_0^\infty m_\mathrm{p} \mathcal{N}_j(m_\mathrm{p}) s\left(\ln \frac{m}{m_\mathrm{p}}\right) \mathrm{d}m_\mathrm{p}, \qquad [8]$$

where $\mathcal{N}_j(m_\mathrm{p})$ is the density of prey of size m_p available to j, and the function $s(\cdot)$ characterises the individual-level predator–prey size-ratio window on a logarithmic scale.

The theory admits essentially arbitrary predator–prey size-ratio windows, but the following plausible constraints shall be imposed: $s(u)$ is non-negative and decays faster than exponentially as $u \to \pm\infty$. The Fourier transform $\hat{s}(\xi)$ of $s(u)$ is then an entire function (i.e. it is finite for any complex ξ). An example satisfying this condition is given by Eqs. (109) and (110).

The density of prey entering Eq. (8) is given by

$$\mathcal{N}_j(m) = \sum_k \theta_{j,k} N_k(m), \qquad [9]$$

with the weights $\theta_{j,k} \in [0; 1]$ characterising dietary preferences, that is, the food web. Dependence of $\theta_{j,k}$ on life stages could be incorporated into the formalism but is not considered here. On the contrary, the analysis will largely be based on a mean-field approximation, that is, the ecosystem mean of $\theta_{j,k}$ is absorbed into the search rate (see below), and all $\theta_{j,k}$ are set to 1. Then $\mathcal{N}_j(m) = \mathcal{N}(m)$ is the same for all predators j, and so the density of available food $\phi_j(m) = \phi(m)$.

Food intake is determined by the density of prey $\phi(m)$, the effective search rate, assumed to be of the form γm^q (with constants γ, $q > 0$), and the physiological maximum food-intake rate of individuals. The latter is assumed to scale as hm^n, with constants $h > 0$ and $0 < n < q$. For simplicity, n is identified with the allometric exponent for metabolic rates. Typically, $n \approx 0.75$ (Peters, 1983), but here only $n < 1$ is required. Specifically, individuals of size m feed at a rate $f(m)hm^n$, where the degree of satiation $f(m) \in [0; 1]$ is given by

$$f(m) = \frac{\gamma m^q \phi(m)}{\gamma m^q \phi(m) + h m^n}. \quad [10]$$

This corresponds to an individual-level Type II functional response with handling time $(hm^n)^{-1}$ (dimensions: Time/Mass). In the limit $h \to \infty$, the special case of a linear functional response $f(m)hm^n \to \gamma m^q \phi(m)$ is recovered.

Food intake is discounted by the assimilation efficiency $0 < \alpha < 1$ and metabolic losses at a rate km^n (with constant $k > 0$), leaving a net uptake of energy $\alpha f(m) h m^n - k m^n$ available for somatic growth and reproduction. It is apportioned between these two uses according to a reproduction-selection function $\psi(m/m_{*j}) \in [0, 1]$, with m_{*j} characterising the size of species j at maturation. That is, individuals grow at a rate $g(m, m_{*j})$ (dimension Mass/Time) and invest into offspring at a rate $g_r(m, m_{*j})$, with

$$\begin{aligned} g(m, m_{*j}) &= [1 - \psi(m/m_{*j})][\alpha f(m) h - k] m^n, \\ g_r(m, m_{*j}) &= \psi(m/m_{*j})[\alpha f(m) h - k] m^n. \end{aligned} \quad [11]$$

Individuals produce offspring, assumed to be of size m_{0j}, at a rate $(\epsilon/2m_{0j}) g_r(m, m_{*j})$ (dimension 1/Time), with the factor 1/2 representing the assumed proportion of females in a population and the reproduction efficiency ϵ discounting for all additional losses from production of eggs to birth or hatching. With the case of fish in mind, Hartvig et al. (2011) assumed the size of hatchlings $m_{0j} = m_0$ to be effectively the same for all species, independent of maturation size m_{0j}. Here, m_{0j} values that vary between species will be admitted. Integrating over spawners of all sizes, species j produces offspring at a rate

$$R_j = \frac{\epsilon}{2m_{0j}} \int_0^\infty N_j(m) g_r(m, m_{*j}) \mathrm{d}m. \quad [12]$$

Many analytic results derived here are independent of the specific form of the reproduction-selection function $\psi(x)$, but the following general characteristics will be used below: whereas maturation is a gradual process, it is sufficiently well defined that, as $x \to 0$, $\psi(x)$ goes to zero, with most of the transition taking place near $x \approx 1$. In order for individuals to have well-defined growth trajectories, $\psi(x)$ should be Lipschitz continuous.[3] Further, it is assumed that $\psi(\eta^{-1}) = 1$ for some constant $0 < \eta < 1$, and that $0 \le \psi(x) < 1$ for $0 < x < \eta^{-1}$.

[3] A function $f(x)$ is called Lipschitz continuous if there is a positive constant K such that $|f(x) - f(y)| < K|x - y|$ for all x, y in the domain of f.

These conditions ensure that individuals cannot reach the size m_*/η, which therefore becomes a sharp upper bound on body size.

The predation mortality of individuals of size m_p follows from the model of food intake above. It is given by

$$\mu_\mathrm{p}(m_\mathrm{p}) = \int_0^\infty s\left(\ln\frac{m}{m_\mathrm{p}}\right)[1-f(m)]\gamma m^q \mathcal{N}(m)\mathrm{d}m. \qquad [13]$$

Mortality from all other causes is summarised in a species-dependent background mortality

$$\mu_j = \mu_0 m_{*j}^{n-1}, \qquad [14]$$

chosen such as to be proportional to inverse generation time. It is assumed here that, as Hartvig et al. (2011) suggested, the parameter $\mu_0 \geq 0$ is sufficiently small that μ_j becomes relevant only for adults. Hartvig et al. (2011) also included starvation mortality in their model, but the situations where this becomes relevant lie beyond the scope of the current theory.

Combining the effects of growth, mortality, and reproduction, one obtains a balance equation for the distribution $N_j(m)$ of the individuals forming a population over body sizes (McKendrick, 1926; von Foerster, 1959):

$$\frac{\partial N_j(m)}{\partial t} + \frac{\partial}{\partial m}\Big[g(m, m_{*j})N_j(m)\Big] = -\Big[\mu_\mathrm{p}(m) + \mu_0 m_{*j}^{n-1}\Big]N_j(m). \qquad [15]$$

The boundary condition $R_j = g(m_{0j}, m_{*j})N_j(m_{0j})$, equating offspring production with outgrowth, closes the model.

5. PROPERTIES OF THE SCALE-INVARIANT COMMUNITY STEADY STATE

5.1. Discussion of the underlying approximations

To obtain an analytic characterisation of the solution of this model, two additional approximations are made. Both are motivated by the empirical fact that the community size spectrum $\mathcal{N}(m)$ often follows a power law $\mathcal{N}(m) \propto m^{-\lambda}$ over a wide range of body sizes m. (Sheldon's hypothesis corresponds to $\lambda \approx 2$.) The first approximation is to coarse-grain over species with similar maturation size m_{*j}, giving a smooth distribution $N(m, m_*)$ of individuals over body sizes m and maturation sizes m_* (Andersen and Beyer, 2006). In this coarse-grained description, the number of individuals in the infinitesimal body size interval $[m;\ m+\mathrm{d}m]$ belonging to species with

maturation body sizes in the infinitesimal interval $[m_*; m_* + \mathrm{d}m_*]$ is given by $\mathcal{V}N\,(m,m_*)\,dmdm_*$ with $\mathcal{V}$ again denoting system volume. It is assumed that the size of hatchlings or newborns m_0 is determined largely by maturation size m_*, so that the former becomes a function of the latter. This can be a linear relationship, a functional relationship where m_0 is constant over some range in m_*, or any other type of non-linear functional relationship. With this and the foregoing mean-field approximation in place, species with similar m_* will typically be similar in all their ecological characteristics. The competitive exclusion dynamics resulting from this approximation is discussed in Section 6.4.

The second approximation is motivated by the scale-invariance of the community size spectrum, highlighted by Camacho and Solé (2001) and Capitán and Delius (2010).[4] It suggests that the underlying intraspecific size distributions $N_j(m)$ are, to some approximation, also scale-invariant when factoring out the dependence on maturation body size m_{*j}. Specifically, conditions will be derived for which $N_j(xm_{*j}) \propto N_k(xm_{*k})$ to a good approximation over a wide range in dimensionless body masses x for most pairs of species (j, k). The obvious truncation of intraspecific size structure below the size of hatchlings m_{0j}, that is, for[5] $x < x_{0j} \stackrel{\text{def}}{=} m_{0j}/m_{*j}$, violates this approximation and will therefore receive special attention below. It turns out that the limit $x_{0j} \to 0$ is often non-singular and taking it yields ecologically consistent results.

The combination of these two approximations leads to an ansatz

$$N(m, m_*) = \begin{cases} m_*^{-\lambda-1}\tilde{N}(m/m_*) & \text{for } m \geq m_0, \\ 0 & \text{for } m < m_0 \end{cases} \qquad [16]$$

for the coarse-grained, scale-invariant distribution of individuals, where m_0 is a function of m_* and the scale-free size distribution $\tilde{N}(x)$ remains to be determined.[6]

In the small-hatchling limit $m_0/m_* \to 0$, the coarse-grained community size spectrum Eq. (9) can be evaluated, by using first Eq. (16) and then substituting $m_* = m/x$, as

[4] Recall that scale invariance in the simple form $\mathcal{N}(cm) = c^{-\lambda}\mathcal{N}(m)$ is equivalent to the power-law condition $\mathcal{N}(m) \propto m^{-\lambda}$: The power law obviously implies scale invariance. The converse can be seen by differentiating the scaling laws with respect to the scale factor c at $c = 1$ and solving the resulting differential equation. As both conditions imply each other, they are equivalent.

[5] The notation $A \stackrel{\text{def}}{=} B$ indicates the definition of A as B.

[6] To streamline notation, a tilde ($\sim$) is used throughout this work to indicate the "scale-invariant part" of some mass-dependent function. This leads to the following modification of the notation used by Andersen and Beyer (2006) and Hartvig et al. (2011): $a \to \tilde{a}, N_c(m) \to \mathcal{N}(m), \kappa_c \to \tilde{\mathcal{N}}, \hbar \to \tilde{g}_0, \alpha_p \to \tilde{\mu}$.

$$\begin{aligned}\mathcal{N}(m) &= \int_0^\infty N(m, m_*)\mathrm{d}m_* \\ &= \int_0^\infty {m_*}^{-\lambda-1}\tilde{N}(m/m_*)\mathrm{d}m_* \\ &= \int_0^\infty x^{\lambda-1}m^{-\lambda}\tilde{N}(x)\mathrm{d}x \\ &= m^{-\lambda}\tilde{\mathcal{N}},\end{aligned} \qquad [17]$$

with a constant

$$\tilde{\mathcal{N}} = \int_0^\infty x^{\lambda-1}\tilde{N}(x)\mathrm{d}x. \qquad [18]$$

Equation (17) confirms the supposed relation between ansatz (16) and power-law size spectra, Eq. (17). Consistency of this result requires that the integral in Eq. (18) converges, which will be verified after computing $\tilde{N}(x)$ and λ in Section 5.4.

5.2. Scale-invariant demographics

The steady-state demographic rates are now evaluated assuming scale-invariance (Eq. (17)) and making use of the mean-field approximation $\mathcal{N}_j(m) = \mathcal{N}(m)$. Prey availability, Eq. (8), then becomes

$$\begin{aligned}\phi(m) &= \int_0^\infty m_\mathrm{p}\mathcal{N}(m_\mathrm{p})s\left(\ln\frac{m}{m_\mathrm{p}}\right)\mathrm{d}m_\mathrm{p} \\ &= m^{2-\lambda}\tilde{\phi},\end{aligned} \qquad [19]$$

where the constant

$$\tilde{\phi} = \tilde{\mathcal{N}}\int_0^\infty \gamma^{\lambda-3}s(\ln\gamma)\mathrm{d}\gamma \qquad [20]$$

is obtained from Eq. (19) using the substitution $m_\mathrm{p} = m/\gamma$. Doing another substitution, $\gamma = e^x$, then noting the formal similarity with a Fourier integral, the integral in the last equation above can be expressed in terms of the Fourier transform $\tilde{s}(\xi)$ of $s(x)$:

$$\begin{aligned}\int_0^\infty \gamma^{\lambda-3}s(\ln\gamma)\mathrm{d}\gamma &= \int_{-\infty}^\infty e^{(\lambda-2)x}s(x)\mathrm{d}x \\ &= \tilde{s}(i(\lambda-2)).\end{aligned} \qquad [21]$$

Below, similar transformations will be applied to evaluate other integrals.

The consumer satiation resulting from the prey availability $\phi(m)$ computed above is

$$f(m) = \frac{\gamma m^{2+q-\lambda}\tilde{\phi}}{\gamma m^{2+q-\lambda}\tilde{\phi} + hm^n}. \quad [22]$$

According to Eq. (11), consumers neither grow nor reproduce when satiation $f(m) < k/\alpha h$. Exclusion of this situation leaves two scenarios for scale-invariance of $f(m)$. In the first case, $\gamma m^{2+q-\lambda}\tilde{\phi} \gg hm^n$ over the body-size (m) range of interest, so $f(m) \approx 1$. This regime breaks down at body sizes $m \approx [h/(\tilde{\phi}\gamma)]^{1/(2+q-\lambda-n)}$, where a crossover to a non-scale-invariant regimes occurs. However, this point can be moved mathematically to arbitrarily large or small m, respectively, by an appropriate choice of γ. In the second case, $2+q-\lambda = n$, so that $f(m) = \tilde{f}$ with constant $\tilde{f} \stackrel{\text{def}}{=} \gamma\tilde{\phi}/(\gamma\tilde{\phi} + h)$. This fixes the size-spectrum exponent as $\lambda = -2+q-n$ (Andersen and Beyer, 2006). Mindful of the caveats discussed in Section 2.1, the first case is called the eutrophic regime and the second the oligotrophic regime.[7]

Both cases lead to scale-invariant somatic and reproductive growth rates:

$$g(m, m_*) = \tilde{g}(m/m_*)m^n, \quad g_r(m/m_*) = \tilde{g}_r(m/m_{r*})m^n, \quad [23]$$

where

$$\tilde{g}(x) = [1 - \psi(x)]\tilde{g}_0, \quad \tilde{g}_r(x) = \psi(x)\tilde{g}_0 \quad [24]$$

with

$$\tilde{g}_0 = \alpha f_0 h - k, \quad [25]$$

and $f_0 = 1$ or $f_0 = \tilde{f}$, depending on the case considered.

To evaluate predation mortality, Eq. (13), in the eutrophic regime, the lowest-order correction to satiation, $f(m) = 1 - hm^{n+\lambda-2-q}\gamma^{-1}\tilde{\phi}^{-1} + \cdots$, needs to be taken into account, giving

$$\begin{aligned}\mu_p(m_p) &= \int_0^\infty s\left(\ln\frac{m}{m_p}\right) hm^{n-2}\tilde{\phi}^{-1}\tilde{\mathcal{N}}\,\mathrm{d}m \\ &= \tilde{\mu}m_p^{n-1},\end{aligned} \quad [26]$$

with a constant

[7] Maury et al. (2007b) investigated a size-spectrum model in which the allometric exponent for maximal ingestion $\propto m^{2/3}$ is smaller than the exponent for metabolic losses $\propto m$, so that ingestion limits are relevant only for the largest organisms. Then other scaling regimes become possible, e.g. such that ingestion balances maintenance cost by having feeding levels $\propto m^{1-2/3} = m^{1/3}$. Their Fig. 5e might represent this scenario for body lengths < 0.1 m. It is not considered here.

$$\tilde{\mu} = \frac{h\tilde{\mathcal{N}}}{\tilde{\phi}} \hat{s}(i(n-1)), \qquad [27]$$

expressed in terms of the Fourier transform of $s(x)$.

In the oligotrophic regime, predation mortality evaluates to a power law of the same form as Eq. (26), but now with coefficient

$$\tilde{\mu} = (1-\tilde{f})\gamma\tilde{\mathcal{N}}\hat{s}(i(n-1)) = \frac{\gamma h\tilde{\mathcal{N}}}{\gamma\tilde{\phi}+h}\hat{s}(i(n-1)). \qquad [28]$$

It is worth noting that, although the demographic parameters derived in this section depend on the exponent λ and coefficient $\tilde{\mathcal{N}}$ characterising the community size spectrum, Eq. (17), the scale-free size distribution $N(x)$ itself does not enter the results. Hence, the results hold also when the community size spectrum follows a power law but is not apportioned to scale-free intrapopulation size distributions. With such a situation in mind, it is instructive to consider the boundary condition $g_j(m_{0j})N_j(m_{0j}) = R_j$ of the McKendrick–von Foerster Equation, while making use of the scale-invariant expressions for the demographic parameters derived above but allowing arbitrary population structures $N_j(m_{0j})$. With $m_{0j} = x_0 m_{*j}$, this yields by Eqs. (12), (23), and (24):

$$[1-\psi(x_0)]\tilde{g}_0 x_0^n m_{*j}^n N_j(x_0 m_{*j}) = \frac{\epsilon\tilde{g}_0 m_{*j}^n}{2x_0}\int_0^\infty N_j(x m_{*j})\psi(x)x^n \mathrm{d}x. \qquad [29]$$

Observing that the maturation selection function for hatchlings $\psi(x_0)$ is generally zero, and cancelling common factors on both sides of the equation, this reduces to

$$N_j(x_0 m_{*j}) = \frac{\epsilon x_0^{-1-n}}{2}\int_0^\infty N_j(x m_{*j})\psi(x)x^n \mathrm{d}x. \qquad [30]$$

The exponent $-1-n$ of x_0 decomposes into a contribution -1, arising from simple book-keeping, and a contribution $-n$ for the ratio of the rates of metabolic activity of adults and hatchlings. Little more ecology enters this power law, Eq. (30), for the scaling of the ratio of hatchling and adult abundance with x_0. It should therefore be robust with respect to variations in the structure of the model and its solutions.

5.3. Scale-free size distribution

The scale-free size distribution $\tilde{N}(x)$ can now be obtained as the equilibrium solution of the McKendrick–von Foerster Equation (15). Taking above results for growth and mortality into account,

$$\frac{\partial}{\partial m}\left[\tilde{g}(m/m_*)m^n\tilde{N}(m/m_*)\right] = -(\tilde{\mu}m^{n-1} + \mu_0 m_*^{n-1})\tilde{N}(m/m_*), \qquad [31]$$

or, substituting $m = m_* x$ and cancelling a factor m_*^{n-1},

$$\frac{\partial}{\partial x}\left[\tilde{g}(x)x^n\tilde{N}(x)\right] = -(\tilde{\mu}x^{n-1} + \mu_0)\tilde{N}(x). \qquad [32]$$

The equation is solved by

$$\tilde{N}(x) = \frac{\tilde{N}_0}{\tilde{g}(x)x^n}\exp\left[-\int_1^x \frac{\tilde{\mu}}{\tilde{g}(x')x'} + \frac{\mu_0}{\tilde{g}(x')x'^n}\mathrm{d}x'\right] \qquad [33]$$

for $x < \eta^{-1}$ and $\tilde{N}(x) = 0 \quad \text{for} \, x \geq \eta^{-1}$. The normalisation factor $\tilde{N}_0$ is related to $\tilde{\mathcal{N}}$ via Eq. (18). Differentiability of $\tilde{N}(x)$ requires the integral in Eq. (33) to diverge at $x = \eta^{-1}$, which is the case when the function $\psi(x)$ is Lipschitz continuous at the point $\psi(\eta^{-1}) = 1$, as demanded above.

To understand the structure of solution (33), recall that for body sizes much smaller than maturation size ($x \ll 1$), all available energy is used for growth ($\psi(x) = 0$), so $\tilde{g}(x)$ reduces to $\tilde{g}_0$ by Eq. (24). The integral in Eq. (33) can then be evaluated, giving

$$\tilde{N}(x) \propto \frac{1}{x^n} x^{-\frac{\tilde{\mu}}{\tilde{g}_0}} \exp\left[-\frac{\mu_0(x^{1-n} - 1)}{\tilde{g}_0(1-n)}\right] \quad (\text{for} \, x \ll 1).$$

With $n < 1$, and therefore $x^{1-n} \to 0$ as $x \to 0$

$$\tilde{N}(x) \propto x^{-n-\tilde{a}} \quad (\text{for} \, x \ll 1), \qquad [34]$$

where the constant

$$\tilde{a} = \frac{\tilde{\mu}}{\tilde{g}_0}, \qquad [35]$$

is the specific physiological mortality (Beyer, 1989) of immature individuals.

5.4. Implications of the boundary condition (part I)

To assure demographic equilibrium, the boundary condition, Eq. (30), still needs to be evaluated. Putting $N_j(m) \propto \tilde{N}(m/m_{*j})$ into this equation and substituting Eq. (34) for the left-hand side, one obtains

$$x_0^{-n-\tilde{a}} \propto x_0^{-1-n}. \qquad [36]$$

As x_0 takes different values for different maturation size classes, existence of a scale-free intrapopulation size distribution $\tilde{N}(x)$ requires that

$$\tilde{a} = 1. \qquad [37]$$

The mechanism by which this condition can be satisfied depends on the size-spectrum regime. In the oligotrophic case, the results of Section 5.2 combine with $\tilde{a}=1$ to the condition

$$\tilde{\mathcal{N}} = \frac{k}{\gamma[(\alpha - kh^{-1})I_1 - I_2]}, \qquad [38]$$

where $I_1 \stackrel{\text{def}}{=} \hat{s}(i(\lambda-2))$ and $I_2 \stackrel{\text{def}}{=} \hat{s}(i(n-1))$. Therefore, $\tilde{a}=1$ implies a constraint on physiological parameters or on the coefficient of the community size spectrum $\tilde{\mathcal{N}}$. For the eutrophic regime, Section 5.2 with $\tilde{a}=1$ implies

$$(\alpha - kh^{-1})I_1 - I_2 = 0. \qquad [39]$$

By varying the size-spectrum slope λ, the value of I_1 can be adjusted to satisfy this condition. Hence, power-law size spectra impose a condition on the size-spectrum slope in the eutrophic regime, and on absolute abundances (with a slope fixed at $\lambda = 2+q-n$) in the oligotrophic regime.

To interpret Eqs. (38) and (39) ecologically, observe first that $\alpha - kh^{-1}$ is the conversion efficiency at *ad libitum* feeding (assimilation minus metabolic losses). Now, consider the special case of a sharply defined predator–prey size ratio β, that is, $s(x) = \delta(x - \ln\beta)$, $\hat{s}(\xi) = \beta^{-i\xi}$. Equation (39) is then equivalent to $\alpha - kh^{-1} = \beta^{n-1}\beta^{2-\lambda}$, which has the form of an energy-balance equation as encountered in early size-spectrum theory (e.g. Platt and Denman, 1978): losses through conversion $\alpha - kh^{-1}$ are matched by a corresponding reduction of metabolic activity at the next trophic level β^{n-1}, corrected by the ratio of predator to prey biomass abundance $\beta^{2-\lambda}$. In the oligotrophic regime, where hypothetical *ad libitum* feeding leads to an energy surplus (a positive denominator in Eq. (38)), a power-law size spectrum is attained with less-efficient feeding at lower abundances. Remarkably, despite the fact that reproduction played a crucial role in deriving Eqs. (38) and (39), the result could have been obtained similarly when disregarding species identity and reproduction.

It is also noteworthy that, to the degree that (i) natural death is negligible so that conversion efficiency equals the Lindeman's trophic transfer efficiency (commonly found to be ≈ 0.1) and (ii) Sheldon's hypothesis $\lambda = 2$ holds, the energy balance discussed above necessarily leads to a predator–prey size ratio $\beta = 0.1^{1/(n-1)} \approx 1000$, which is similar to observed values, without any reference to mechanical constraints on feeding interactions.

One might therefore wonder whether the size of a fish's gape is determined by community-level constraints, rather than *vice versa*.

We can now ask under which conditions the integral in Eq. (18) converges for small x, in other words, under which conditions the contribution of large species to the abundance of small individuals in a community is small. By Eqs. (34) and (37), this requires $\lambda > 1 + n$. Therefore, there is with $n \approx 3/4$ little scope for size-spectrum slopes much smaller than the Sheldon slope $\lambda = 2$.

5.5. Total biomass per size class

From Eq. (16), the total biomass of species belonging to a small maturation size interval $[m_*; m_* + \Delta m_*]$ can be computed for the scale-invariant solution as $\mathcal{V} B_{\mathrm{tot}}(m_*) \Delta m_*$, with

$$\begin{aligned} B_{\mathrm{tot}}(m_*) &= \int_{m_0}^{\infty} m N(m, m_*) \mathrm{d}m \\ &= \int_{m_0}^{\infty} m\, m_*^{-\lambda-1} \tilde{N}(m/m_*) \mathrm{d}m \\ &= m_*^{-\lambda+1} \tilde{B}_{\mathrm{tot}}(m_0/m_*) \end{aligned} \qquad [40]$$

and

$$\tilde{B}_{\mathrm{tot}}(x_0) = \int_{x_0}^{\infty} x \tilde{N}(x) \mathrm{d}x. \qquad [41]$$

From the asymptotic form of $\tilde{N}(x)$, Eq. (34), it follows that the integrand above scales as x^{-n} for small x, implying that the contribution from small individuals to the total biomass is small as long as $n < 1$. The biomass of a maturation size class or species is dominated by its adults.

5.6. Total metabolic loss rate per size class

Contrasting with population biomass, the rate of metabolic losses of a maturation size class or species contains a large contribution from small individuals and diverges in the limit $x_0 \to 0$. Specifically, the total losses $k m^n$ of individuals belonging to a small maturation size interval $[m_*; m_* + \Delta m_*]$ evaluates to $\mathcal{V} K_{\mathrm{tot}}(m_*) \Delta m_*$, with

$$\begin{aligned} K_{\mathrm{tot}}(m_*) &= \int_{m_0}^{\infty} k m^n N(m, m_*) \mathrm{d}m \\ &= \int_{m_0}^{\infty} k m^n m_*^{-\lambda-1} \tilde{N}(m/m_*) \mathrm{d}m \\ &= m_*^{-\lambda+n} \tilde{K}_{\mathrm{tot}}(m_0/m_*) \end{aligned} \qquad [42]$$

and

$$\tilde{K}_{\mathrm{tot}}(x_0) = k \int_{x_0}^{\infty} x^n \tilde{N}(x) \mathrm{d}x. \qquad [43]$$

By Eqs. (34) and (37), the integrand above is proportional to x^{-1} for small x, implying a logarithmic divergence of the integral as $x_0 \to 0$. It is easily verified that a similar logarithmic divergence arises for biomass loss by predation mortality and biomass gain by somatic growth. Consistency of model solutions in the limit $x_0 \to 0$ requires that these contributions cancel each other out.

5.7. Implications of the boundary condition (part II)

The conditions derived in the foregoing section leave no free parameter that could be adjusted to ensure that boundary condition Eq. (29) is satisfied not only by order of magnitude but also exactly. Below, it is shown that exact satisfaction is possible only under special, artificial assumptions, so deviations of the population structure $N(m, m_*)$ from the ideal scale-invariant form $m_*^{-\lambda-1} N(m/m_*)$ must be expected. Then, the qualitative nature of the expected deviations is discussed.

Consider first the case of vanishing background mortality $\mu_0 = 0$ and assume $\tilde{a} = 1$ (i.e. $\tilde{\mu} = \tilde{g}_0$) and scale-invariance: $N_0(m) \propto \tilde{N}(m/m_{*j})$ for $m_0 \le m \le \eta^{-1} m_*$ and $N_j(m) = 0$ otherwise. Define the function

$$E(x) = \exp\left[-\int_1^x \frac{1}{[1-\psi(x')]x'} \mathrm{d}x' \right], \qquad [44]$$

which satisfies the identify

$$\begin{aligned} \int_{x_0}^{\eta^{-1}} \frac{\psi(x)}{1-\psi(x)} E(x) \mathrm{d}x &= \int_{x_0}^{\eta^{-1}} \left[\frac{1}{1-\psi(x)} - 1 \right] E(x) \mathrm{d}x \\ &= \int_{x_0}^{\eta^{-1}} -x \frac{\mathrm{d}E(x)}{\mathrm{d}x} - E(x) \mathrm{d}x \qquad [45] \\ &= -\int_{x_0}^{\eta^{-1}} \frac{\mathrm{d}}{\mathrm{d}x} [xE(x)] \mathrm{d}x = x_0 E(x_0). \end{aligned}$$

Using Eqs. (24), (33), (44), and (45), one can re-evaluate the general boundary condition (29) as

$$[1-\psi(x_0)]\tilde{N}(x_0)=\frac{\tilde{N}_0 x_0^{-n}}{\tilde{g}_0}E(x_0) \quad =\frac{\epsilon x_0^{-1-n}}{2}\int_{x_0}^{\eta^{-1}}\tilde{N}(x)\psi(x)x^n\,\mathrm{d}x$$
$$=\frac{\epsilon\tilde{N}_0 x_0^{-1-n}}{2\tilde{g}_0}\int_{x_0}^{\eta^{-1}}\frac{\psi(x)}{1-\psi(x)}E(x)\mathrm{d}x$$
$$=\frac{\epsilon\tilde{N}_0 x_0^{-n}}{2\tilde{g}_0}E(x_0). \qquad [46]$$

Hence, boundary condition (46) will be satisfied for scale-invariant solutions only when $\epsilon/2=1$. This requires an energetically impossible reproduction efficiency $\epsilon>1$. When natural mortality (μ_0) is taken into account, the value of the left-hand side in Eq. (46) would reduce further, requiring even larger values of ϵ. Perfect scale-invariant solutions are ecologically infeasible, so what happens instead?

Losses caused by reproduction efficiencies $\epsilon<2$ need to be compensated by accelerated growth or reduced mortality, that is, reduced physiological mortality over some phase of life history, typically in the immature phase. In the current model, specific physiological mortality before maturation depends only on body size, not on species identity. Therefore, if specific physiological mortality is reduced for one species over a given body-size range, so as to increase abundances by $2/\epsilon$ compared with the unmodified case, it will lead to an increase of abundances by $2/\epsilon$ for all other species covering this range too, effectively compensating their inefficiency in reproduction. Species covering a larger body-size range can therefore exploit conditions generated by other species contained within this range (this may be one of the reasons why large body-size ranges are encountered in nature).

The resulting picture for the case of fish is illustrated in Fig. 3: as hatchling size, m_0, is approximately the same for all fish (Cury and Pauly, 2000), independent of maturation size, specific physiological mortality will be reduced only within a size range covered by the smallest species. Larger species are affected only in early life history. For most fish species, setting $\epsilon=2$ and assuming the universal population structure given by Eq. (33) will therefore yield legitimate approximations of the true population structure, provided it can be shown that the effects of deviations from this structure at small body sizes are negligible.

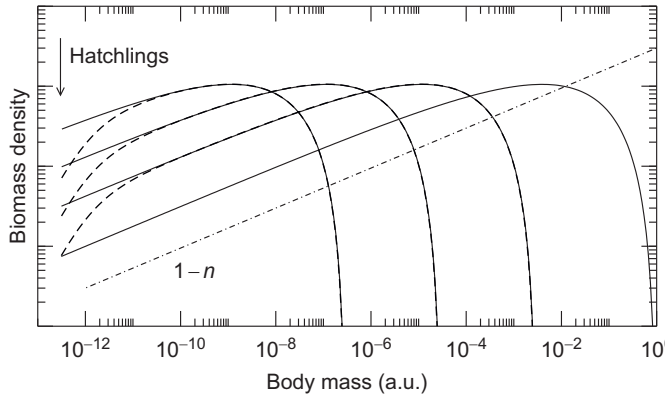

Figure 3 Schematic representation of intrapopulation size distributions. Body-mass ranges are exaggerated. Curves show the density of a population's biomass along the logarithmic size axis, given by $m^2 N_j(m)$ up to a constant factor. Solid lines correspond to scale-invariant distributions, which have a small-size tail scaling as m^{1-n} (dash-dotted line) by Eqs. (16), (34), and (37). Dashed lines represent conceivable corrections due to reproductive losses. Because juvenile specific physiological mortality, which controls the local slope of the curves, does not depend on species identity, corrections for all species occur in the same size range.

This picture explains the observed discrepancies between the simulation results of Hartvig et al. (2011) and their analytic equilibrium theory, which predicts another value for $\tilde{a}$. Specifically, the scenario sketched in Fig. 3 agrees with simulations by Hartvig et al. (2011) (i) in the predicted deformation of population structures for the smallest individuals, (ii) in its prediction for the scaling of offspring abundance with maturation size (corresponding to $\tilde{a} = 1$), (iii) in its prediction of power-law scaling of survival to a given size corresponding to $\tilde{a} = 1$, after a short phase of lower mortality. See Hartvig et al. (2011) for details.

Outside the range covered by fish, one can expect other regions on the logarithmic body-size axis where $\tilde{a}$ is depleted relative to 1, so as to compensate for inefficient reproduction of the species overlapping these regions, and values of $\tilde{a}$ near 1 in between. The locations and relative proportions of these regions on the body-size axis are currently unclear. On the condition that most species in a community cover wide ranges in body size, few regions of depleted $\tilde{a}$ will be necessary to compensate for $\epsilon < 2$, and these will, for most maturation size classes, fall outside their adult size ranges.

This completes the characterisation of the model's steady state. In what follows, the response of this steady state to perturbations will be evaluated in a linear approximation. To understand the impact of short regions

of depleted $\tilde{a}$ on the logarithmic body-size axis, some critical calculations below will be carried out along two tracks: first for the *general* case of arbitrary $\epsilon \leq 2$, $m_0(m_*)$ and resulting forms for $g(m, m_*)$, $\mu_p(m)$, and $N(m, m_*)$, taking the considerations above into account, and then for the *scale-invariant* case of $\epsilon = 2$, $m_0(m_*) \ll m_*$, with scale-invariant $N(m, m_*)$ and life-history parameters. It will be argued that, as far as regions of depleted specific physiological mortality fall outside the adult body-size ranges of species, the *scale-invariant* case is a reasonable approximation of the *general* case. To aid orientation of the reader, the terms *general* and *scale-invariant* are italicised in the subsequent Section 6 when used with these particular meanings. Later, an additional simplification $\mu_0 = 0$ is introduced for the *scale-invariant* case, which is then explicitly stated.

6. DERIVATION OF THE SPECIES SIZE-SPECTRUM MODEL

6.1. General framework

As an effective and accurate method to reduce models for the dynamics of interacting structured populations to models in which each population is described by a single variable only (e.g. population biomass), Rossberg and Farnsworth (2011) introduce the QNA. The QNA for a system of S structured populations, described by vectors $\boldsymbol{n}_j = \mathbf{n}_j(t)$ of abundances by stage ($1 \leq j \leq S$), satisfying $d\mathbf{n}_j/dt = \mathbf{A}_j(\mathbf{n}_1, \ldots, \mathbf{n}_S)\mathbf{n}_j$ with a density-dependent population matrix $\mathbf{A}_j(\mathbf{n}_1, \ldots, \mathbf{n}_S)$, can be carried out by following a simple recipe. (1) Obtain an approximate description of the community steady state and use it to construct for each species j an approximation of its steady-state population matrix $\underline{\mathbf{A}}_j$, that is, a constant matrix of transition rates between different population stages in the community steady state. Ensure that, because the system is in steady state and populations neither grow nor decay on average, all matrices $\underline{\mathbf{A}}_j$ have an eigenvalue zero. (2) Compute the eigenvector $\mathbf{w}_j$ and adjoint eigenvector $\mathbf{v}_j$ corresponding to eigenvalue zero for each $\underline{\mathbf{A}}_j$, choosing normalisations such that the equilibrium population structure $\mathbf{w}_j$ corresponds to a population of unit size (e.g. 1 kg of biomass), and that $\mathbf{v}_j^{\mathrm{T}}\mathbf{w}_j = 1$. (3) Approximate the dynamics of population sizes, defined by $B_j(t) = \mathbf{v}_j^{\mathrm{T}}\mathbf{n}_j(t)$, as $\mathrm{d}B_j/\mathrm{d}t = \mathbf{v}_j^{\mathrm{T}}\mathbf{A}(\mathbf{w}_1 B_1, \ldots, \mathbf{w}_S B_S)\mathbf{w}_j B_j$, which is an ordinary differential equation in the variables B_j. Using this result, approximate the full community dynamics as $\mathbf{n}_j(t) \approx \mathbf{w}_j B_j(t)$. The components of the vectors $\mathbf{v}_j$ are interpreted as the reproductive values of the corresponding population stage.

6.2. Operators and eigenfunctions

Applying the QNA to obtain a simplified description of the dynamics of the density of individuals, $N(m, m_*)$, requires adapting it to a continuum of life-history stages indexed by body mass m and a continuum of populations characterised by maturation size m_*. Functional analysis (Section 3) provides the necessary formal tools. The first step of the recipe (approximation of the steady state) has been completed in the Section 5. To obtain a description of dynamics in a form appropriate for the second step, the McKendrick–von Foerster Equation (15) is written as $\mathrm{d}N(m, m_*)/\mathrm{d}t = L_{m_*}N(m, m_*)$, where the linear operator L_{m_*}, parametrised by m_*, is modified such as to include the production of hatchlings explicitly:

$$L_{m_*}N(m, m_*) = -\frac{\partial}{\partial m}\Big[g(m, m_*)N(m, m_*)\Big] - \Big[\mu_p(m) + \mu_0 m_*^{n-1}\Big]N(m, m_*) + \delta(m - m_0)\frac{\epsilon}{2m_0}\int_0^\infty N(m', m_*)g_r(m', m_*)\mathrm{d}m'. \quad [47]$$

Here, m_0 is again understood to be a function of m_*. The boundary condition for $N(m, m_*)$ then becomes $N(m, m_*) = 0$ for any $m < m_0$. The facts that the last term correctly enforces the original boundary condition $g(m, m_*)$ $N(m, m_*) = R_{m_*}$ (with R_{m_*} given after obvious adjustments by Eq. (12)) is readily verified by integrating Eq. (47) over a small interval $[m_0 - \Delta m/2;$ $m_0 + \Delta m/2]$.

The *general* steady-state McKendrick-von Foerster operator $\underline{L}_{m_*}$ is obtained from L_{m_*} by replacing the functions $g(m, m_*)$, $g_r(m, m_*)$, and $\mu_\mathrm{p}(m)$ with the results $\underline{g}(m, m_*)$, $\underline{g}_r(m, m_*)$, and $\underline{\mu}(m)$ for a particular *general* steady-state community size spectrum $\mathcal{N}(m) = \underline{\mathcal{N}}(m)$. The null-eigenvectors required by the QNA, that is, the equilibrium population structures $W_{m*}(m)$ satisfying $\underline{L}_{m_*}W_{m_*}(m) = 0$, can be obtained as

$$W_{m_*}(m) = B_{m_*}^{-1}\underline{N}(m, m_*), \quad [48]$$

where $\underline{N}(m, m_*)$ is $N(m, m_*)$ evaluated at a *general* steady state (which may or may not be scale-invariant), and a normalisation to unit biomass (actually biomass density) is obtained by setting

$$B_{m_*} = \int_0^\infty m\underline{N}(m, m_*)dm. \quad [49]$$

As for the *scale-invariant* case in Section 5.5, this integral is dominated by adult individuals in the *general* case as well. Therefore, for maturation size classes m_* where the *general* population structures $\underline{N}(m, m_*)$ do not differ much from the *scale-invariant* case in the adult range of m, the *scale-invariant* form of W_{m_*} is a good approximation of *general* W_{m_*} in the adult range. In the *scale-invariant* case, W_{m_*} is obtained from Eqs. (48), (16), (49), and (40) as

$$W_{m_*}(m) = \begin{cases} m_*^{-2} \tilde{B}_{\text{tot}}^{-1} \tilde{N}(m/m_*) & \text{for } m \geq m_0 \\ 0 & \text{for } m < m_0, \end{cases} \quad [50]$$

with $\tilde{N}(m/m_*)$ given by Eq. (33) and $\tilde{B}_{\text{tot}}$ standing as shorthand for $\tilde{B}_{\text{tot}}(m_0/m_*)$.

For populations described by a finite number of stages (Section 6.1), the steady-state population matrices $\underline{\mathbf{A}}_j$ only have a finite number of eigenvalues. The eigenvalue 0, assumed to be the one with the largest real part and to have multiplicity one, is therefore always separated by a gap from the real parts of the other eigenvalues. This leads to a separation between the timescales of intra- and interspecific population dynamics that is exploited in the QNA. However, when populations are described by a continuum of life-history stages, as is the case here, the corresponding linear operator $\underline{L}_{m_*}$ has an infinite number of eigenvalues. Thus, the existence of a spectral gap between 0 and the other eigenvalues is not guaranteed. In Appendix, the spectrum of operator $\underline{L}_{m_*}$ is studied for a numerical example of the *scale-invariant* case. It is concluded that indeed 0 is the unique eigenvalue of $\underline{L}_{m_*}$ with largest real part, and that all other eigenvalues have real parts smaller than $-1 \times$ (mortality of the largest individuals of the population). These observations can plausibly be expected to generalise to the *general* class of operators $\underline{L}_{m_*}$ considered here, so the eigenvalue zero will be separated from the subdominant eigenvalues by a gap of size $\underline{\mu}(m_*/\eta) + \mu_0 m_*^{n-1}$. The resulting separation of timescales is estimated in Section 9.5.

To obtain the adjoint eigenvectors (here eigenfunctions), the adjoint linear operator $\underline{L}_{m_*}^+$ of $\underline{L}_{m_*}$ needs to be computed. Application of the method described in Section 3 yields

$$\underline{L}_{m_*}^+ V(m) = \underline{g}(m, m_*) \frac{\partial V(m)}{\partial m} - \left[\underline{\mu}(m) + \mu_0 m_*^{n-1}\right] V(m) + \underline{g}_r(m, m_*) \frac{\epsilon V(m_0)}{2m_0}. \quad [51]$$

Following the general prescription (Section 6.1), the reproductive value of an individual of size m and maturation size m_* is given by the solution $V_{m_*}(m)$ of $\underline{L}^+_{m_*} V(m) = 0$, subject to the normalisation condition $\langle V_{m_*} | W_{m_*} \rangle = 1$. As, for any species of maturation size class m_*, the equilibrium density of individuals along the m axis for a population of unit biomass is given by $W_{m_*}(m)$, the equilibrium density of reproductive value for a unit population along the m axis is given by the product $V_{m_*}(m) W_{m_*}(m)$. Multiplying this with the equilibrium growth rate, $\underline{g}(m, m_*)$ gives the equilibrium flow of reproductive value along the size axis for a unit population, $\underline{J}_{m_*}(m) \stackrel{\text{def}}{=} \underline{g}(m, m_*) V_{m_*}(m) W_{m_*}(m)$. It is readily verified using $L_{m_*} W_{m_*} = L^+_{m_*} V_{m_*} = 0$ and Eqs. (47) and (51) that for $m > m_0$

$$\frac{\mathrm{d}\underline{J}_{m_*}}{\mathrm{d}m} = \frac{\mathrm{d}}{\mathrm{d}m}\left[\underline{g}(m, m_*) V_{m_*}(m) W_{m_*}(m)\right] = -\frac{\epsilon V_{m_*}(m_0)}{2m_0} \underline{g}_r(m, m_*) W_{m_*}(m). \quad [52]$$

That is, until maturation $\underline{J}_{m_*}(m)$ is constant and then it declines. Obviously, $\underline{J}_{m_*}(m) = 0$ for $m < m_0$ and $m \geq m_*/\eta$. Therefore, one can compute *general* reproductive values from a given *general* population structure $W_{m_*}(m)$ by integrating Eq. (52) as

$$V_{m_*}(m) = \frac{1}{C_{m_*} \underline{g}(m, m_*) W_{m_*}(m)} \int_m^{m_*/\eta} \underline{g}_r(m', m_*) W_{m_*}(m') \mathrm{d}m', \quad [53]$$

where the correct normalisation $\langle V_{m_*} | W_{m_*} \rangle = 1$ is assured by setting

$$\frac{2m_0}{\epsilon V_{m_*}(m_0)} = C_{m_*} = \int_{m_0}^{m_*/\eta} \frac{1}{\underline{g}(m, m_*)} \int_m^{m_*/\eta} \underline{g}_r(m', m_*) W_{m_*}(m') \mathrm{d}m' \mathrm{d}m. \quad [54]$$

An important observation now is that, because $\underline{g}(m, m_*)$ scales as m^n with $n < 1$ for $m \ll m_*$, and $\underline{g}_r(m, m_*)$ is localised near m_*, the integral over m in Eq. (54) is dominated by contributions from large m. The value of C_{m_*} therefore depends only on $W_{m_*}(m)$ and the size spectrum near m_*, and these will often be well approximated by the *scale-invariant* forms.

If natural mortality (μ_0) is negligible in the *scale-invariant* case, Eq. (53) evaluates by manipulations similar to Eq. (45) to the simple form

$$V_{m_*}(m) = m. \quad [55]$$

In this approximation, reproductive value therefore exactly equals body mass. This result is most easily verified by directly confirming $\underline{L}^{+}_{m_*} V(m) = 0$ and $\langle V_{m_*} | W_{m_*} \rangle = 1$. The simplicity of this result allows carrying out the QNA analytically, which is done in the next section.

A generalisation of Eq. (55) to the case with natural mortality gives an enhancement of reproductive value by an amount of the order of magnitude $m\mu_0 / \tilde{g}_0$ for old individuals, and a corresponding proportional reduction for all others. As this does not much affect the overall structure of $V_{m_*}(m)$, natural mortality is not considered further in detail below.

6.3. Reduced dynamics

Following the recipe of the QNA, define a reduced description $B(m_*)$ of the community state as

$$B(m_*) = \left\langle V_{m_*} | N(\cdot, m_*) \right\rangle = \int_0^\infty V_{m_*}(m) N(m, m_*) \mathrm{d}m \qquad [56]$$

for an arbitrary, time-dependent distribution of individuals $N(m, m_*)$. In the approximation that reproductive value equals body mass, the function $B(m_*)$ approximates the time-dependent distribution of biomass over maturation body sizes. To the accuracy of the QNA, the dynamics of $B(m_*)$ follow

$$\begin{aligned} \frac{1}{B(m_*)} \frac{\partial B(m_*)}{\partial t} &= \left\langle V_{m_*} | L_{m_*} W_{m_*} \right\rangle \\ &= \int_0^\infty V_{m_*}(m) \left\{ -\frac{\partial}{\partial m} \left[g(m, m_*) W_{m_*}(m) \right] - \left[\mu_\mathrm{p}(m) + \mu_0 m_*^{n-1} \right] W_{m_*}(m) \right\} \mathrm{d}m, \\ &\quad + \frac{\epsilon V_{m_*}(m_0)}{2 m_0} \int_0^\infty W_{m_*}(m) g_r(m, m_*) \mathrm{d}m \end{aligned} \qquad [57]$$

where $g(m, m_*), g_r(m, m_*)$, and $\mu_\mathrm{p}(m)$ are evaluated for a variable size spectrum given by

$$\mathcal{N}(m) = \int_0^\infty B(m_*) W_{m_*}(m) \mathrm{d}m_*. \qquad [58]$$

By Eq. (57), one can read $\langle V_{m_*} | L_{m_*} W_{m_*} \rangle$ as the momentary growth rate of biomass in maturation size class m_*.

In the *scale-invariant* case without natural mortality ($\mu_0 = 0$), the simple results (50) and (55) for the null-eigenfunctions hold and the right-hand side of Eq. (57) simplifies through integration by parts to

$$\left\langle V_{m_*}|L_{m_*}W_{m_*}\right\rangle = \int_{m_0}^{\infty}\left[g(m,m_*)+g_r(m,m_*)-m\mu_{\mathrm{p}}(m)\right]\frac{\tilde{N}(m/m_*)}{m_*^2\tilde{B}_{\mathrm{tot}}}\mathrm{d}m$$
$$= \int_{m_0}^{\infty}\left[(\alpha f(m)h-k)m^n-m\mu_{\mathrm{p}}(m)\right]\frac{\tilde{N}(m/m_*)}{m_*^2\tilde{B}_{\mathrm{tot}}}\mathrm{d}m. \qquad [59]$$

The second step implies that the density-dependencies of investments into somatic and reproductive growth are here equivalent in their population-dynamic effects. This is remarkable when recalling that the causal chains through which these effects are achieved are fundamentally different.

Careful inspection reveals that Eq. (59) holds to a good degree also in the *general* case. To see this, observe first that, using $\underline{L}^+_{m_*}V_{m_*}(m)=0$, Eqs. (51), and (54),

$$\frac{\partial V_{m_*}(m)}{\partial m} = V_{m_*}(m)\left[\frac{\underline{a}(m,m_*)}{m}-\frac{\underline{g}_r(m,m_*)}{C_{m_*}\underline{g}(m,m_*)V_{m_*}(m)}\right], \qquad [60]$$

where $\underline{a}(m,m_*)\overset{\mathrm{def}}{=}m\left[\underline{\mu}_{\mathrm{p}}(m)+\mu_0 m_*^{n-1}\right]/\underline{g}(m,m_*)$ is the steady-state specific physiological mortality. Then integrate the somatic growth term in Eq. (57) by parts, eliminate $\partial V_{m_*}/\partial m$ through Eq. (60), and, finally, eliminate ϵ using Eq. (54), to obtain

$$\left\langle V_{m_*}|L_{m_*}W_{m_*}\right\rangle = \int_0^{\infty} g(m,m_*)V_{m_*}(m)W_{m_*}(m)\frac{\underline{a}(m,m_*)-a(m,m_*)}{m}\mathrm{d}m$$
$$+\int_0^{\infty}\frac{W_{m_*}(m)}{C_{m_*}}\left[\frac{g_r(m,m_*)\underline{g}(m,m_*)-\underline{g}_r(m,m_*)g(m,m_*)}{\underline{g}(m,m_*)}\right]\mathrm{d}m$$
$$= \int_0^{\infty} g(m,m_*)V_{m_*}(m)W_{m_*}(m)\frac{\underline{a}(m,m_*)-a(m,m_*)}{m}\mathrm{d}m$$
$$= \int_0^{\infty}\underline{J}_{m_*}(m)\frac{\underline{a}(m,m_*)-a(m,m_*)}{m}\mathrm{d}m+\mathrm{h.o.t.} \qquad [61]$$

with $a(m,m_*)\overset{\mathrm{def}}{=}m\left[\mu_{\mathrm{p}}(m)+\mu_0 m_*^{n-1}\right]/g(m,m_*)$. In the second step the second integral vanishes because the term in brackets becomes zero when inserting the definitions of $g(m,m_*)$ and $g_r(m,m_*)$ from Eqs. (23) and (24). Below, only effects linear in deviations of growth, reproduction and mortality from the steady-state rates will be investigated, and to linear

order one can substitute $g(m, m_*)$ by $\underline{g}(m, m_*)$ in the remaining integral, so $g(m, m_*) V_{m_*}(m) W_{m_*}(m)$ reduces to $\underline{J}_{m_*}(m)$ in the last line, up to higher-order contributions indicated by h.o.t.

Denote by $\underline{B}(m_*)$ the equilibrium values of the reduced dynamic variables $B(m_*)$ defined in Eq. (56). To investigate the community response to perturbations of this equilibrium state, the linearization of $\langle V_{m_*} | L_{m_*} W_{m_*} \rangle$ for small deviations $\Delta B(m_*) = B(m_*) - \underline{B}(m_*)$ from this state is now constructed. Specifically, an integral kernel $K(m_*, m'_*)$ is sought such that

$$\left\langle V_{m_*} | L_{m_*} W_{m_*} \right\rangle = \int_0^\infty K(m_*, m'_*) \Delta B(m'_*) \mathrm{d}m'_* + \text{h.o.t.}, \qquad [62]$$

with h.o.t. denoting higher-order terms in ΔB. As $\langle V_{m_*} | L_{m_*} W_{m_*} \rangle$ depends on $B(m_*)$ only through the size spectrum $\mathcal{N}(m)$, the chain rule for functional derivatives can be applied before using Eqs. (58) and (61) to obtain

$$\begin{aligned} K\left(m_*, m'_*\right) &= \frac{\delta \left\langle V_{m_*} | L_{m_*} W_{m_*} \right\rangle}{\delta B(m'_*)} \\ &= \int_0^\infty \frac{\delta \left\langle V_{m_*} | L_{m_*} W_{m_*} \right\rangle}{\delta \mathcal{N}(m')} \frac{\delta \mathcal{N}(m')}{\delta B(m'_*)} \mathrm{d}m' \\ &= \int_0^\infty \int_0^\infty \frac{\underline{J}_{m_*}(m)}{m} \frac{\delta a(m, m_*)}{\delta \mathcal{N}(m')} W_{m'_*}(m') \mathrm{d}m \mathrm{d}m' \\ &= \int_0^\infty \int_0^\infty \frac{\underline{J}_{m_*}(m)}{m\left[1 - \psi\left(m/m_*\right)\right]} \frac{\delta\left[1 - \psi\left(m/m_*\right)\right] a\left(m, m_*\right)}{\delta \mathcal{N}(m')} W_{m'_*}(m') \mathrm{d}m' \mathrm{d}m. \end{aligned} \qquad [63]$$

This expression needs to be evaluated at the equilibrium state. By multiplying $a(m, m_*)$ with $[1 - \psi(m/m_*)]$ in the last step, a divergence of $a(m, m_*)$ at the size of the largest adults caused by cessation of growth, Eq. (24), is suppressed. This effectively removes the distinction between somatic and reproductive growth. The division by $[1 - \psi(m/m_*)]$ in the first factor of the integrand cancels with a corresponding factor entering $\underline{J}_{m_*}(m) = \underline{g}(m, m_*) V_{m_*}(m) W_{m_*}(m)$ through $\underline{g}(m, m_*)$ and, therefore, does not cause a divergence for large adults. Equations (57), (62), and (63) together specify the QNA for the *general* case.

To understand to what extent deviations from scale-invariance affect Eq. (63), it is useful to investigate how the value of the integrand scales for small m and m' while $m > m_0(m_*)$, $m' > m_0(m'_*)$. As $\underline{J}_{m_*}(m)$ is constant for

small m, the first factor scales as m^{-1}. The second factor describes the dependence of the specific physiological mortality of individuals of size m on the density of individuals of size m'. The body-size ratios of interacting individuals are constrained by the predator–prey size-ratio window $s(x)$. The second factor will therefore be significantly different from zero only when m and m' are of roughly similar magnitude. For such a situation, the functional derivative operator $\delta/\delta\mathcal{N}(m')$ shows the same scaling behaviour as $\delta(m-m')/\mathcal{N}(m')$, with $\delta(m-m')$ denoting Dirac's delta functional (as can be verified by evaluating the derivative). The operand $[1-\psi(m/m_*)]a(m,m_*)$ will be of the order of magnitude of one, even in the *general* case. In the *scale-invariant* case, the last factor grows for small m' as $(m')^{-n-1}$ by Eqs. (50), (34), and (37). In the *general* case, it may grow slower to accommodate inefficient reproduction (Section 5.7), but it will never grow faster. After performing the integration over m', the integrand does therefore not increase faster than $m^{-1}\times m^{\lambda}\times m^{-n-1}=m^{\lambda-n-2}$ for small m. Small m dominates the integral if the integrand increases faster than m^{-1}, implying that $\lambda<1+n$. This is unlikely to be the case, because it violates a condition for the existence of a *scale-invariant* steady state (Section 5.4). Therefore, the integrand is generally dominated by contributions where m and m' are of similar order of magnitude as m'_*.

These considerations have two important implications. As explained in Section 6.2, *general* $J_{\bar{m}_*}(m)$ and $W_{m_*}(m)$ can be approximated by their *scale-invariant* forms in the adult range, at least as long as m_* is not in a size range of depleted specific physiological mortality. Further, $J_{\bar{m}_*}(m)$ attains in the juvenile range a constant value that depends only on the life-history parameter in the adult range. The first implication is therefore that, except for cases where m_* or m'_* are in or near one of the regions of depleted specific physiological mortality described in Section 5.7, the right-hand side of (63) can be approximated by the corresponding *scale-invariant* form. Because contributions from small m and m' do not dominate the integral, a second consequence is that the mathematical limit $m_0(m_*), m_0(m'_*)\to 0$ of infinitely small offspring is regular and approximates the case of general but small $m_0(m_*)/m_*$. The calculations are therefore continued from here on using the simplifying approximations of *scale-invariant* population structures with $m_0(m_*)\to 0$ for any m_*. To simplify matters further, natural mortality is not taken into consideration ($\mu_0=0$), as it has only minor effects on dynamics (see also Hartvig et al., 2011).

Therefore, starting from Eq. (59) and making use of Eq. (50) for *scale-invariant* population structures,

$$\begin{aligned} K\left(m_*, m'_*\right) &= \frac{\delta\left\langle V_{m_*} | L_{m_*} W_{m_*}\right\rangle}{\delta B\left(m'_*\right)} \\ &= \int_0^\infty \frac{\delta\left\langle V_{m_*} | L_{m_*} W_{m_*}\right\rangle}{\delta \mathcal{N}(m')} \frac{\delta \mathcal{N}(m')}{\delta B\left(m'_*\right)} \mathrm{d}m' \\ &= \int_0^\infty \left\{ \int_0^\infty \left[\alpha h m^n \frac{\delta f(m)}{\delta \mathcal{N}(m')} - m \frac{\delta \mu_\mathrm{p}(m)}{\delta \mathcal{N}(m')} \right] \frac{\tilde{N}\left(m/m_*\right)}{m_*^2 \tilde{B}_\mathrm{tot}} \mathrm{d}m \right\} \frac{\tilde{N}\left(m'/m'_*\right)}{m_*'^2 \tilde{B}_\mathrm{tot}} \mathrm{d}m'. \end{aligned} \quad [64]$$

The functional derivatives of $f(m)$ and $\mu_\mathrm{p}(m)$ can be evaluated based on results of Section 5.2. For the eutrophic regime, one obtains

$$\frac{\delta f(m)}{\delta \mathcal{N}(m')} = \frac{h}{\gamma \tilde{\phi}^2} m' m^{2\lambda+n-q-4} s\left(\ln \frac{m}{m'}\right) \quad [65]$$

and

$$\frac{\delta \mu_\mathrm{p}(m)}{\delta \mathcal{N}(m')} = \frac{h}{\tilde{\phi}} \left[s\left(\ln \frac{m'}{m}\right) - \frac{1}{I_1} \Sigma\left(\ln \frac{m'}{m}, \lambda - 4 + n\right) \right] m'^{\lambda+n-2}, \quad [66]$$

using $I_1 = \hat{s}(i(\lambda - 2))$ as above and the abbreviation

$$\begin{aligned} \Sigma(\gamma, c) &= \int_0^\infty x^c s(\ln x) s(\gamma + \ln x) \mathrm{d}x \\ &= \int_{-\infty}^\infty \mathrm{e}^{(c+1)u} s(u) s(\gamma + u) \mathrm{d}u. \end{aligned} \quad [67]$$

In Eq. (66), the first term in brackets describes direct predation mortality, the second term a release from predation pressure in the presence of other prey of similar size. It follows from the condition $\gamma m^{2+q-\lambda} \tilde{\phi} \gg h m^n$, which defines the eutrophic regime, that the functional derivative of $f(m')$ in Eq. (64) will generally be negligible compared with that of $\mu_\mathrm{p}(m')$. It is discarded hereafter.

In the oligotrophic regime,

$$\frac{\delta f(m)}{\delta \mathcal{N}(m')} = \frac{\gamma h}{\left(\gamma \tilde{\phi} + h\right)^2} m' m^{q-n} s\left(\ln \frac{m}{m'}\right) \quad [68]$$

and, using Eq. (38),

$$\frac{\delta\mu_\mathrm{p}(m)}{\delta\mathcal{N}(m')}=\frac{\gamma h}{\gamma\tilde{\phi}+h}\left[s\left(\ln\frac{m'}{m}\right)-\frac{k}{h(\alpha I_1-I_2)}\Sigma\left(\ln\frac{m'}{m},q-2\right)\right]m'^q. \qquad [69]$$

To simplify Eq. (64), define first the individual-level interaction kernel

$$\kappa_0\left(\ln\frac{m}{m'}\right)=\frac{m'^{-\lambda-n+2}}{m}\left[\alpha h m^n\frac{\delta f(m)}{\delta\mathcal{N}(m')}-m\frac{\delta\mu_\mathrm{p}(m)}{\delta\mathcal{N}(m')}\right]. \qquad [70]$$

It follows from Eqs. (66) to (69) that the right-hand side of Eq. (70) does indeed depend only on the ratio m/m'. Further, let

$$\tilde{\beta}(w)=\tilde{B}_\mathrm{tot}^{-1}\mathrm{e}^{2w}\tilde{N}(\mathrm{e}^w) \qquad [71]$$

describe the scale-free distribution of a species' biomass over the logarithmic body mass axis for $m_0, x_0\to 0$, normalised to $\int_{-\infty}^{\infty}\tilde{\beta}(w)\mathrm{d}w=1$. Equation (64) can then be rewritten in terms of convolution integrals by performing the substitutions $m=\mathrm{e}^{-w}m_*$ and $m'=\mathrm{e}^{-v}m_*$, which yield, after some calculation,

$$\begin{aligned}K\left(m_*,m'_*\right)&=m_*^{-\nu}\int_{-\infty}^{\infty}\int_{-\infty}^{\infty}\mathrm{e}^{\nu v}\kappa_0(v-w)\tilde{\beta}(-w)\tilde{\beta}\left(-v+\ln\frac{m_*}{m'_*}\right)\mathrm{d}w\,\mathrm{d}v\\&=m_*^{-\nu}\left[\kappa*\tilde{\beta}\right]\left(\ln\frac{m_*}{m'_*}\right),\end{aligned} \qquad [72]$$

with the abbreviations $\nu=3-\lambda-n$ and

$$\kappa(v)=\mathrm{e}^{\nu v}\left[\kappa_0*\tilde{\beta}^-\right](v), \qquad [73]$$

where $\tilde{\beta}^-(v)\overset{\mathrm{def}}{=}\tilde{\beta}(-v)$.

In order to fully go over to logarithmic scales, introduce the scale-invariant interaction kernel

$$\tilde{K}(w)=\tilde{B}_\mathrm{tot}\left[\kappa*\tilde{\beta}\right](w), \qquad [74]$$

and a logarithmic mass axis $u=\ln(m_*/M)$, where M denotes a unit mass (e.g. $M=1\,\mathrm{g}$). Deviations $b(u)$ of the distribution of biomass on the u-axis from the power-law steady state are given by

$$b(u)=Me^u\Delta B(Me^u). \qquad [75]$$

The density-dependent growth rate, given by Eq. (62), then becomes, up to higher-order terms,

$$\begin{aligned}\left\langle V_{m_*} | L_{m_*} W_{m_*} \right\rangle &= \tilde{B}_{\text{tot}}^{-1} m_*^{-\nu} \left[\tilde{K} * b\right] \left(\ln \frac{m_*}{M}\right) \\ &= \frac{m_*^{n-2}}{B_{\text{tot}}(m_*)} \left[\tilde{K} * b\right] \left(\ln \frac{m_*}{M}\right),\end{aligned} \tag{76}$$

where Eq. (40) was applied in the second step.

The response of size spectra to external perturbations is of great practical interest: here, we concentrate on the effects of fishing. Assume a size-selective fishing regime that enhances mortality of individuals by up to F over a range centred at m_{F} with logarithmic width σ_{F}; that is, next to predation and natural mortality, there is additional mortality $\mu_{\text{F}}(m) = F W_{\sigma_{\text{F}}}(\ln m/m_{\text{F}})$ with the Gaussian window $W_{\sigma_{\text{F}}}(x)$ defined in Section 3. Putting this into Eq. (57) and using Eqs. (50) and (71) leads, in the limit $m_0 \to 0$, in addition to natural community dynamics, to a pressure on populations with maturation size m_*, corresponding to a rate of decline (dimension 1/Time):

$$\begin{aligned}\int_0^\infty m \mu_{\text{F}}(m) W_{m_*}(m) \mathrm{d}m &= F \int_{-\infty}^{\infty} W_{\sigma_{\text{F}}}\left(u + \ln \frac{m_*}{m_{\text{F}}}\right) \tilde{\beta}(u) \mathrm{d}u \\ &= F \int_{-\infty}^{\infty} W_{\sigma_{\text{F}}}\left(-u + \ln \frac{m_*}{m_{\text{F}}}\right) \tilde{\beta}^-(u) \mathrm{d}u \\ &= F \left[W_{\sigma_{\text{F}}} * \tilde{\beta}^-\right] \left(\ln \frac{m_*}{m_{\text{F}}}\right).\end{aligned} \tag{77}$$

One can then, by applying Eqs. (76), (75), and $B(m_*) = \Delta B(m_*) + B_{\text{tot}}(m_*)$ to Eq. (57) and including of the effect of fishing, Eq. (77), express system dynamics in response to fishing pressure that sets in at $t = 0$ by the integro-differential equation

$$\frac{\partial b(u)}{\partial t} = (M \mathrm{e}^u)^{n-1} \left[\tilde{K} * b\right](u) - (M \mathrm{e}^u)^{2-\lambda} \Phi(u) \Theta(t), \tag{78}$$

where

$$\Phi(u) = \tilde{B}_{\text{tot}} F \left[W_{\sigma_{\text{F}}} * \tilde{\beta}^-\right] \left(u - \ln \frac{m_{\text{F}}}{M}\right) \tag{79}$$

describes the fishing pressure, and $\Theta(t)$ denotes the unit step function: $\Theta(t)=0$ for $t<0$ and $\Theta(t)=1$ for $t\geq 1$. If fishing was specific to the maturation size of species rather than to the size of individuals, Eqs. (79) would be modified to

$$\Phi(u) = \tilde{B}_{\text{tot}} F W_{\sigma_F}\left(u - \ln\frac{m_F}{M}\right). \qquad [80]$$

Equation (78) represents the Species Size-Spectrum Model. It describes the dynamics of deviations of the size spectrum from the steady state in the linearised QNA. Linearised versions of other size-spectrum models proposed in the literature would assume similar forms. The main difference between these models lies in the interaction kernels they contain. In practice, the interaction kernel derived here, $\tilde{K}(w) = \tilde{B}_{\text{tot}}\left[\kappa * \tilde{\beta}\right](w)$, is best evaluated via its Fourier transform

$$\hat{K}(\xi) = \tilde{B}_{\text{tot}}\hat{\kappa}(\xi)\hat{\beta}(\xi) = \tilde{B}_{\text{tot}}\hat{\kappa}_0(\xi+\nu i)\hat{\beta}(-\xi-\nu i)\hat{\beta}(\xi), \qquad [81]$$

which follows from Eqs. (73) and (74) and some manipulations of convolution integrals.

Making use of Eq. (70), the preceding explicit formulae (65) to (69) for the functional derivatives, and the observation that the Fourier transform of $\Sigma(\gamma, c)$ with respect to γ is

$$\hat{\Sigma}(\xi, c) = \hat{s}(-\xi + (c+1)i)\hat{s}(\xi) \qquad [82]$$

give the Fourier transform of the individual-level interaction kernel

$$\hat{\kappa}_0(\xi) = \frac{h}{\tilde{\phi}}\left[-[\hat{s}(\xi^*)]^* + \frac{\hat{s}(\xi-\nu i)[\hat{s}(\xi^*)]^*}{\hat{s}((\lambda-2)i)}\right] \qquad [83]$$

in the eutrophic regime and

$$\begin{aligned}\hat{\kappa}_0(\xi) = {} & \frac{\alpha h^2\gamma}{(\gamma\tilde{\phi}+h)^2}\hat{s}(\xi-\nu i) - \frac{\gamma h}{\gamma\tilde{\phi}+h}[\hat{s}(\xi^*)]^* \\ & + \frac{\gamma^2\tilde{N}h}{(\gamma\tilde{\phi}+h)^2}\hat{s}(\xi-\nu i)[\hat{s}(\xi^*)]^*\end{aligned} \qquad [84]$$

in the oligotrophic regime. The last expression can be brought into alternative forms by using the identity

$$\frac{\gamma\tilde{\mathcal{N}}}{\gamma\tilde{\phi}+h} = \frac{k}{h(\alpha I_1 - I_2)}, \qquad [85]$$

which follows from results in Section 5.

6.4. Food-web effects

Simulations show that Eq. (78) with the kernel given by (74) is structurally unstable, as indicated in Section 5.1. As a result of combining coarse graining with the mean-field approximation, the equation effectively describes competition among a continuum of species along the species-size axis. This destabilises the system by mechanisms similar to those involved in the scenarios described by Pigolotti et al. (2007), leading ultimately to a breakup of the continuum into a set of distinct species (isolated spikes on the size axis). In real communities, this distinct set of species is already established and, as a result, dynamics will be modified. Deriving these modifications of dynamics from first principles would require a better understanding of food-web structure and dynamics than we currently have. But the following heuristic arguments suggest the general pattern that can be expected.

Consider perturbations of $b(u)$ of the form $\imath \sin(\xi u + \psi)$ with small amplitude $\imath$ and arbitrary phase ψ. For species *randomly* distributed along the u-axis and sufficiently small wavelengths $2\pi/\xi$, the perturbations received by each species become uncorrelated. Such short-wavelength perturbations of the size spectrum are therefore effectively equivalent to random perturbations with a distribution independent of the wave number ξ and, relative to species biomass, independent and identical among species. The relaxation of the system from such perturbations to the equilibrium state (or the attractor) can be expected to be rather complicated in detail and involves a range of timescales (Rossberg and Farnsworth, 2011), but, as a simple model, linear relaxation at a constant rate proportional with m_*^n and independent of ξ (if large enough) should provide an appropriate picture. Unfortunately, these heuristic considerations do not provide a value for the relaxation rate, except for the general principle that rates become larger for larger $\tilde{B}_{\mathrm{tot}}$. Because the community effect of perturbations of food-web nodes is typically diffuse (Yodzis, 1998) and decays swiftly with the degree of separation from the perturbed node (Berlowa et al., 2009), a periodic perturbation has effectively a random effect when the wavelength $2\pi/\xi$ is small compared to the typical distance in u among the main prey and predators of a species. As wavelengths become larger—and wave numbers ξ smaller—these food-web effects will gradually subside. Food-web effects might therefore be modelled by adding a correction of the form $-r\tilde{B}_{\mathrm{tot}}\left[1 - \exp(-\sigma_r^2\xi^2/2)\right]$ to the Fourier transform of the interaction kernel $\hat{K}(\xi)$. The constant σ_r controls the cut-off-wavelength for food-web effects. The relaxation-rate constant r has the same dimensions as the search-rate coefficient γ, and it may therefore be assumed to be of comparable magnitude, presumably somewhat smaller (Rossberg and Farnsworth, 2011).

Back-transforming, this leads to a corrected interaction kernel

$$\tilde{K}(w) = \tilde{B}_{\text{tot}}\left\{\left[\kappa * \tilde{\beta}\right](w) + X(w)\right\} \qquad [86]$$

with food-web effects being given by

$$X(w) = -r\left[\frac{1}{\sqrt{2\pi}\sigma_r}\exp\left(-\frac{w^2}{2\sigma_r^2}\right) - \delta(w)\right]. \qquad [87]$$

7. SOLUTION OF THE SPECIES SIZE-SPECTRUM MODEL

The factor $(Me^u)^{n-1}$ in Eq. (78) expresses the slowing-down of effective ecological activity of larger species attributable to allometric scaling of metabolic rates. This factor makes the solution of Eq. (78), either numerically or analytically, difficult. Datta et al. (2010) and Capitán and Delius (2010) avoided this problem by imposing conditions equivalent to $n=1$, i.e. absence of allometric scaling of metabolism. Three analytical approaches that do not require this constraint will be explored here.

7.1. Approximation for times shortly after onset of fishing

For the time before the onset of fishing, assume an unperturbed power-law size spectrum, $b(u)=0$. Shortly after the onset at $t=0$, when $b(u)$ is still close to zero, the first term on the right-hand side of Eq. (78) will be small compared with the second term. Disregarding the first term, the solution of Eq. (78) can be approximated as $b(u) \approx -(Me^u)^{2-\lambda}\,\Phi(u)t$. This corresponds to a depletion of populations in response to fishing without consideration of density-dependent effects. Early density-dependent responses by prey and predators can be obtained by putting this first-order approximation into Eq. (78) and integrating in time, which leads to the second-order approximation

$$b(u) = -(Me^u)^{2-\lambda}\Phi(u)t - \frac{1}{2}M^{n+1-\lambda}e^{(n-1)u}\left\{\tilde{K}(u) * \left[e^{(2-\lambda)u}\Phi(u)\right]\right\}t^2 + \text{h.o.t.} \qquad [88]$$

Here, h.o.t. stands for higher-order terms in t, which could be computed by iterating this procedure. However, it is quite likely that a series expansion in t would not converge for any value of t. Inclusion of higher-order terms would then not generally improve the approximation. It is valid only

asymptotically, as $t \to 0$. To describe the system's long-term response to fishing, other approaches are required.

7.2. Tentative steady-state solution

An idea that comes to mind for understanding the long-term dynamics of Eq. (78) is to consider its steady-state ($\partial b/\partial t = 0$). A formal steady-state solution $b(u) = b_0(u)$ is easily derived. Dividing the right-hand side of Eq. (78) by $(Me^u)^{n-1}$ and Fourier transforming, it becomes

$$0 = \hat{K}(\xi)\hat{b}_0(\xi) - M^v\hat{\Phi}(\xi + v\mathrm{i}), \qquad [89]$$

with $\hat{K}(\xi)$ denoting the Fourier transform of $\tilde{K}(u)$ and $\hat{\Phi}(\xi) = \tilde{B}_{\mathrm{tot}} F \hat{W}_{\sigma_F}(\xi)\hat{\beta}(-\xi)\exp\left(-\mathrm{i}\xi \ln\frac{m_F}{M}\right)$ the Fourier transform of $\Phi(u)$. As $\hat{K}(\xi)$ generally has no zeros on the real ξ axis, we can solve for

$$\hat{b}_0(\xi) = \frac{M^v\hat{\Phi}(\xi + v\mathrm{i})}{\hat{K}(\xi)}, \qquad [90]$$

from which $b_0(u)$ is obtained by back-transforming. However, care must be taken, because not all steady-state solutions $b(u)$ necessarily have a Fourier transform. To understand why, the analytic properties of $\hat{K}(\xi)$ need to be discussed.

7.3. The roles of complex poles and zeros of $\hat{K}(\xi)$

Consider, for some complex $\xi \in \mathbb{C}$, the convolution integral

$$\tilde{K}(u) * e^{i\xi u} = \int_{-\infty}^{\infty} \tilde{K}(v) e^{i(u-v)\xi} dv = e^{iu\xi} \int_{-\infty}^{\infty} \tilde{K}(v) e^{-i\xi v} dv. \qquad [91]$$

The integral exists if and essentially only if $\left|\tilde{K}(u)\right|$ decays faster than $|e^{i\xi u}| = e^{-u\,\mathrm{Im}\{\xi\}}$ as $u \to \pm\infty$, with $\pm$ given by the sign of $\mathrm{Im}\{\xi\}$. If the integral exists, it equals $e^{iu\xi}$ times the analytic continuation of the Fourier transform $\hat{K}(\xi)$ into the complex plane. The range of Im $\{\xi\}$ values over which Eq. (91) converges determines a stripe in the complex plane, parallel to and covering the real axis. Typically, as is the case here, the stripe is limited by poles of $\hat{K}(\xi)$, which correspond to exponentially decaying "tails" of $\tilde{K}(u)$ as $u \to \pm\infty$. To find these poles, recall that

$$\hat{K}(\xi) = \tilde{B}_{\mathrm{tot}}\hat{\kappa}_0(\xi + v\mathrm{i})\hat{\beta}(-\xi - v\mathrm{i})\hat{\beta}(\xi) - r\tilde{B}_{\mathrm{tot}}\left[1 - \exp\left(-\sigma_r^2\xi^2/2\right)\right], \qquad [92]$$

and that $\hat{\beta}(\xi)$ has a pole at $\xi = -(1-n)i$ because of the hatchling tail of $\tilde{N}(x)$, Eq. (34), and possibly more poles farther from the real axis. This is the only source of poles of $\hat{K}(\xi)$. The Fourier transform $\hat{k}_0(\xi)$ of $k_0(w)$ is an entire function by Eqs. (83) and (84) and the assumption that $\hat{s}(\xi)$ is an entire function. In the oligotrophic regime $\hat{K}(\xi)$ therefore has poles at $\xi = -(1-n)i$ and $\xi = (q-n)i$, corresponding to decays of $\tilde{K}(u)$ as $e^{(1-n)u}$ for $u \to -\infty$ and as $e^{-(q-n)u}$ for $u \to +\infty$, and these two poles generally limit the range over which the integral (91) exists. In the eutrophic regime the pole $\xi = (1-n-\nu)i$ of $\hat{\beta}(-\xi - \nu i)$ coincides with a zero of $\hat{k}_0(\xi + \nu i)$ by Eq. (83), eliminating the corresponding pole of $\hat{K}(\xi)$, but other poles of $\hat{\beta}(-\xi - \nu i)$ may persist. Denote by Ξ the maximal (open) stripe in the complex plane parallel to the real axis for which $\hat{K}(\xi)$ is analytic ($\Xi = \{\xi : -(1-n) < \mathrm{Im}\{\xi\} < q-n\}$ in the oligotrophic regime).

Now, if $\xi_0 \in \Xi$ is a complex zero of $\hat{K}(\xi)$, and A_0 is any complex number, then with every solution $b_0(u)$ of Eq. (78), $b(u) = b_0(u) + A_0 \exp(i\xi_0 u)$ is, by Eq. (91), a solution of Eq. (78), too. Such additional exponential terms do not have finite Fourier integrals for any ξ and therefore cannot be found using Eq. (90). The correct choice of these corrections to the Fourier transform solution $b_0(u)$ of (78) follows, as for corresponding problems in physics (Jackson, 1962), from causality considerations: the corrections should be added if localised perturbations trigger waves or fronts that increase in magnitude as they propagate towards $|u| \to \infty$. However, because of the factor $(Me^u)^{n-1}$ in Eq. (78), standard methods for deciding when to make these corrections cannot be applied directly. Instead, this problem will here be (partially) solved by first investigating explicitly time-dependent solutions of Eq. (78).

7.4. Analytic approximation of time-dependent size-spectrum dynamics

Above, it was explained how complex zeros of $\hat{K}(\xi)$ lead to complications when solving Eq. (78). The idea of the approach described in this section is that, under certain conditions, the dynamics of $b(u)$ can indeed be dominated by the effects of these zeros. For example, it is evident from Eq. (90) that the Fourier transform $\hat{b}_0(\xi)$ of the steady-state solution $b_0(u)$ derived there generally has poles wherever $\hat{K}(\xi)$ has zeros. These poles are likely to have strong effects when the inhomogeneity (the fishing term) in Eq. (78) is not too broadly spread out on the logarithmic species size axis, that is, if its Fourier transform is not too localised along the real ξ axis. Specifically, the spread σ_F should be smaller than the typical logarithmic predator–prey

size ratio, that is, fishing should not target more than about two trophic levels. This is often the case in practice.

Firstly, only zeros of $\hat{K}(\xi)$ within the stripe Ξ are considered. Denote by $\xi_1, \xi_2, \ldots$ an enumeration of these zeros (which may be finite or infinite in number). To isolate the effect of these zeros on the time-dependent solution of Eq. (78), we seek a representation of the solution in the form

$$b(u,t) = b_c(u,t) + \sum_j a_j(u,t)\exp(i\xi_j u), \qquad [93]$$

with the functions $b_c(u,t)$ and $a_j(u,t)$ to be specified below. The condition that $b(u,t)$ is real-valued requires that $a_j(u,t) = (a_k(u,t))^*$ when $\xi_j = -\xi_k{}^*$ (the asterisk * denotes complex conjugation).

Eliminating b in Eq. (78) by Eq. (93), one obtains an equation for b_c,

$$\frac{\partial b_c(u,t)}{\partial t} = (M\mathrm{e}^u)^{n-1}\left[\tilde{K} * b_c\right](u,t) + (M\mathrm{e}^u)^{n-1}\Psi(u,t), \qquad [94]$$

with

$$\begin{aligned}\Psi(u,t) = &-(M\mathrm{e}^u)^{\gamma}\Phi(u)\Theta(t) + \sum_j \int_{-\infty}^{\infty} \tilde{K}(u-\upsilon)a_j(\upsilon,t)\mathrm{e}^{i\xi_j\upsilon}\mathrm{d}\upsilon \\ &- \sum_j (M\mathrm{e}^u)^{1-n}\frac{\partial a_j(u,t)}{\partial t}\mathrm{e}^{i\xi_j u}.\end{aligned} \qquad [95]$$

The condition for choosing the functions $a_j(u,t)$ is now that they should vary slowly in u and t in a sense explained below, and that, even in the limit $t \to \infty$, the Fourier transform $\hat{b}_c(\xi,t)$ of $b_c(u,t)$ exists and can be continued analytically into Ξ. This implies that, even in the limit $t \to \infty$, $b_c(u,t)$ decays at least as fast as $\tilde{K}(u)$ for $u \to +\infty$ and $-\infty$, that is, $b_c(u,t)$ is at least as localised as $\tilde{K}(u)$. The impacts of fishing on species much smaller or larger than the target species should then be completely captured by the functions $a_j(u,t)$.

The strategy to achieve this goal is to assure that the Fourier transform $\hat{\Psi}(\xi,t)$ of $\Psi(u,t)$ has zeros at the points $\xi_k \in \Xi$ at all times, so as not to excite these modes in $b_c(u,t)$. This gives the condition

$$0 = \hat{\Psi}(\xi_k,t), \qquad [96]$$

and one can require $\hat{\Psi}(\xi,t)$ to be small also in the vicinity of these points. An interesting implication of this condition stems from the Fourier transform of the convolution integral in Eq. (95). Let ζ be an arbitrary complex number in Ξ.

Using information about the exponential decay of $\tilde{K}(u)$ as $u \to \pm\infty$ derived above and the fact that $\int_{-\infty}^{\infty} \tilde{K}(u)\exp(-i\xi_j u)\mathrm{d}u = \hat{K}(\xi_j) = 0$, one finds that

$$\int_{-\infty}^{\infty} \mathrm{e}^{-i\zeta u} \int_{-\infty}^{\infty} \tilde{K}(u-v) a_j(v,t) \mathrm{e}^{i\xi_j v} \mathrm{d}v\, \mathrm{d}u$$

becomes, after multiplying and dividing by $\mathrm{e}^{i\xi_j u}$

$$= \int_{-\infty}^{\infty} \mathrm{e}^{i(\xi_j-\zeta)u} \int_{-\infty}^{\infty} \tilde{K}(u-v) a_j(v,t) \mathrm{e}^{i\xi_j(u-v)} \mathrm{d}v\, \mathrm{d}u,$$

after integrating by parts in v

$$= \int_{-\infty}^{\infty} \mathrm{e}^{i(\xi_j-\zeta)u} \int_{-\infty}^{\infty} \int_{-\infty}^{u-v} \tilde{K}(w) \mathrm{e}^{-i\xi_j u} \mathrm{d}w \frac{\partial a_j(v,t)}{\partial v} \mathrm{d}v\, \mathrm{d}u,$$

after changing order of integration and substituting $u \to u+v$

$$\int_{-\infty}^{\infty} \int_{-\infty}^{\infty} \mathrm{e}^{i(\xi_j-\zeta)(u+v)} \int_{-\infty}^{u} \tilde{K}(w) \mathrm{e}^{-i\xi_j w} \mathrm{d}w \frac{\partial a_j(v,t)}{\partial v} \mathrm{d}u\, \mathrm{d}v,$$

and after factoring out a constant

$$= \left(\int_{-\infty}^{\infty} \mathrm{e}^{i(\xi_j-\zeta)u} \int_{-\infty}^{u} \tilde{K}(w) \mathrm{e}^{-i\xi_j w} \mathrm{d}w\, \mathrm{d}u \right) \left(\int_{-\infty}^{\infty} \mathrm{e}^{i(\xi_j-\zeta)u} \frac{\partial a_j(v,t)}{\partial v} \mathrm{d}v \right).$$

If $\xi_j \neq \zeta$, the first factor evaluates, integrating by parts in u, to

$$\begin{aligned} \frac{1}{i(\zeta-\xi_j)} \int_{-\infty}^{\infty} \mathrm{e}^{i(\xi_j-\zeta)u} \tilde{K}(u) \mathrm{e}^{-i\xi_j u} \mathrm{d}u &= \frac{1}{i(\zeta-\xi_j)} \int_{-\infty}^{\infty} \mathrm{e}^{-i\zeta u} \tilde{K}(u) \mathrm{d}u \\ &= \frac{\hat{K}(\zeta)}{i(\zeta-\xi_j)}, \end{aligned} \qquad [97]$$

whereas for $\xi_j = \zeta$, it becomes, again integrating by parts,

$$-\int_{-\infty}^{\infty} u \mathrm{e}^{-i\xi_j u} \tilde{K}(u) \mathrm{d}u = -i\frac{\mathrm{d}}{\mathrm{d}\xi} \int_{-\infty}^{\infty} \mathrm{e}^{-i\xi u} \tilde{K}(u) \mathrm{d}u \big|_{\xi=\xi_j} = -i\hat{K}'(\xi_j), \qquad [98]$$

with the prime denoting the derivative with respect to the argument. Therefore, in the vicinity of the points $\zeta = \xi_k$, the Fourier transform of the convolution integrals is either zero (or small) by Eq. (97) or approximated by Eq. (98) when $\xi_k = \xi_j$.

For reasons to become clear later, define

$$v_k = i(1-n)M^{n-1}\hat{K}'(\xi_k). \qquad [99]$$

With respect to a Fourier transform near ξ_k, the sum over convolution integrals in Eq. (95) is then equivalent to a term $-(1-n)^{-1}v_k e^{i\xi_k u}M^{1-n}\partial a_k(u,t)/\partial u$. One can now attempt to choose the functions $a_k(u,t)$ such that, with this substitution, the right-hand side of Eq. (95) for $\Psi(u)$ vanishes identically for all u. This leads, for each k, to the condition

$$\frac{\partial a_k(u,t)}{\partial t} = -\frac{v_k e^{u(n-1)}}{1-n}\frac{\partial a_k(u,t)}{\partial u} - (Me^u)^{2-\lambda}e^{-i\xi_k u}\Phi(u)\Theta(t) - \sum_{j\neq k} e^{i(\xi_j-\xi_k)u}\frac{\partial a_j(u,t)}{\partial t}. \qquad [100]$$

An alternative route to Eq. (100), currently under development, employs a multiple-scale singular perturbation formalism (Kevorkian and Cole, 1996). In this approach, the functions $a_k(u,t)$ vary formally on slow spatial and temporal scales, admitting a gradient expansion of the convolution, of which the derivative in u above is the lowest-order contribution.

Now, a new independent variable $z = e^{u(1-n)}$ is introduced, so, because $dz/du = (1-n)e^{u(1-n)} = (1-n)z$, one gets $\partial f/\partial u = (\partial f/\partial z)(dz/du) = (1-n)z\,\partial f/\partial z$ for any function $f(u)$. Writing $A_k(z,t) = a_k(u,t)$, Eq. (100) then becomes

$$\frac{\partial A_k(z,t)}{\partial t} = -v_k\frac{\partial A_k(z,t)}{\partial z} - M^{2-\lambda}z^{\frac{2-\lambda-i\xi_k}{1-n}}\Phi\left(\frac{\ln z}{1-n}\right)\Theta(t) - \sum_{j\neq k} z\frac{i(\xi_j-\xi_k)}{1-n}\frac{\partial A_j(z,t)}{\partial t}. \qquad [101]$$

When reading this equation as

$$\frac{\partial A_k(z,t)}{\partial t} = -v_k\frac{\partial A_k(z,t)}{\partial z} + H_k(z,t), \qquad [102]$$

it formally describes fronts that are generated by the inhomogeneity $H_k(z,t)$ and move away from it at a velocity v_k. However, complicating matters, the velocity v_k can here be a complex numbers. Yet, for $H_k(z,t)$ analytic in z, one can write a formal solution of Eq. (102),

$$A_k(z,t) = \int_0^\infty H_k(z-v_k\tau, t-\tau)d\tau, \qquad [103]$$

which is easily verified. The solution is causal: $A(z, t)$ depends on $H_k(z', t')$ only for times $t' \leq t$. To understand this result better, consider first the hypothetical special case that $H_k(z,t) = \exp(-(z-z_0)^2/2\sigma^2)\Theta(t)/\sqrt{2\pi\sigma^2}$, with arbitrary $\sigma, z_0 > 0$. Then

$$A_k(z,t) = \frac{\Theta(t)}{2\nu_k}\left[\operatorname{erf}\left(\frac{z-z_0}{\sqrt{2}\sigma}\right) - \operatorname{erf}\left(\frac{z-z_0-\nu_k t}{\sqrt{2}\sigma}\right)\right]. \qquad [104]$$

The error function $\operatorname{erf}(x)$ for complex arguments x approaches $\pm 1 = \operatorname{sign}\operatorname{Re}\{x\}$ for large $|x|$ when $|\operatorname{Re}\{x\}| > |\operatorname{Im}\{x\}|$, but for $|\operatorname{Re}\{x\}| < |\operatorname{Im}\{x\}|$, it oscillates heavily. It follows that, as $H_k(z,t)$ converges to $\delta(z-z_0)\Theta(t)$ for small σ, one can approximate

$$\begin{aligned} A_k(z,t) &\approx \nu_k^{-1}\Theta(t)[\Theta(z-z_0) - \Theta(z-z_0-\operatorname{Re}\{\nu_k\}t)] \\ &= \begin{cases} +\nu_k^{-1} & \text{for } \operatorname{Re}\{\nu_k\} > 0, t > 0 \text{ and } z_0 < z < z_0 + \operatorname{Re}\{\nu_k\}t, \\ -\nu_k^{-1} & \text{for } \operatorname{Re}\{\nu_k\} < 0, t > 0 \text{ and } z_0 + \operatorname{Re}\{\nu_k\}t < z < z_0, \\ 0 & \text{otherwise} \end{cases} \end{aligned} \qquad [105]$$

when $|\operatorname{Re}\{\nu_k\}| > |\operatorname{Im}\{\nu_k\}| \geq 0$. This describes a sharp front moving at velocity $\operatorname{Re}\{\nu_k\}$ away from $z = z_0$. The heavy oscillations in z and t arising when $|\operatorname{Re}\{\nu_k\}| < |\operatorname{Im}\{\nu_k\}|$ violate the assumptions that $A_k(z,t)$ varies slowly along z and bring $A_k(z,t)$ outside the range of validity of Eq. (102). Generally, one would assume such oscillations to be suppressed by higher-order derivative terms not included in Eq. (102), resulting, again, in a front moving at velocity $\approx \operatorname{Re}\{\nu_k\}$. Below, Eq. (105) will be used to approximate the response of $A_k(z,t)$ to any sharply localised perturbation $\delta(z-z_0)\Theta(t)$ "switched on" at $t=0$, as long as $\operatorname{Re}\{\nu_k\} \neq 0$. The case $\operatorname{Re}\{\nu_k\} = 0$ does not generally arise and is not considered here. The approximate response of $A_k(z,t)$ to general $H_k(z,t)$ can be obtained as a linear combination of solutions of the form (105).

According to Eq. (105), $\partial A_k/\partial t$ is localised at the tip of the travelling fronts generated by inhomogeneities elsewhere on the z-axis. The last term in Eq. (101) describes secondary excitations of fronts/waves by fronts pertaining to other zeros ξ_j. In the singular perturbation formalism, it arises as a higher-order correction. Its effect can be observed in simulations of the system (see Section 8.4.1) but are disregarded in the following analytic calculations, for simplicity. The term containing the fishing pressure $\Phi(\cdot)$ in Eq. (100) is then the only contribution to $H_k(z,t)$ and, using approximation (101), one obtains

$$A_k(z,t) \approx -\frac{M^{2-\lambda}\Theta(t)}{\nu_k}\int_{z_1}^{z} \gamma^{\frac{2-\lambda-i\xi_k}{1-n}}\Phi\left(\frac{\ln\gamma}{1-n}\right)\mathrm{d}\gamma \qquad [106]$$

where $z_1 = \max(0, z - \mathrm{Re}\{\nu_k\}t)$.

On the logarithmic maturation size scale, this becomes

$$a_k(u,t) \approx -\frac{M^{2-\lambda}\Theta(t)(1-n)}{\nu_k}\int_{u_1}^{u} \mathrm{e}^{(\nu-i\xi_k)w}\Phi(w)\mathrm{d}w, \qquad [107]$$

with $u_1 = u_1(u,t) = (1-n)^{-1}\ln[\mathrm{e}^{(1-n)u} - \mathrm{Re}\{\nu_k\}t]$ if the expression in brackets is positive, and $u_1 = -\infty$ otherwise. For fishing pressure specific to maturation size rather than individual size (i.e. using Eq. (80)), the integral can be evaluated analytically, leading to

$$a_k(u,t) \approx -\frac{\sqrt{\pi}\tilde{B}_{\mathrm{tot}}M^{2-\lambda}F\sigma_{\mathrm{F}}\Theta(t)(1-n)}{\sqrt{2}\nu_k}\exp\left[(\nu-i\xi_k)u_{\mathrm{F}} + \frac{(\nu-i\xi_k)^2\sigma_{\mathrm{F}}^2}{2}\right] \times\left\{\mathrm{erf}\left[\frac{(\nu-i\xi_k)\sigma_{\mathrm{F}}^2 + u_{\mathrm{F}} - u_1}{\sqrt{2}\sigma_{\mathrm{F}}}\right] - \mathrm{erf}\left[\frac{(\nu-i\xi_k)\sigma_{\mathrm{F}}^2 + u_{\mathrm{F}} - u}{\sqrt{2}\sigma_{\mathrm{F}}}\right]\right\}, \qquad [108]$$

where $u_{\mathrm{F}} = \ln(m_{\mathrm{F}}/M)$ and u_1 is as defined above. Once the front generated by the onset of fishing has run over a given point u on the logarithmic species-size axis, which happens at time $t \approx (\mathrm{e}^{(1-n)u} - \mathrm{e}^{(1-n)u_{\mathrm{F}}})/\mathrm{Re}\{\nu_k\}$, the expression in braces evaluates to $2\,\mathrm{sign}\,\mathrm{Re}\{\nu_k\}$, and the amplitude of the community response to fishing is controlled by the constant of dimension Mass/Volume given by the first two factors in Eq. (108). The first factor accounts for the available biomass ($B_{\mathrm{tot}}M^{2-\lambda}$ of dimensions Mass/Volume), the fishing pressure applied to it ($F\sigma_{\mathrm{F}}$ dimension 1/Time), and the rate at which this pressure is diverted to other size classes (ν_k, dimension 1/Time). The exponential function in the second factor combines the allometric scaling laws of response rates ($1-n$) and available biomass ($2-\lambda$, recall $\nu = 3-\lambda-n$), a weight and phase factor $\exp(-i\xi_k u_{\mathrm{F}})$ attributable the modulation of the kth mode, and a correction factor relevant when fishing is spread out over a broad body mass range.

The time-dependent community response to size-selective fishing can be approximated analytically by inserting Eq. (108) into Eq. (93) and setting the localised core contribution $b_{\mathrm{c}}(u,t)$ to zero. According to this approximation, fronts travelling towards smaller body sizes ($\mathrm{Re}\{\nu_k\} < 0$) accelerate and

reach $u=-\infty$, that is, $z, m_*=0$, after the finite time $t=\mathrm{e}^{(1-n)u_\mathrm{F}}/|\mathrm{Re}\{\nu_k\}|=(m_\mathrm{F}/M)^{(1-n)}/|\mathrm{Re}\{\nu_k\}|$. Fronts travelling towards larger body sizes ($\mathrm{Re}\{\nu_k\}>0$) decelerate logarithmically on the u-axis. All fronts travel at constant speed on the $z=(m_*/M)^{(1-n)}$ axis. If $\mathrm{Re}\{\nu_k\}$ and $\mathrm{Im}\{\xi_k\}$ have the same sign, the front described by $a_k(u,t)\exp(-i\xi_k u)$ travels into the direction in which $|\exp(-i\xi_k u)|$ decreases. The contribution from $a_k(u,t)\exp(-i\xi_k u)$ is then bounded and its Fourier transform exists. In the opposite case ($\mathrm{sign}\,\mathrm{Re}\{\nu_k\}\neq\mathrm{sign}\,\mathrm{Im}\{\xi_k\}$), the contribution by $a_k(u,t)\exp(-i\xi_k u)$ grows beyond all bounds as time proceeds. These contributions are of the amplifying type not captured by the Fourier transform steady-state solution Eq. (90). This phenomenon is closely related to what the physics and engineering literature calls a *convective instability*. It is characterised by the fact that, although the system response to a pulse perturbation remains finite at any fixed point on the u-axis, it grows beyond all bounds applicable uniformly for the entire infinite u-axis.[8] In reality, logarithmic size u is limited from both above and below, and the community response to perturbations remains finite. Convective instabilities are distinguished from *absolute instabilities*, where perturbation responses grow beyond all bounds for some given value of u. Such instabilities are conceivable also for size spectra and can be observed in simulations for specific parameter values, but the analysis described here is unable to capture them. An adaptation of standard methods for identifying absolute instabilities (e.g. Akhiezer and Polovin, 1971) to the particular form of Eq. (78) is therefore highly desirable.

7.5. Extension of the method to all zeros of $\hat{K}(\xi)$

It turns out that the approximation constructed above can be improved further by including also the zeros of $\hat{K}(\xi)$ outside the stripe Ξ, although some care needs to be taken. For zeros ξ_k outside the strip, the exponentially decaying tails of $\hat{K}(u)$ are "flat" compared with the rate of increase or decrease of $\mathrm{e}^{-i\xi_k}$. The tails can therefore mediate long-range interactions and delocalise the dynamics of the modes $a_k(u,t)$. An analysis of the special case where $\hat{K}(\xi)$ is the ratio of two linear polynomials (not discussed here) reveals that this can lead to the suppression of convective instabilities even when $\mathrm{sign}\,\mathrm{Re}\{\nu_k\}\neq\mathrm{sign}\,\mathrm{Im}\{\xi_k\}$: the response of $a_k(u,t)$ is then in the direction on the u-axis opposite to $\mathrm{Re}\{\nu_k\}$. To take this into account, the following heuristics suppressing convective instabilities are employed. In the rare cases

[8] As here press perturbations are considered here rather than pulse perturbation, not all unbounded responses necessarily correspond to convective instabilities.

where $\mathrm{Re}\{\nu_k\}$ and $\mathrm{Im}\{\xi_k\}$ have opposite signs for zeros $\xi_k \notin \Xi$, the value of u_1 in Eq. (107) or (108) is, for all times $t > 0$, set to $+\infty$ for $\mathrm{Re}\{\nu_k\} > 0$ and to $-\infty$ for $\mathrm{Re}\{\nu_k\} < 0$. Because of the rapid decay of these modes along u, the discontinuity of $b(u)$ in t resulting from this approximation is hardly noticeable. If $\mathrm{Re}\{\nu_k\}$ and $\mathrm{Im}\{\xi_k\}$ have the same signs, $a_k(u,t)$ is computed according to Eq. (107) or (108) without modifications. Although convective instabilities for zeros outside Ξ have not been observed in simulations, there is some risk that exceptions to these heuristics exist.

Provided the extension of this method to all zeros ξ_k of $\tilde{K}(\xi)$ is successful so that $\lim_{t\to\infty} \hat{\Psi}(\xi_k, t) = 0$, one can expect that, by Eq. (94), the Fourier transform of the residual $b_c(u,t)$ converges to an entire function as $t \to \infty$. That is, $|\lim_{t\to\infty} b_c(u,t)|$ decays faster than exponentially for $u \to \pm\infty$. The steady-state residual $\lim_{t\to\infty} b_c(u,t)$ unaccounted for by the approximation developed above is then, in this sense, strongly localised near the size class targeted by fishing. When using the approximation method below, the contribution by $b_c(u,t)$ is not included.

8. COMPARISON OF ANALYTIC THEORY AND SIMULATIONS

8.1. A specific parametrisation

To visualise typical responses of size spectra to fishing and to test the analytic predictions of Section 7.4 by comparison with simulations, specific choices for the free model parameters need to be made. This includes, in particular, choices for the predator–prey size-ratio window $s(x)$ and the maturation selection function $\psi(x)$. Standard values used for the scalar parameters are listed in Table 3. The choices follow Hartvig et al. (2011), and the reader is referred to their work for detailed motivations. All body masses are measured in units of the body mass class targeted by fishing ($M = m_\mathrm{F}$). To report simulation results independent of the specific choice of m_F, time is measured in units of the approximate age of the targeted size class at maturation (i.e. the age when $m = m_* = m_\mathrm{F}$), computed for $\psi(x) = 0$ and $m_0 \to 0$ for simplicity. The growth trajectories of individuals then follow $\mathrm{d}m/\mathrm{d}t = \tilde{g}_0 m^n$ and time to maturation is $T_\mathrm{mat} = m_\mathrm{F}^{1-n} \tilde{g}_0^{-1} (1-n)^{-1}$. For $m_\mathrm{F} = 1\,\mathrm{kg}$, this equals 3.0 years with standard parameters. Fishing pressure F was fixed so that, in response to the onset of fishing, species of size m_F initially decline at a rate $F = 0.1\, T_\mathrm{mat}{}^{-1}$.

Table 3 Standard parameters used in simulations

Symbol	Value	Unit	Description
n	3/4		Exponent of physiological activity
h	85	$g^{1-n}yr^{-1}$	Coefficient of maximal food intake
k	10	$g^{1-n}yr^{-1}$	Coefficient of metabolic loss rate
q	0.8		Exponent of search/attack rate
γ	Cancels out	$g^{1-q}m^{-3}yr^{-1}$	Coefficient search/attack rate
α	0.6		Conversion efficiency
β	100		Preferred predator–prey mass ratio
σ_s	1		Width of predator–prey size-ratio window
F	See text	yr^{-1}	Fishing mortality
σ_F	ln 10		Width of harvested size range
η	0.25		Maturation over asymptotic mass
σ_r	0.5		Cut-off length for food-web effects
r	0.5γ	$g^{1-q}m^{-3}yr^{-1}$	Strength of food-web effects

The parameters values $r=0.5\gamma$ and $\sigma_r=0.5$ of the heuristic submodel for food-web effects where chosen, following the reasoning of Section 6.4, according to the observation that γ is the only other model parameter of the same dimension as r, so that both might be of similar magnitude, and that $\exp(\sigma_r)$ corresponds to the typical mass ratio between prey in the diet of a consumer.

8.1.1 Choice of the predator–prey size-ratio window

With β standing for the preferred predator–prey mass ratio (not to be confused with the size distribution $\tilde{\beta}(w)$) and x for the actual logarithmic predator–prey mass ratio, the predator–prey size-ratio window is chosen following Hartvig et al. (2011) as a Gaussian window:

$$s(x) = \exp\left[-\frac{(x-\ln\beta)^2}{2\sigma_s^2}\right]. \qquad [109]$$

Its Fourier transform is

$$\hat{s}(\xi) = (2\pi)^{1/2}\sigma_s \exp\left[-\frac{\sigma_s^2\xi^2}{2}\right]\beta^{-i\xi}. \qquad [110]$$

8.1.2 Choice of the reproduction-selection function and its implications

Hartvig et al. (2011) showed that with a reproduction-selection function of the form

$$\psi(x) = (\eta x)^{1-n}, \qquad [111]$$

growth of individuals follows a von Bertalanffy trajectory. The coefficient η stands for the ratio of maturation size to asymptotic size. Hartvig et al. (2011) multiplied this form with a smoothed step function to describe the onset of maturation at $x = 1$, but here I stick with Eq. (111) for the sake of analytic tractability. In fact, population structures resulting from $\psi(x)$ with or without this additional factor do not differ much.

For the special case that the allometric exponent for the metabolic loss rate is exactly $n = 3/4$, and that background mortality is negligible ($\mu_0 = 0$), the scale-free population size structure $\tilde{N}(x)$ (Eqs. 33 and 24) with $\psi(x)$ given by Eq. (111), and $\tilde{\mu} = \tilde{g}_0$ (i.e. $\tilde{a} = 1$) evaluates to

$$\tilde{N}(x) = \frac{\tilde{N}_0 \left[1 - (\eta x)^{1/4}\right]^3}{\tilde{g}_0 \left[1 - \eta^{1/4}\right]^4 x^{7/4}} \qquad [112]$$

for $x \leq \eta^{-1}$ and $\tilde{N}(x) = 0$ otherwise. This result follows after verifying that $E(x)$, defined by Eq. (44), is given by $E(x) = [1 - (\eta x)^{1/4}]^4 [1 - \eta^{1/4}]^{-4} x$ (compute $E'(x)/E(x)$ to see this).

From Eq. (112) one gets, according to Eq. (41),

$$\begin{aligned} \tilde{B}_{\text{tot}} = \tilde{B}_{\text{tot}}(0) &= \int_0^\infty x \tilde{N}(x) \mathrm{d}x \\ &= \frac{\tilde{N}_0}{\tilde{g}_0 \left[1 - \eta^{1/4}\right]^4 \eta^{1/4}}. \end{aligned} \qquad [113]$$

Consequently, the distribution of a species' biomass over the logarithmic size axis is given, following Eq. (71), by

$$\tilde{\beta}(w) = (\eta \mathrm{e}^w)^{1/4} \left[1 - (\eta \mathrm{e}^w)^{1/4}\right]^3 \qquad [114]$$

for $w \leq -\ln \eta$ and $\tilde{\beta}(w) = 0$ otherwise. This function has the Fourier transform

$$\hat{\beta}(\xi) = \frac{\eta^{i\xi}}{(i+\xi)(i+4\xi/3)(i+2\xi)(i+4\xi)}. \qquad [115]$$

Next to the pole at $\xi = -i/4$, expected from the general asymptotic form of $\tilde{N}(x)$ for small x, Eq. (34), the analytic continuation of $\hat{\beta}(\xi)$ has poles also at $\xi = -i/2$, $\xi = -3i/4$, and $\xi = -i$. Interestingly, all poles are located at multiples of $-i(1-n)$.

As Eq. (113) contains the unknown $\tilde{N}_0$, it does not give a numerical value for $\tilde{B}_{\text{tot}}$. To compute $\tilde{B}_{\text{tot}}$, use Eq. (71) to express $\tilde{N}(x)$ by $\tilde{\beta}(w)$ in Eq. (18). The resulting equation can be solved for $\tilde{B}_{\text{tot}}$, to obtain

$$\tilde{B}_{\text{tot}} = \frac{\tilde{\mathcal{N}}}{\hat{\beta}(i(\lambda-2))}. \qquad [116]$$

As $\tilde{\beta}(0) = 1$ by normalisation, the two coefficients $\tilde{B}_{\text{tot}}$ and $\tilde{\mathcal{N}}$ are therefore nearly identical when $\lambda \approx 2$.

8.2. Simulation technique

Simulation of the Species Size-Spectrum Model, Eq. (78), over a large range in u is difficult because, by the factor $(Me^u)^{n-1}$, a broad range of timescales has to be covered. The u-axis was discretized to 256 points at distance 0.5, ranging from $u = u_{\min} = -128/3$ to $u = 254.5/3$. This corresponds to a range from about 10^{-19}M to 10^{37}M in maturation size, which is much larger than the size range covered in real size spectra. The reason for choosing this broad range is to isolate the effects of scale-invariant dynamics, which can be approximated analytically, from conceivable complications due to boundary effects. To gain some qualitative understanding of the modifications of dynamics that could result from boundary effects, a variant of the model (constrained-domain variant) was simulated where Eq. (78) was applied only over the interval $e^u M = 10^{-15}$M to 10^3M, and $b(u) = 0$ held fixed otherwise.

The right-hand-side of Eq. (78) was evaluated using a pseudospectral method: the convolution was evaluated in Fourier space by multiplication of $\hat{b}(\xi)$ with the result for $\hat{K}(\xi)$, Eq. (92), with either Eq. (83) or (84). To reduce aliasing, the u-axis was extended by another 256 points for this operation. To suppress numerical instabilities developing at the lower edge of the u-axis, a stabilising extra term $-8(Me^u)^{n-1}b(u)/\{1+\exp[0.6(u-u_{\min}-\ln\beta)]\}$ was added to Eq. (78). Over most of the u-axis, this term has no effect. The discretized system was then solved using the implicit ODE solver CVODE included in the SUNDIALS package (Hindmarsh et al., 2005). This solver automatically adjusts the approximation order and the step size to achieve a prescribed accuracy (here 10^{-4} per step). In

addition, upper limits on step size, scaling as the square-root of time since the start of simulations, were imposed to suppress numerical instabilities.

8.3. Numerical evaluation of the analytic approximation

The analytic formula for the Fourier transform of the interaction kernel, $\tilde{K}(\xi)$, was converted into a subroutine which takes arbitrary complex ξ as arguments and outputs $\tilde{K}(\xi)$. The zeros of $\tilde{K}(\xi)$ in the vicinity of $\xi = 0$ were then determined using a simple secant search algorithm, initiated at all points on a grid with resolution $\pi/(8 \ln \beta)$ spanning the range $0 \leq \mathrm{Re}\,\xi \leq 8\pi/\ln \beta, \quad |\mathrm{Im}\,\xi| \leq 4\pi/\beta$. It was verified that enlarging this range did not change the results markedly. Zeros found repeatedly were discarded. The derivatives of $\tilde{K}(\xi)$ at the zeros, required to evaluate the analytic approximation of dynamics, are most easily computed numerically.

The programming language used (C++) did not include an implementation of the error function for complex arguments in its mathematical library. This function is required when computing the analytic approximation of size-spectrum dynamics using Eq. (108). The function was therefore implemented using the method proposed by Hui et al. (1978). Alternatively, the integrals in Eq. (107) could have been evaluated numerically. This second approach has the advantage of being applicable for arbitrary external perturbations $\Phi(w)$ but is slightly more computation-intensive.

8.4. Case studies

8.4.1 Standard parameters

Equation (78) for the oligotrophic case was solved with standard parameters both numerically and in the analytic approximation described in Section 8.1. The evolution of the system state is shown in Fig. 4. One observes the formation of two trophic cascades, one downwards from m_F to smaller species, the other one upwards, towards larger species. In a later phase, an upward-moving front emerges that bends the size spectrum downward and carries an additional downward cascade in its wake.

The initial dynamics are not reproduced well by the analytic result in Eqs. (93) and (108). The theory overestimates the initial decay of the targeted size class (which is well described by the small-t approximation, Eq. (88)) and is late in predicting the formation of a weak downward trophic cascade. The analytic solution predicts the timing of the saturation of the downward cascade around 3.3–10 T_{mat} reasonably well. It makes an excellent prediction of its final, saturated state.

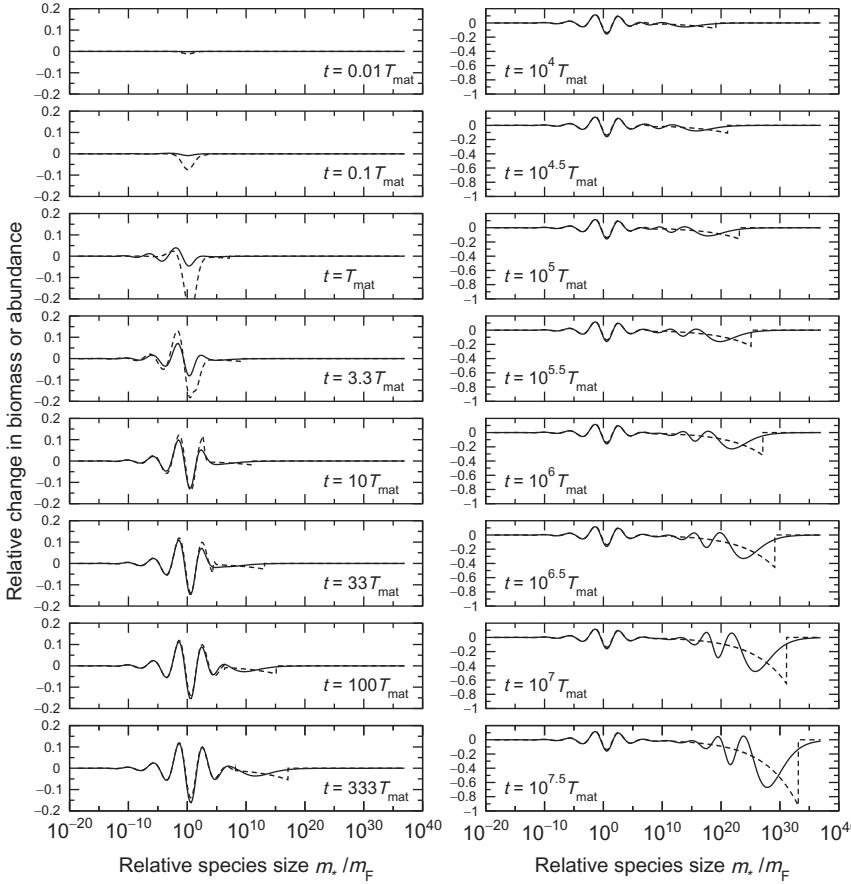

Figure 4 Time-dependent response of a size spectrum to size-specific exploitation targeting maturation sizes around m_F, for the oligotrophic regime in the standard parametrisation described in Section 8.1. Solid lines: simulations. Dashed lines: analytic theory. T_{mat} is the approximate age at which individuals maturing at m_F reach this size. In the second column, corresponding to later stages, the vertical axis is expanded.

The upward cascade evolves much slower than the downward cascade. This is mostly a consequence of the allometric scaling of biological rates, encapsulated in the factor $(Me^u)^{n-1}$ in Eq. (78). The analytic approximation captures reasonably well the timing of the formation of the first maximum of the upward cascade around 10–33 T_{mat}, the formation of the second minimum around 100 T_{mat}, and the full emergence of the second maximum around 333 T_{mat}. Thereafter (second column in Fig. 4), the two trophic cascades have mostly stabilised.

What follows is the propagation of a downward-bending front to larger species sizes. Continuation of the simulation until $t = 10^{7.5} T_{\mathrm{mat}}$ and over an (unrealistically) large body-size range demonstrates three general facts. Firstly, the analytic theory makes a good prediction of the velocity of the downward-bending front on the u-axis. Secondly, the modulations behind the front travel in its wake, and, after sufficient waiting time, subside (compare, e.g. the simulation results at the point $m/m_{\mathrm{F}} = 10^{10}$ for $t = 10^{5} T_{\mathrm{mat}}$ and $t = 10^{7.5} T_{\mathrm{mat}}$). Presumably, these secondary excitations of the size spectrum would be captured when including the neglected sum over j in Eq. (100) as an additional inhomogeneity contributing to $H_k(z, t)$. Thirdly, whereas in the analytic approximation the front quickly becomes sharp as it moves to larger u (as does the front of the upward trophic cascade), it is blurred in simulations. This indicates the presence of additional diffusive effects along the u-axis that were not captured in the present approximation.

The case displayed in Fig. 4 is a typical example for the degree of agreement between simulations and analytic approximations. Despite many differences in detail, the analytic approximation captures the main features and the times of their emergence.

8.4.2 The constrained-domain variant

In Fig. 5, it is shown how the response of the size spectrum changes in simulations when dynamics are constrained to a narrower domain. The dynamic domain was chosen so that with $m_{\mathrm{F}} = 1\,\mathrm{kg}$ it corresponds approximately to the realised range of species sizes in marine communities. The resulting modification of dynamics evident in Fig. 5 can be interpreted as a minimal adaptation (a reflection on the upper boundary?) required to keep $b(u)$ continuous at the domain boundaries. Otherwise, the effect on dynamics is small, at least for the case considered here. Small dynamic effects of the boundaries do not imply that their effects on the steady-state size spectrum will be small.[9] The latter are discussed briefly in Section 9.6.

[9] The correct form of the boundary conditions that represent the upper and lower size limits of real communities in the Species Size-Spectrum Model is unknown. In an approximation consistent with the model, one can expect them to take the form of a set of inhomogeneous linear conditions on $b(u)$ (Cross and Hohenberg, 1993). A particular, stationary solution of the model compatible with these inhomogeneous boundary conditions represents the effect of "press perturbations by the boundaries" discussed in Sec. IX.F below. These perturbations will be stronger the larger the inhomogeneities in the boundary conditions. After subtracting this particular solution from $b(u)$, the reminder is constrained by a set of homogeneous boundary conditions. Of these, the condition applied here ($b(u) = 0$ for u outside the domain) is one example. As it is independent of the magnitude of the inhomogeneities, its effect on the dynamics inside the domain can be small even when boundary perturbations are strong.

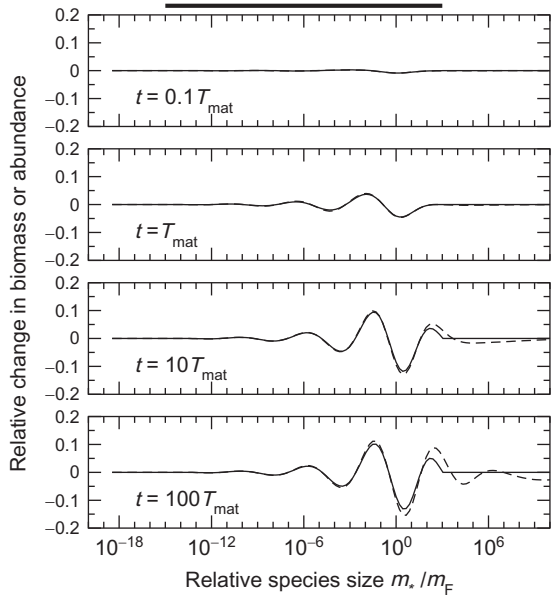

Figure 5 Effect of constraining the domain of the dynamic response of the size spectrum to the size range indicated by the bar above. Simulations with standard parameters in the oligotrophic regime as in Fig. 4, at four points in time t. Solid lines: constrained-domain variant. Dashed line: unconstrained variant for comparison.

8.4.3 Characterisation of size-spectrum dynamics by the zeros of $\hat{K}(\xi)$

The solution of Eq. (78) is controlled by the Fourier transform $\hat{K}(\xi)$ of the interaction kernel $\tilde{K}(u)$ entering Eq. (78), specifically by its complex zeros and its first derivatives at these points. A good qualitative understanding of the solution of Eq. (78) can therefore be gained already by studying the geometry of these zeros in the complex plane. For the standard parameter set used here, the zeros of $\hat{K}(\xi)$ and its analytic continuation are marked as open circles in Fig. 6. The arrow attached to each open circle indicates the argument of the first derivative of $\hat{K}(\xi)$ at this point (an arrow pointing straight right would mean a real, positive first derivative). The filled circles represent poles of $\hat{K}(\xi)$. Figure 6B offers a broader view of the same configuration.

Results derived in Section 7.4 translate into the following geometric picture: zeros of $\hat{K}(\xi)$ located below the real axis ($\mathrm{Im}\{\xi\} = 0$) correspond to modulations or bending of $b(u)$ that increases towards larger u (larger body sizes), and *vice versa* for zeros above the real axis. A non-modulated (bending) contribution corresponds to a zero on the imaginary axis ($\mathrm{Re}\{\xi\} = 0$).

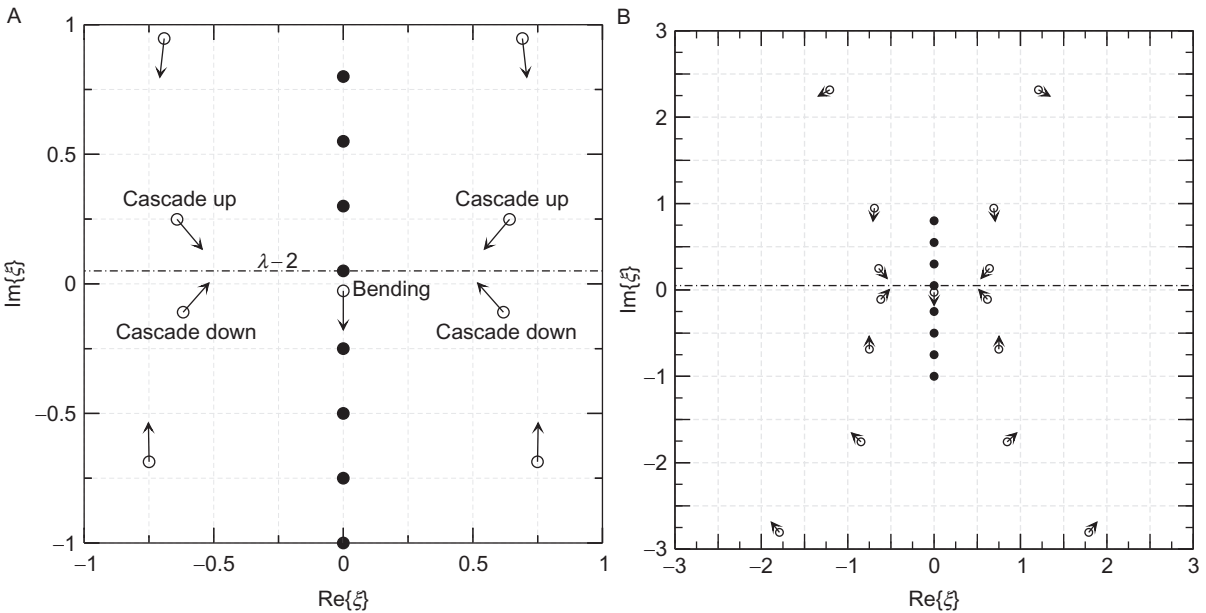

Figure 6 (A) Locations of zero (open circles) and poles (closed circles) of $\hat{K}(\xi)$ in the complex plane as well as the argument of $\hat{K}'(\xi)$ at the zeros (arrows), annotated with the corresponding perturbation responses. Standard parameters. (B) gives a wider perspective.

All other zeros always come in pairs ($\xi = \pm\xi_r + \mathrm{i}\xi_i$), guaranteeing that the sum of all contributions approximating $b(u)$ by Eq. (93) is real-valued. When expressing deviations from the unperturbed equilibrium state in terms of relative changes in biomass or abundance (rather than by absolute differences in biomass density), modulations and bending increase towards positive u if the corresponding zero is located below the line $\mathrm{Im}\{\xi\} = \lambda - 2$, and *vice versa*.

The direction into which the front corresponding to each of these contributions propagates is determined by the vertical component of the orientation of the attached arrows. Arrows pointing downwards correspond to fronts propagating into the direction of positive u (upward cascades), that is, towards larger body size. Arrows pointing upwards correspond to fronts propagating in the direction of smaller body size (downward cascades). Combining the positions of zeros with the orientations of arrows, it follows that for zeros with arrows pointing towards the line $\mathrm{Im}\{\xi\} = \lambda - 2$ the corresponding modulations of relative abundance (or non-modulated bending) become smaller away from the size class targeted by fishing, or any other press perturbation. Effects on relative abundance corresponding to zeros with arrows pointing away from the line $\mathrm{Im}\{\xi\} = \lambda - 2$ increase as they propagate along the size axis. Such contributions correspond to the amplifying contributions mentioned at the end of Section 7.4. For the standard parameter set, the only contribution of this type is the upward-moving front of size-spectrum bent.[10]

Among zeros with attached arrows pointing towards the line $\mathrm{Im}\{\xi\} = \lambda - 2$, their contributions decay the faster along the u-axis the farther they are from the line $\mathrm{Im}\{\xi\} = \lambda - 2$. Further, zeros at some distance from $\mathrm{Im}\{\xi\} = \lambda - 2$ generally appear to be of the convectively stable type (see Figs. 6B, 6.7B, and 8B). Often, good qualitative images of the system response to press perturbations can be obtained from considering just a few zeros close to the line $\mathrm{Im}\{\xi\} = \lambda - 2$. In Fig. 6A, the five zeros of $\hat{K}(\xi)$ closest to this line have been annotated.

[10] The fact that in the oligotrophic regime there is always a purely imaginary zero corresponding to an amplifying, upward-moving front follows from the observation that $\hat{K}(\xi)$ is real along the imaginary axis, the existence of the two poles of $\hat{K}(\xi)$ at $\xi = -(1-n)i$ and $\xi = (q-n)i$, their respective sign structures, and continuity considerations. The sign structure follows heuristically from the fact that $\tilde{K}(u)$ describes feeding on smaller species and predation by larger species. The corresponding analytic argument makes use of the observation that the denominator in Eq. (46) is positive, so $\alpha I_1 - I_2 > kh^{-1} I_1$, a comparison of Eqs. (83) and (84), and the observation that Eq. (83) has a zero coinciding with the pole at $\xi = (q-n)i$.

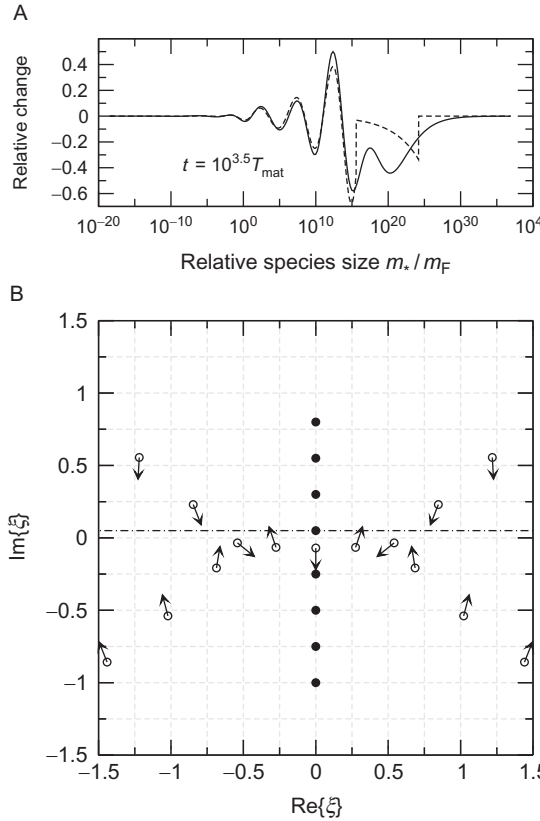

Figure 7 Perturbation response of the size spectrum (A) and graphic characterisation of $\hat{K}(\xi)$ (B) for the case discussed in Section 8.4.4, which leads to an amplifying upward trophic cascade. As in Fig. 4, solid and dashed lines in panel (A) correspond to simulation and analytic approximation, respectively. As in Fig. 6, open and closed circles in (B) correspond to zeros and poles of $\hat{K}(\xi)$ respectively, and arrows to the argument of $\hat{K}'(\xi)$ at the zeros.

8.4.4 An amplifying upward trophic cascade

When changing model parameters, other types of dynamics can be found. Figure 7A displays simulation and analytic results when, compared with the previous case, the preferred predator–prey mass ratio is increased from $\beta = 10^2$ to $\beta = 10^5$. The upward cascade now becomes amplifying, which means that the modulated system response becomes stronger towards species sizes larger than m_F (Fig. 7). Figure 7B displays the configuration of zeros and poles of $\hat{K}(\xi)$ in the complex plane. The amplifying upward cascade is generated by the pair of zeros near ± 0.5 with attached arrows pointing away from the line $\mathrm{Im}\{\xi\} = \lambda - 2$.

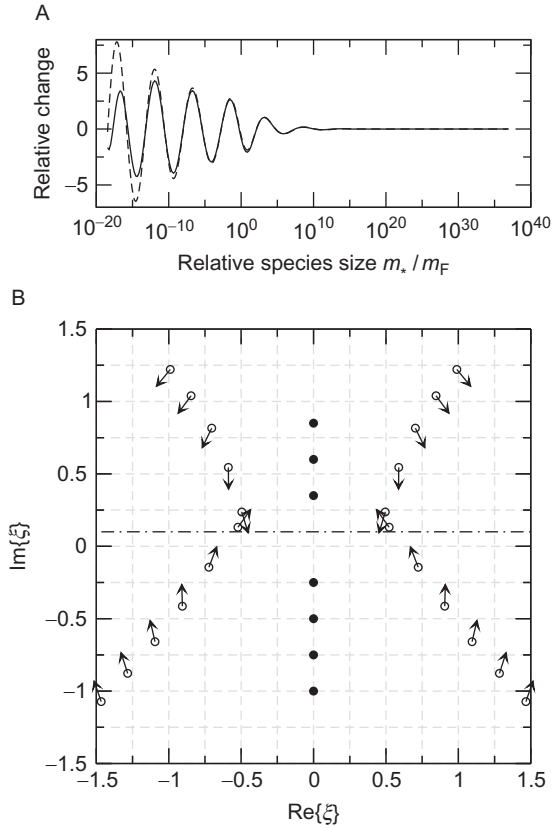

Figure 8 Perturbation response of the size spectrum (A) and graphic characterisation of $\hat{K}(\xi)$ (B) for the case discussed in Section 8.4.5, which leads to an amplifying downward trophic cascade. Symbols as in Figs. 4 and 6. As in Fig. 6, solid and dashed lines in (A) correspond to simulation and analytic approximation, respectively. As in Fig. 6, open and closed circles in (B) correspond to zeros and poles of $\hat{K}(\xi)$, respectively, and arrows to the argument of $\hat{K}'(\xi)$ at the zeros.

8.4.5 An amplifying downward trophic cascade

Finally, an example for the eutrophic regime is considered. In addition to setting $\beta = 10^5$ as in the previous example, standard parameters are modified by increasing the width of the predator–prey size-ratio window (Eq. 109) from $\sigma = 1$ to $\sigma = 3$. The coefficient of the allometric scaling law for respiration is increased from $k = 10\, g^{1-n}\,\mathrm{year}^{-1}$ to $k = 49.09\, g^{1-n}\,\mathrm{year}^{-1}$, giving a size-spectrum slope of $\lambda = 2.1$ via the constraint Eq. (39). For ecological consistency, all biomasses and abundances must be sufficiently large to fully

satiate all consumers. For the system response to the fishing regime used here, this is clearly not the case. As can be seen in Fig. 8A, the predicted linear response grossly exceeds changes by 100% in biomass. Realistically, one should therefore apply less fishing pressure. Reducing fishing pressure by, say, one-tenth would yield exactly the same response as shown in Fig. 8, only with a ten times lower amplitude. Fishing pressure was retained at the standard value in Fig. 8A to allow easy comparison with the previous examples.

Now, the downward cascade becomes amplifying: abundance modulations increase towards lower species sizes. As the downward cascade propagates at constant speed on the m_*^{1-n}-axis, it reaches the lower end of the simulated range after finite time (about $100\,T_{\mathrm{mat}}$). The simulation results differ from the analytic predictions for very low species sizes because of the numerical stabilisation applied near the lower boundary (see Section 8.2). The occurrence of a convectively unstable downward cascade can be predicted from the fact that in Fig. 8B there is one pair of zeros above the line $\mathrm{Im}\{\xi\} = \lambda - 2$ with attached arrows pointing away from it. The observation that the amplitude of the system response here is considerably larger than in the previous cases might be related to the fact that these two zeros are both close to other zeros, which could lead to small derivatives of $\hat{K}(\xi)$ at these zeros (when $\hat{K}(\xi)$ has a double zero, $\hat{K}'(\xi)$ vanishes), small values of $|\nu_k|$, and hence large modulation amplitudes by Eq. (108).

Comparing Figs. 7A and 8A, one can see that in the eutrophic regime the pole of $\hat{\beta}(-\xi - \nu i)$ at $\xi = (\lambda - 2)i$ has disappeared. It has been cancelled in $\hat{K}(\xi)$ by the zero of $\hat{\kappa}_0(\xi + \nu i)$, Eq. (83), at the same position. This zero results from the interplay between predation mortality (first term in Eq. (83)) and release from predation (second term in Eq. (83)) under *ad libitum* feeding. The pole of $\hat{\beta}(-\xi - \nu i)$ is a result of taking the limit $m_0, x_0 \to 0$ in Section 6.3. When regularising $\hat{\beta}(\xi)$, for example, by fixing x_0 at some small but positive value, $\hat{\beta}(-\xi - \nu i)$ would instead attain a large, but finite, value at $\xi = (\lambda - 2)i$. Then $\hat{K}(\xi)$ at this point would be zero and $\hat{K}'(\xi)$ large, corresponding to perturbation responses in the form of small amplitude, rapidly upward-moving fronts, by Eqs. (99) and (108). These fronts represent the mechanism by which the overall abundances of larger species are adjusted to match those of smaller species in the eutrophic regime. In the limit $m_0, x_0 \to 0$, this mechanism degenerates to an immediate, rigid regulation, concealing the regulating dynamics.

9. IMPLICATIONS, DISCUSSION, AND OUTLOOK

9.1. The final steady state of a perturbed species size spectrum

The theory of size-spectrum dynamics developed in Section 8 now allows the problem of computing the steady-state solution reached long after initiating a size-specific press perturbation to be revisited. As argued in Section 7.2, this solution must be of the form

$$b(u) = b_0(u) + \sum_j A_j \mathrm{e}^{i\xi_j u}, \qquad [117]$$

where $b_0(u)$ is given by its Fourier transform in Eq. (90) and A_j are constants to be determined. By comparing with the related decomposition Eq. (93) of the time-dependent solution and taking the limit $t \to +\infty$, one obtains

$$\lim_{t\to+\infty} b_c(u,t) = b_0(u) + \sum_j \left[A_j - \lim_{t\to+\infty} a_j(u,t)\right] \mathrm{e}^{i\xi_j u}. \qquad [118]$$

The fact that $b_0(u)$ has a Fourier transform and the conjecture that $\lim_{t\to+\infty} b_c(u,t)$ is strongly localised (Section 7.5) and can now be used to compute the coefficients A_j. Consider first those cases where $|\exp(i\xi_j u)|$ diverges as $u \to +\infty$ (i.e. where $\mathrm{Im}\{\xi_j\} < 0$). The conditions on $b_c(u)$ and $b_0(u)$ require that

$$A_j = \lim_{t,u\to+\infty} a_j(u,t). \qquad [119]$$

For fronts propagating to negative u, that is, $\mathrm{Re}\{\nu_j\} < 0$, this implies $A_j = 0$. In the opposite case, $\mathrm{Re}\{\nu_j\} > 0$, application of Eqs. (107) and (99) gives

$$\begin{aligned} A_j &= -\frac{M^{2-\lambda}(1-n)}{\nu_j}\hat{\Phi}(\xi_j + \nu i) \\ &= \frac{iM^{\nu}\hat{\Phi}(\xi_j + \nu i)}{\hat{K}'(\xi_j)}. \end{aligned} \qquad [120]$$

The corresponding results in the case $\mathrm{Im}\{\xi\} > 0$ has the opposite sign for A_j. The close similarity between this expression for A_j and Eq. (90)

for $\hat{b}_0(\xi)$ has the interesting consequence that the final steady state $b(u) = \lim_{t\to+\infty} b(u,t)$ can be computed by formally evaluating the inverse Fourier transformation, Eq. (1), of $\hat{b}_0(\xi)$,

$$b(u) = \frac{1}{2\pi}\int_C \hat{b}_0(\xi) e^{i\xi u} d\xi. \qquad [121]$$

However, the path of integration C in the complex plane must be chosen such that, in the geometric picture introduced in Fig. 6A, it remains above all zeros ξ_j (open circles) with attached arrows pointing upwards, and below all zeros with attached arrows pointing downwards. Using Eq. (120) and the residue theorem of functional analysis, it is easily verified that the additional terms resulting form deviations of this path C from the real axis are exactly the non-zero contributions $A_j e^{i\xi_j u}$ in Eq. (117).

9.2. Distribution of individual sizes in the final steady state

From $b(u)$, the final deviations of the distribution of biomass over logarithmic species sizes from the unperturbed distribution, one can compute the corresponding deviations $c(u)$ of the distribution of biomass over logarithmic individual sizes by a convolution with the intraspecific mass distribution $c(u) = \left[\tilde{\beta} * b\right](u)$. For simplicity, only those situations are considered here where $\mathrm{Im}\{\xi_k\} > -(1-n)$ for all k for which $A_k \neq 0$. Graphically, this means that all zeros (open circles) with attached arrows pointing away form the dash-dotted line must lie above the highest pole (filled circle) in the lower half plane. In all scenarios considered above (Figs. 6–8), this is the case. Using Eq. (117) and again invoking the residue theorem, one can then evaluate

$$\begin{aligned} c(u) &= \left[\tilde{\beta} * b_0\right](u) + \sum_j \hat{\beta}(\xi_j) A_j e^{i\xi_j u} \\ &= \frac{1}{2\pi}\int_C \hat{c}_0(\xi) e^{i\xi u} d\xi, \end{aligned} \qquad [122]$$

with $\hat{c}_0(\xi) = \hat{\beta}(\xi)\hat{b}_0(\xi)$ and the path C taken identical to that in Eq. (121). Interestingly, when considering the case of fishing specific to the size of individuals (rather than species) and ignoring food-web effects, Eqs. (90), (79), and (92) evaluate $\hat{c}_0(\xi)$ to the simple expression

$$\begin{aligned}\hat{c}_0(\xi) &= \frac{\hat{\beta}(\xi) M^{\nu} \hat{\Phi}(\xi + \nu i)}{\hat{K}(\xi)} \\ &= \frac{\hat{\beta}(\xi) M^{\nu} \tilde{B}_{\mathrm{tot}} F \hat{W}_{\sigma_{\mathrm{F}}}(\xi + \nu i) \hat{\beta}(-\xi - \nu i) (M/m_{\mathrm{F}})^{i\xi - \nu}}{\tilde{B}_{\mathrm{tot}} \hat{\kappa}_0(\xi + \nu i) \hat{\beta}(-\xi - \nu i) \hat{\beta}(\xi)} \\ &= \frac{F M^{\nu} \hat{W}_{\sigma_{\mathrm{F}}}(\xi + \nu i)}{\hat{\kappa}_0(\xi + \nu i)} \left(\frac{M}{m_{\mathrm{F}}}\right)^{i\xi - \nu}.\end{aligned} \qquad [123]$$

This result depends on ecological detail only through the feeding interactions described through $\hat{\kappa}_0$, not through the life-history characteristics of species. These enter $c(u)$ only through path C determined by $\hat{K}(\xi)$. Formally, $c(u)$ is a steady-state solution of the balance equation

$$\frac{\partial c(u)}{\partial t} = (M \mathrm{e}^{u})^{n-1} \left[\tilde{K}_1 * c\right](u) - \tilde{B}_{\mathrm{tot}} F (M \mathrm{e}^{u})^{2-\lambda} W_{\sigma_{\mathrm{F}}}\left(u - \ln\frac{m_{\mathrm{F}}}{M}\right), \qquad [124]$$

with $\tilde{K}_1(u) = \tilde{B}_{\mathrm{tot}} \mathrm{e}^{\nu u} \kappa_0(u)$ (so that $\hat{K}_1(\xi) = \tilde{B}_{\mathrm{tot}} \hat{\kappa}_0(\xi + \nu i)$). Making use of the definition of $\kappa_0(u)$, Eq. (70), $\tilde{K}_1(u)$ can be expressed as

$$\tilde{K}_1\left(\ln\frac{m}{m'}\right) = \tilde{B}_{\mathrm{tot}} m^{2-\lambda} \left[\alpha h \frac{\delta f(m)}{\delta \mathcal{B}(m')} - m^{1-n} \frac{\delta \mu_{\mathrm{p}}(m)}{\delta \mathcal{B}(m')}\right], \qquad [125]$$

were $\mathcal{B}(m) = m\mathcal{N}(m)$ denotes the density of biomass on the (linear) body-size scale. The two terms in brackets describe effects on individuals of size m by trophic interactions with individual of size m'. The leading factor $\tilde{B}_{\mathrm{tot}} m^{2-\lambda}$ scales as the size-dependence of the biomass of affected individuals.

Oddly, Eq. (124) therefore describes the mass balance in a size-structured community of individuals that feed upon each other but, akin to microorganisms, essentially only to multiply their numbers rather than to grow in size—despite the fact that the equation was obtained from a model for interacting highly size-structured populations. The fact that the true steady-state $c(u)$ solves Eq. (124) justifies the use of simplifying pictures where "large species eat small species" in verbal arguments. However, over-interpretation of such pictures or corresponding numerical models can be fatal: the dynamic response of $c(u)$ to fishing pressure predicted by the Eq. (124) will generally be very different from that predicted via the Species Size-Spectrum Model, Eq. (78), by setting $c(u) = \left[\tilde{\beta} * b\right](u)$. There can be differences in the timing of events, as demonstrated in Section 9.4, when the propagation velocities $\mathrm{Re}\{\nu_k\}$ of perturbation responses (see Eq. (105)) have different magnitudes but the same signs in both cases, and

the dynamic selection of entirely different steady states when some velocities $\mathrm{Re}\{v_k\}$ have different signs.

9.3. The population-level predator–prey size-ratio window

Models of interacting size-structured populations often invoke an individual-level predator–prey size-ratio window such as the function $s(w)$ entering the model of Hartvig et al. (2011). On the other hand, models of unstructured populations differentiating species by size (e.g. Brännström et al., 2010) often depend on a population-level predator–prey size-ratio window $S(w)$ that describes the size-dependence of the amount consumed of a species of size m_* by another species of size $m'_* = e^w m_*$. The QNA in the form developed in Section 6 allows the derivation of $S(w)$ from $s(w)$.

The computation is analogous to the derivation of the interaction kernel $\tilde{K}(u)$ from individual-level interactions, but now contributions related to active and passive feeding are handled separately. Consider the special case of a linear functional response ($h \to \infty$) in the oligotrophic regime. The contribution of predation mortality to $\kappa_0(w)$, Eq. (70), then simplifies to $-\gamma s(w)$. Verifying that $K(m_*, m'_*)$ specifies, according to Eqs. (57) and (62), a rate of change (dimension 1/Time) normalised to the biomass density of the affecting species, and replacing $\kappa_0(w)$ by $-\gamma s(w)$ in the formula for $K(m_*, m'_*)$, Eq. (72), one obtains—in the mean-field approximation underlying this calculation—the rate of population decay of a species of size m_* resulting from consumption by a species of size m'_* with biomass density B' as $\gamma {m'_*}^{q-1} S(\ln(m'_*/m_*))B'$, where

$$S(w) = \left[s * \tilde{\beta} * \tilde{\beta}_\nu^-\right](w), \quad \text{with } \tilde{\beta}_\nu^- \stackrel{\text{def}}{=} \mathrm{e}^{\nu w}\tilde{\beta}(-w) = \mathrm{e}^{(1-q)w}\tilde{\beta}(-w). \qquad [126]$$

The quantity $\gamma {m'_*}^{q-1}$ was factored out to make this result comparable with the corresponding formula for $s(w)$, that is, Eq. (13) with $\mathcal{N}(m)$ expressed in terms of biomass density $\mathcal{B}(m) = m\mathcal{N}(m)$.

Conversely, the rate of population growth of a species of size m'_* resulting from consumption of a species of size m_* with biomass density B evaluates to $\alpha\gamma {m'_*}^{q-1} S(\ln(m'_*/m_*))B$. Therefore, surprisingly, the population-level assimilation efficiency is here identical to the individual-level assimilation efficiency α.

The convolutions in Eq. (126) generally need to be evaluated numerically, for example using Fourier techniques. The resulting form of $S(w)$ for standard parameters is shown in Fig. 9. However, some general characteristics of $S(w)$ can be derived directly from Eq. (126). Recalling the

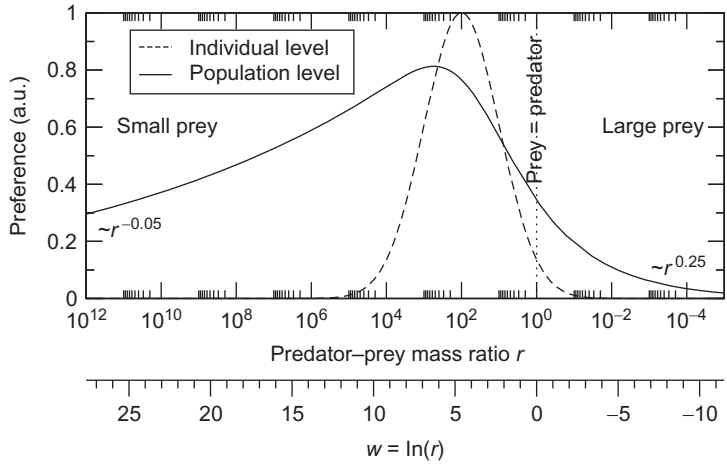

Figure 9 Comparison between the predator–prey size-ratio windows at individual level $s(w)$ and at population level $S(w)$. The mass ratio $r = e^w$ is the body-size ratio m'/m for $s(w)$ and the species-size m'_*/m_* for $S(w)$, with the prime denoting the predator. To display the curves from the predator's perspective, the horizontal axis is inverted. Curves correspond to standard parameters with $x_0 \to 0$. For finite parent-offspring size ratios, the tails of $S(w)$ will be truncated.

assumption that $s(w)$ decays faster than exponentially for $w \to \pm\infty$ (Section 4) and the observation that $\tilde{\beta}(w) \propto e^{(1-n)w}$ as $w \to -\infty$ (see Eqs. (34), (37), and (71)), it follows immediately that (i) $S(\ln(m'_*/m_*)) \propto (m'_*/m_*)^{1-n}$ for predator species smaller than their prey, (ii) $S(\ln(m'_*/m_*)) \propto (m_*/m'_*)^{q-n}$ for prey species much smaller than their predators, and (iii) typical $s(w)$, localised much sharper than intraspecific size structures $\tilde{\beta}(w)$, have little influence on the structure of $S(w)$ apart from determining a preferred predator–prey size ratio.

The conclusion that the population-level predator–prey size-ratio window is wide appears at odds with the conclusion reached analytically by Nakazawa et al. (2011), consistent with empirical analyses by Woodward and Warren (2007) (see also Gilljam et al., 2011; Woodward et al., 2010b), that the mean predator–prey size ratio at population level must be smaller than that at individual level. However, the paradox is easily resolved by noting that Nakazawa et al. (2011) and Woodward and Warren (2007) weighted all individuals equally when averaging over populations, whereas here each individual is weighted by its body mass as a proxy for reproductive value. With this modification, the analysis by Nakazawa et al. (2011) does indeed lead to the opposite conclusions: the

mean population-level predator–prey size ratio is larger than that at individual level. This is the more adequate choice. As demonstrated by Rossberg and Farnsworth (2011) analytically and through simulations, weighting individuals within populations by reproductive value leads to better predictions of community dynamics than equal weighting.

9.4. Slow and fast responses to size-selective fishing

The timescale for the long-term community responses to fishing is determined by the constants ν_k entering Eq. (107), which are defined as $\nu_k = i(1-n)M^{n-1}\hat{K}'(\xi_k)$. These depend on ecological details through the factor $\hat{K}'(\xi_k)$, given by Eq. (92).

If intraspecific biomass distributions over the logarithmic mass scale $\tilde{\beta}(w)$ are wide and smooth, then their Fourier transforms $\hat{\beta}(\xi)$ are narrow on the $\mathrm{Re}\{\xi\}$-axis, as exemplified by Eq. (115). As a result, all ξ_k (except for the purely imaginary zero) are likely to lie outside the region where $\hat{\beta}(\xi)$ is large. Typically, this is the case when the logarithmic predator–prey mass ratio $\ln\beta$ is small compared with the width of $\tilde{\beta}(w)$, evidenced by cannibalistic feeding. This leads, by Eq. (92), to small $\hat{K}'(\xi_k)$ and a sluggish formation of trophic cascades compared, for example, with expectations from the naive picture of Eq. (124)—at least as long as $\hat{K}'(\xi_k)$ is not dominated by food-web effects through the second term in Eq. (92). Expressed in ecological terms, trophic cascades form slowly because population-level predator–prey size-ratio windows are broad: even species differing in maturation sizes by exactly the predator–prey mass ratio β do not form a simple predator–prey pair, rather they interact through a mixture of predator–prey, prey–predator, and competitive relationships resulting from the tremendous ontogenetic growth of fish and other aquatic organisms.

For the purely imaginary zero corresponding to size-spectrum bending, the situation is opposite. As shown in Figs. 6 and 7, this zero of $\hat{K}(\xi)$ is typically located near the pole of $\hat{K}(\xi)$ that corresponds to the first pole of $\hat{\beta}(-\xi-\nu i)$. Because of the resulting rapid transition of $\hat{K}(\xi)$ from zero to infinity, $\hat{K}'(\xi_k)$ is generally large for this zero. The downward bending of the size spectrum for large species is therefore fast, at least when compared with the biological rates of these species (despite being slow in absolute terms, see Fig. 4). The underlying ecological mechanism, which follows immediately from back-tracing how $\hat{\beta}(-\xi-\nu i)$ enters this result, is that larger species are being depleted directly through fishing mortality of their juveniles, even if the proportion of these in the catch—which scales

as $(m_F/m_*)^{1-n}$—is relatively low. The mechanism is further amplified by a depletion of the food resources of juveniles of large species.

The effects of intraspecific size structure on response times can be demonstrated by a comparison of simulations of the Species Size-Spectrum Model with simulations of Eq. (124), which does not account for intraspecific size structure. To stabilise solutions of Eq. (124), some technical adjustments are required (caption of Fig. 10). As seen in Fig. 10, the initial response of the two systems to exploitation targeting a narrow range of body sizes is very different. Formation of the downward cascade is by a factor 3–10 slower in the full model than in Eq. (124). Depletion of larger organisms, however, proceeds by about a factor 3 faster for the reasons explained above. Yet, the equilibrium states approached by both systems are very similar: indeed, by the arguments of Section 9.2, they are possibly the same.

9.5. Neutrality and the validity of the QNA

Perfect ecological neutrality in the sense of Hubbell (2001) is a situation of perfectly even competition. Apart from drift driven by stochastic processes (which are not modelled here), communities of neutrally competing species are demographically stable for any combination of their relative abundances. In situations of approximate neutrality, populations approach particular equilibrium values, but only slowly in comparison with typical life-history time scales. The QNA, invoked in Section 6, exploits the resulting separation of the timescales of intraspecific and interspecific population dynamics to simplify descriptions of community dynamics (Rossberg and Farnsworth, 2011). Approximate neutrality among species with similar maturation sizes in a size-structured community is a likely phenomenon (O'Dwyer et al., 2009). Indeed, in the Species Size-Spectrum Model, the contribution from food-web effects had to be included in the interaction kernel $\tilde{K}(u)$ exactly to regularise model artefacts arising from perfect neutrality within size classes (Section 6.4).

The QNA as applied in the Species Size-Spectrum Model, however, invokes approximate neutrality not only within size classes, but, to a certain degree, also across size classes. This is justified *a posteriori* by the substantial competitive components in the interactions between species of different size, which arise from broad population-level predator–prey size-ratio windows, leading to slow dynamics. To quantify the resulting degree of timescale separation, and hence to gauge the reliability of the QNA, one can compare typical intra- and interspecific relaxation times in the model. In the simulation with standard parameters, shown in Fig. 4, population sizes near the targeted size class $m_* = m_F$ relax on a timescale of 4–10 T_{mat}, with

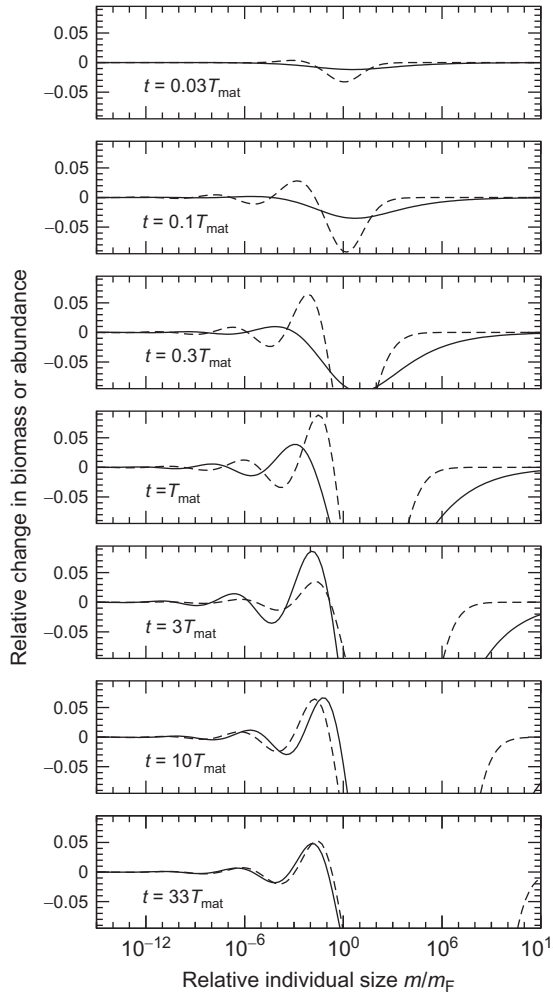

Figure 10 Comparison of the response of individual (i.e. Sheldon-type) size spectra to size-specific feeding as predicted by the Species Size-Spectrum Model (Eqs. (78) and (79), solid lines) and a corresponding model that disregards intraspecific size structure (Eq. (124), dashed lines). Simulations with standard parameters for the oligotrophic regime, however, with 10-fold fishing mortality F, with $\tilde{K}_1(u) = \tilde{B}_{\text{tot}}[e^{\gamma}\kappa_0(u) + X(u)]$ in Eq. (124) to stabilise short-wavelength instabilities, $X(w)$ in Eq. (86) replaced by $\left[X * \beta * \tilde{\beta}_{\gamma}^{-}\right](w)$ for consistency, and the parameter r in $X(w)$ set to 20γ to suppress amplifying cascades that would otherwise arise.

$T_{\text{mat}} = m_{\text{F}}^{1-n}\tilde{g}_0^{-1}(1-n)^{-1}$. The intraspecific relaxation timescale is given by the inverse size of the spectral gap of the McKendrick–von Foerster operator $\underline{L}_{m_*}$, which is estimated in Appendix as $\tilde{\mu}(m_*/\eta)^{n-1}$. As $\tilde{\mu} = \tilde{g}_0$ by Eqs. (35) and (37), the ratio between the two timescales is 4–10 times $(1-n)^{-1}\eta^{n-1}$,

which is ≈ 20 to 60. These are fairly large values, from which at least a semi-quantitative validity of the QNA can be expected. Indeed, Hartvig et al. (2011) find for their closely related model, using simulations that explicitly account for both intra- and interspecific population dynamics in small communities, that dynamical details are generally much more complex than the Species Size-Spectrum Model predicts. Yet, the structures emerging when averaging across time and communities (Hartvig et al., 2011) are similar to those derived here.

9.6. How do power-law size spectra arise?

Just as in the paper of Andersen and Beyer (2006), the current analysis began with the assumption of a power-law size spectrum and then investigated its consequences, for example, constraints on the power-law exponent. This does not immediately answer the question of why power laws emerge in the first place. In addressing this question, the oligotrophic and eutrophic regimes have to be distinguished.

In the oligotrophic regime, where $\lambda = 2 + q - n$, conditions on overall abundance, Eq. (38) for $\tilde{\mathcal{N}}$ or Eq. (116) for $\tilde{B}_{\mathrm{tot}}$, must be satisfied for steady-state power-law size spectra. Press perturbations of the size spectrum lead to modifications of the power law that spread on the m_*-axis away from the point of perturbation. Pulse perturbations can be described as two press perturbations of opposite sign initiated with a short delay. These are therefore predicted to lead to pulses travelling along the m_*-axis away from the point of perturbation. Assuming that any deviation of the size spectrum from the ideal form can be generated by applying appropriate pulse perturbations, one can conclude that any such deviations will eventually travel towards the upper and lower ends of the m_* range realised in a community, and there, depending on the effective boundary conditions, either be reflected back or disappear. When reflection is sufficiently weak and/or all modes are sufficiently damped, all deviations will eventually disappear when no further perturbations are applied. What remains is a power-law size spectrum.

Complications of this scenario can arise only when the boundaries of the ecologically realised m_* range effectively impose press perturbations on the size spectrum, which will then lead to persistent upward or downward cascades or bends originating at the upper or lower end of the realised range. In particular, insufficient biomass at the lower end acts as a press perturbation which will generate an upward-travelling front of reduced abundance corresponding to the purely imaginary zero of $\hat{K}(\xi)$ (Fig. 6A), and

eventually to a bent-down steady-state size spectrum. This has, after back-translating result of Section 7 to the linear m_*-axis and disregarding trophic cascades, the form

$$B(m_*) = m_*^{-\lambda+1}\tilde{B}_{\text{tot}}\left(1 + Qm_*^{-\lambda-2-\text{Im}\{\xi_1\}} + \text{h.o.t.}\right), \qquad [127]$$

with a scale parameter $Q<0$, rather than following a power law. Overabundance of biomass at the lower end corresponds to $Q>0$. Higher-order terms in Q, not captured by the linearised QNA, are indicated by h.o.t. However, the exponent $\lambda-2-\text{Im}\{\xi_1\}$ can be numerically quite small (Fig. 6A), so the deviations from a perfect power law described by Eq. (127) might remain undetected in empirical data. Possibly, all that can be seen is a change in the best-fitting power-law exponent ("slope").

Besides, mechanisms not considered here could help satisfying Eq. (38) at least approximately, to keep deviations from a power law in Eq. (127) small. For example, temporal modulations of abundances, as observed by Hartvig et al. (2011), can modify the effective value of the interaction coefficient γ in Eq. (38). An effect observed in simulations of size-structured food webs may also be important (Rossberg et al., 2008): evolutionary forces can lead to adjustments of attack rates at community level such that effective food availability becomes of similar magnitude as physiological food demand. In the present case, this would mean that $\gamma\tilde{N}/k$ becomes approximately of the order of magnitude of one, which is indeed what Eq. (38) requires.

In the eutrophic regime, a power-law spectrum can form at any abundance level $\tilde{\mathcal{N}}$, provided $\tilde{\mathcal{N}}$ is sufficiently large to guarantee *ad libitum* feeding. Perturbations of the size spectrum will, over time, subside as in the oligotrophic case, leaving a power-law size spectrum, possibly overlaid with boundary-induced trophic cascades. Therefore, power-law size spectra form naturally in the eutrophic regime.

In size-spectrum theories pre-dating Benoît and Rochet (2004), an individual's rate of food uptake is generally thought to be density independent, as here in the eutrophic regime (e.g. Brown et al., 2004; Platt and Denman, 1977, 1978), leading to perfect power laws over a wide range of conditions. A similar situation arises in the models investigated analytically by Benoît and Rochet (2004) and Law et al. (2009), where all growth and mortality terms scale linearly with abundance, so that abundance can be factored out. Contrary to a statement by Capitán and Delius (2010), the two cases (no density dependence or uniform linear density dependence) are neither ecologically nor mathematically the same. Yet, it is characteristic for both

that power-law size spectra can form at any abundance level, and that the size-spectrum slope λ depends on several physiological parameters (in the present case, according to Eq. (39), on α, h, k, n, and the predator–prey size-ratio window $s(\cdot)$).

9.7. Comparison with the theory of Andersen and Beyer (2006)

An important result of the present work is that in size-structured communities of populations covering wide size distributions the boundary condition of the McKendrick–von Foerster Equation (which balances production and outgrowth of newborns) implies that the specific physiological mortality of immature individuals is constrained to $\tilde{a}=1$ over most of their life history. This finding differs from the analytic results of Andersen and Beyer (2006), which Hartvig et al. (2011), similar to Andersen et al. (2008), evaluate to $\tilde{a}\approx 0.42$ for parameters as in Table 3. The theory of (Andersen and Beyer, 2006) does not consider the boundary condition and is therefore not "complete" in the sense used here. As a result, it predicts "equilibrium" population structures that violate the condition that mean lifetime reproductive output per individual (known as R_0) should equal one (Andersen et al., 2008). Resolution of the discrepancy between the two approaches requires understanding how Andersen and Beyer (2006) arrive at their constraint on $\tilde{a}$.

The case considered by Andersen and Beyer (2006) corresponds to the oligotrophic regime, because the feeding level is assumed fixed at an intermediate value $0<f_0<1$. They were the first to observe that this alone determines the size-spectrum slope as $\lambda=2+p-n$ (Capitán and Delius, 2010, make a similar observation). The crucial difference from the model of Hartvig et al. (2011)—investigated here—seems to be that Andersen and Beyer (2006) assume the rate of food intake to follow a different allometric scaling law than metabolic loss so that the loss becomes relevant only as individuals approach their maximal attainable size. For younger individuals, both growth $g(m, m_*)$ and predation mortality $\mu_\mathrm{p}(m)$ are proportional to what Andersen and Beyer (2006) call the *metabolic requirement for food*. This leads to a value $\tilde{a}=\lim_{m/m_*\to 0} m\mu_\mathrm{p}(m)/g(m, m_*)$ that is fully determined by basic physiological parameters. By contrast, the density-dependent bioenergy available for growth in the model of Hartvig et al. (2011) is always discounted by substantial density-independent metabolic loss so that $\tilde{a}$ (mortality over growth) becomes density dependent. This leaves room for $\tilde{a}$ to be adjusted at community level by the mechanisms explored in Sections 5 and 9.6.

9.8. Outlook

Although providing answers and clarifications to many questions related to community dynamics, the present analysis also led to a number of new questions and challenges. In closing, some of these are discussed briefly.

The distinction between the mechanisms shaping size spectra in oligotrophic and eutrophic regime made throughout the analysis immediately raises the question as to which empirical systems are best described by which regime, or whether either of these exclusively describes the situation in the field. An easy approach to this question would be to measure how close somatic growth and reproduction rates in a given community are to those found in laboratory experiments with *ad libitum* feeding. By the definition of the eutrophic regime, they should be identical in this case, whereas for the oligotrophic regime, growth and reproduction would be slower in the field than in the laboratory.

Based on such identifications of the relevant regimes, further progress may be possible in relating size-spectrum slopes to trophic status (Ahrens and Peters, 1991; Sprules and Munawar, 1986), temperature (Yvon-Durocher et al., 2011), and other environmental conditions. Obviously, changes in the slope resulting from environmental change can have great impacts on the production at higher trophic levels available to human consumption.

Another question that deserves further study is the distinction between damped and amplifying upward and downward cascades in field data. As mentioned in Section 2.5, this will probably require analysis of temporally resolved size-spectrum data. Clearly, the distinction between upward and downward cascades has implications for approaches to management of size-structured communities. Provided that amplifying cascades can be identified, the theoretical problem arises of extending the linear theory for size-spectrum dynamics to include non-linear corrections, because these could limit the amplification. Perturbative approaches developed in other contexts (Newell and Whitehead, 1969) might be employed usefully here.

Important in the context of fisheries management are the three related questions of what determines the upper cut-off of the size spectrum (i.e. the natural size of the largest species), how the boundary condition resulting from this cut-off is best incorporated into size-spectrum models, and how large the expected perturbation of the size spectrum resulting from this boundary conditions is. A way forward on these questions might be to study them first in corresponding species-resolved models of size-structured

communities (Hartvig et al., 2011; Rossberg et al., 2008; Shephard et al., 2012), where the upper cut-off naturally emerges.

Finally, the observations of Section 9.4 highlight that care must be taken to incorporate population size structure and trophic interactions at all life stages adequately into management models, because this may drastically modify dynamics. Consistency of model steady states with observed conditions is an insufficient criterion for model validation: this insight might allow improvements of some models currently in use.

As exemplified throughout this work, the language of mathematics has its use in science not only for reasons of numerical precision. Often, the outcome is just precision of thought: the definition of a quantity through a formula allows investigation of logical relations to other quantities; equations stating mechanistic relations between quantities allow tracking down their implications; a description of a system by combinations of such equations (rather than verbal models) allows evaluation of its logical consistency, its descriptive completeness, its mechanical consistency, and at least the qualitative consistency of its predictions with observations. Verbal descriptions and analyses of complex systems are more prone to the risks of being incomplete, overlooking essential feedback loops, or incorporating hidden inconsistencies. Ecology as a field might be underestimating the benefits inherent to the mathematical idiom.

Especially in a context of rapid, global change leading into a world with environmental conditions not experienced before, there is need for good understanding of the general mechanisms controlling high-level ecosystem states (Mintenbeck et al., 2012; Möllmann and Diekmann, 2012). This understanding should ideally derive not solely from syntheses of past observations but be anchored in systematic analyses of the consequences of fundamental principles.

Formal reasoning using mathematical language can help to navigate the complexities of such analyses. The present work hopefully, therefore, does not only provide insights into the workings of size-structured communities but also encourages researchers to make greater use of formal reasoning in order to advance our understanding of complex ecological patterns and processes.

ACKNOWLEDGEMENTS

Discussion and comments on this work by Eric Benoît, Martin Hartvig, Ken Haste Andersen, Linus Carlsson, Åke Brännström, Christian Mulder, Andy Payne, and three anonymous reviewers, as well as editorial input by Julia Reiss, Gabriel Yvon-Durocher, Ute Jacob, and Guy Woodward are gratefully acknowledged. This Beaufort Marine Research Award

is carried out under the *Sea Change* Strategy and the Strategy for Science Technology and Innovation (2006–2013), with the support of the Marine Institute, funded under the Marine Research Sub-Programme of the Irish National Development Plan 2007–2013.

APPENDIX. NUMERICAL STUDY OF THE SPECTRUM OF THE MCKENDRICK–VON FOERSTER OPERATOR

This appendix reports results of a numerical study of the spectrum of the linear operator $\underline{L}_{m_*}$, as defined by Eq. (47). Parameters were chosen as in Section 8.1. To avoid numerical difficulties at small body size, the eigenvalue problem $\underline{L}_{m_*} W(m) = lW(m)$ for the density of individuals along the linear mass axis was transformed into the corresponding eigenvalue problem for the density of biomass along the logarithmic mass axis $f(u) = e^{2u} W(e^u)$, with $u = \ln(m/m_*)$. The equivalent eigenvalue problem is then $H_{m_*} f(u) = lf(u)$, with

$$H_{m_*} f(u) = \tilde{\mu} m_*^{n-1} \left[\left(\frac{1}{4} e^{-u/4} - \eta^{1/4} \right) f(u) - \left(e^{-u/4} - \eta^{1/4} \right) \frac{df(u)}{du} + \eta^{1/4} \delta(u - u_0) \int_{u_0}^{-\ln\eta} f(v) dv \right] \quad [128]$$

conditional to $f(u) = 0$ for $u < u_0$, where $u_0 \stackrel{\text{def}}{=} \ln(m_0/m_*) = \ln(x_0)$. As in Sec. VIII.A, the maximum attainable relative body mass was set to $\eta^{-1} = 4$. Results reported here are for $x_0 = 10^{-5}$. Results depend only weakly on this particular choice. The last term in Eq. (128) enforces the condition

$$f(u_0) = \eta^{1/4} (x_0^{-1/4} - \eta^{1/4})^{-1} \int_{u_0}^{-\ln\eta} f(v) dv \quad [129]$$

on eigenfunctions $f(u)$.

The problem was discretized on a grid with G points, spaced equally on the u-axis from $u_0 + \Delta u$ to $-\ln \eta$, where $\Delta u = (-\ln \eta - u_0)/G$. The derivative of $f(u)$ in Eq. (128) was approximated by backward differences. To compute this difference for the first point, $u = u_0 + \Delta u$, that is, $f'(u_0 + \Delta u) \approx (\Delta u)^{-1} [f(u_0 + \Delta u) - f(u_0)]$, Eq. (129) (trivially approximated by a sum) was used for $f(u_0)$. The factor $\tilde{\mu} m_*^{n-1}$ in Eq. (128) can be eliminated by rescaling all eigenvalues. The eigenvalue problem for H_{m_*} is then approximated by a corresponding numerical eigenvalue problem for a $G \times G$ matrix H_{jk}.

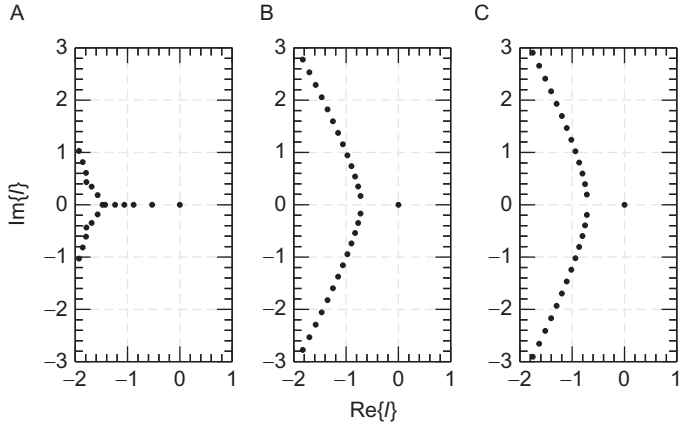

Figure 11 Eigenvalues l of the matrix H_{ij}, a discretization of the McKendrick–von Foerster operator, Eq. (47). (A) Naive implementation, exhibiting discretization artefacts. (B) Regularised version, obtained by removing the last two rows and columns of H_{ij}. (C) After removal of yet another row and column. All eigenvalues are given in units of $\tilde{\mu} m_*^{n-1}$.

Figure 11A shows the eigenvalues of H_{jk} for $G = 2000$. All eigenvalues have multiplicity one. The largest eigenvalue found, $l = -0.00018\,\tilde{\mu} m_*^{n-1}$, is close to zero. Further, one can distinguish 5–6 negative real eigenvalues, and a family of complex eigenvalues.[11] The negative real eigenvalues are numerical artefacts. They arise from the fact that, because $g(e^u m_*, m_*)$ approaches 0 linearly as $u \to -\ln \eta$ (the largest adults do not grow), the matrix H_{jk} has for large G in its lower right corner the approximate structure

$$\begin{pmatrix} \ddots & & \vdots & & \\ -4A-B & 0 & 0 & 0 & 0 \\ 3A & -3A-B & 0 & 0 & 0 \\ \cdots \quad 0 & 2A & -2A-B & 0 & 0 \\ 0 & 0 & A & -A-B & 0 \\ 0 & 0 & 0 & 0 & -B \end{pmatrix}, \qquad [130]$$

with positive constants A and B that are independent of G. This leads to one eigenvector with eigenvalue $-B$, localised on the last lattice point with small contributions in all other components, and a series of eigenvectors of the approximate forms $(\ldots, 0, 0, -1, 1, 0)^{\mathrm{T}}$, $(\ldots, 0, 1, -2, 1, 0)^{\mathrm{T}}$, $(\ldots, -1, 3, -3, 1, 0)^{\mathrm{T}}$, … and corresponding eigenvalues $-(2A+B)$, $-(3A+B)$, $-(4A+B)$, … The strong localisation of these eigenvectors on the u-axis

in the limit $G \to \infty$ and their alternating sign structures exclude them from the set of possible eigenvectors of the exact problem.

These artefacts can be suppressed by removing the last two points of the discretization lattice. The spectrum of the regularised $(G-2)\times(G-2)$ matrix is shown in Fig. 11B. When removing instead the last three lattice point, reducing H_{jk} to a $(G-3)\times(G-3)$ matrix, the structure of the spectrum remains unchanged (Fig. 11C), indicating that the regularisation was successful. The leading eigenvalue $l = -0.00018\,\tilde{\mu} m_*^{n-1}$ remains essentially unchanged close to zero. The corresponding eigenvector, appropriately normalised, differs by no more than 0.5×10^{-5} at any lattice point from the exact solution of $H_{m_*} f(u) = 0$, given for $u_0 < u < -\ln \eta$ by $f(u) = \tilde{\beta}(u)$ (as in Eq. (114)) and $f(u) = 0$ otherwise. This result confirms the numerical method used.

All eigenvalues but the leading one are complex. They are separated from the leading eigenvalue by a gap of about $0.7\,\tilde{\mu} m_*^{n-1}$. The size of the gap approximately equals $\tilde{\mu}(m_*/\eta)^{n-1}$, the mortality of the largest adults, and it was verified to exhibit the corresponding dependence on η. The density of the subdominant eigenvalues along a line in the complex plane (Fig. 11B) was verified to increase approximately as $G^{1/2}$. The results suggest that these subdominant eigenvalues becomes a continuous family of eigenvalues in the limit $G \to \infty$, separated from zero by gap of a size given by the mortality of the largest adults of the m_* size class considered.

REFERENCES

Ahrens, M.A., Peters, R.H., 1991. Patterns and limitations in limnoplankton size spectra. Can. J. Fish. Aquat. Sci. 48 (10), 1967–1978.

Akhiezer, A., Polovin, R., 1971. Criteria for wave growth. Soviet Phys. Uspekhi 14, 278.

Andersen, K.H., Beyer, J.E., 2006. Asymptotic size determines species abundance in the marine size spectrum. Am. Nat. 168 (1), 54–61.

Andersen, K.H., Pedersen, M., 2010. Damped trophic cascades driven by fishing in model marine ecosystems. Proc. R. Soc. B 277 (1682), 795–802.

Andersen, K., Ursin, E., 1977. A multispecies extension to the Beverton and Holt theory of fishing, with accounts of phosphorus circulation and primary production. Meddr. Danm. Fisk.- og Havunders 7, 319–435.

Andersen, K.H., Beyer, J.E., Pedersen, M., Andersen, N.G., Gislason, H., 2008. Life-history constraints on the success of the many small eggs reproductive strategy. Theor. Popul. Biol. 73, 490–497.

Arino, O., Shin, Y.-J., Mullon, C., 2004. A mathematical derivation of size spectra in fish populations. C. R. Biol. 327 (3), 245–254.

Arim, M., Berazategui, M., Barreneche, J.M., Ziegler, L., Zarucki, M., Abades, S.R., 2011. Determinants of density-body size scaling within food webs and tools for their detection. Adv. Ecol. Res. 45, 1–39.

Bays, J.S., Crisman, T.L., 1983. Zooplankton—trophic state relationships in Florida lakes. Can. J. Fish. Aquat. Sci. 40, 1813–1819.

Belgrano, A., Reiss, J., 2011. The Role of Body Size in Multispecies Systems. Advances in Ecological ResearchVol. 45. Academic Press, London.
Bender, E.A., Case, T.J., Gilpin, M.E., 1984. Perturbation experiments in community ecology: theory and practice. Ecology 65, 1–13.
Benoît, E., Rochet, M.-J., 2004. A continuous model of biomass size spectra governed by predation and the effects of fishing on them. J. Theor. Biol. 226 (1), 9–21.
Berlowa, L., Dunne, J.A., Martinez, N.D., Starke, P.B., Williams, R.J., Brose, U., 2009. Simple prediction of interaction strengths in complex food webs. Proc. Natl. Acad. Sci. U.S.A. 106 (1), 187–191.
Beyer, J., 1989. Recruitment stability and survival: simple size-specific theory with examples from the early life dynamic of marine fish. Dana 7, 45–147.
Blanchard, J.L., Jennings, S., Law, R., Castle, M.D., McCloghrie, P., Rochet, M.J., Benoît, E., 2009. How does abundance scale with body size in coupled size-structured food webs? J. Anim. Ecol. 78 (1), 270–280.
Blanco, J., Echevarria, F., Garcia, C., 1994. Dealing with size-spectra: some conceptual and mathematical problems. Sci. Mar. (Barcelona) 58 (1), 17–29.
Boccara, N., 1990. Functional Analysis: An Introduction for Physicists. Academic Press, New York.
Boudreau, P., Dickie, L., 1992. Biomass spectra of aquatic ecosystems in relation to fisheries yield. Can. J. Fish. Aquat. Sci. 49 (8), 1528–1538.
Bourassa, N., Morin, A., 1995. Relationships between size structure of invertebrate assemblages and trophy and substrate composition in streams. J. N. Am. Benthol. Soc. 14 (3), 393–403.
Brännström, Å., Loeuille, N., Loreau, M., Dieckmann, U., 2010. Emergence and maintenance of biodiversity in an evolutionary food-web model. Theor. Ecol. 4 (4), 467–478.
Brown, J.H., Gillooly, J.F., Allen, A.P., Savage, V.M., West, G.B., 2004. Toward a metabolic theory of ecology. Ecology 85 (7), 1771–1789.
Camacho, J., Solé, R., 2001. Scaling in ecological size spectra. Europhys. Lett. 55 (6), 774–780.
Capitán, J.A., Delius, G.W., 2010. Scale-invariant model of marine population dynamics. Phys. Rev. E 81 (6), 061901.
Castle, M.D., Blanchard, J.L., Jennings, S., 2011. Predicted effects of behavioural movement and passive transport on individual growth and community size structure in marine ecosystems. Adv. Ecol. Res. 45, 41–66.
Christensen, V., Pauly, D., 1992. Ecopath II—a software for balancing steady-state ecosystem models and calculating network characteristics. Ecol. Model. 61, 169–185.
Cross, M.C., Hohenberg, P.C., 1993. Pattern formation outside of equilibrium. Rev. Mod. Phys. 65, 851.
Cury, P., Pauly, D., 2000. Patterns and propensities in reproduction and growth of marine fishes. Ecol. Res. 15, 101–106.
Daan, N., Gislason, H., Pope, J.G., Rice, J.C., 2005. Changes in the North Sea fish community: evidence of indirect effects of fishing? ICES J. Mar. Sci. 62, 177–188.
Datta, S., Delius, G.W., Law, R., Plank, M.J., 2010. A stability analysis of the power-law steady state of marine size spectra. J. Math. Biol. 63 (4), 779–799.
Dortch, Q., Packard, T.T., 1989. Differences in biomass structure between oligotrophic and eutrophic marine ecosystems. Deep Sea Res. Part A Oceanogr. Res. Pap. 2, 223–240.
Duplisea, D.E., 2000. Benthic organism biomass size-spectra in the Baltic Sea in relation to the sediment environment. Limnol. Oceanogr. 45 (3), 558–568.
European Commission, 2010. Commission Decision on criteria and methodological standards on good environmental status of marine waters. Official Journal of the European Union 232(14), 2.9.2010.
Fisher, R.A., 1930. The Genetical Theory of Natural Selection. Oxford University Press, Oxford.

Friberg, N., Bonada, N., Bradley, D.C., Dunbar, M.J., Edwards, F.K., Grey, J., Hayes, R.B., Hildrew, A.G., Lamouroux, N., Trimmer, M., Woodward, G., 2011. Biomonitoring of human impacts in freshwater ecosystems: the good, the bad, and the ugly. Adv. Ecol. Res. 44, 1–68.

Fung, T., Farnsworth, K.D., Reid, D.G., Rossberg, A.G., 2012a. Recent data suggest no further recovery in North Sea Large Fish Indicator. ICES J. Mar. Sci. 69 (2), 235–239.

Fung, T., Farnsworth, K.D., Shephard, S., Reid, D.G., Rossberg, A.G., 2012b. Recovery of community size-structure from fishing requires multiple decades, submitted for publication.

Gaedke, U., 1992a. Identifying ecosystem properties: a case study using plankton biomass size distributions. Ecol. Model. 63, 277–298.

Gaedke, U., 1992b. The size distribution of plankton biomass in a large lake and its seasonal variability. Limnol. Oceanogr. 37 (6), 1202–1220.

Gaedke, U., Seifried, A., Adrian, R., 2004. Biomass size spectra and plankton diversity in a shallow eutrophic lake. Int. Rev. Hydrobiol. 89 (1), 1–20.

Garcia, H.E., Locarnini, R.A., Boyer, T.P., Antonov, J.I., 2006. World Ocean Atlas 2005 Volume 4: Nutrients (phosphate, nitrate, silicate). Vol. 64 of NOAA Atlas NESDIS 64. U.S. Government Printing Office, Washington, DC.

Gerlach, S., Hahn, A., Schrage, M., 1985. Size spectra of benthic biomass and metabolism. Mar. Ecol. Prog. Ser. 26 (1–2), 161–173.

Gilljam, D., Thierry, A., Edwards, F.K., Figueroa, D., Ibbotson, A.T., Jones, J.I., Lauridsen, R.B., Petchey, O.L., Woodward, G., Ebenman, B., 2011. Seeing double: size-based and taxonomic views of food web structure. Adv. Ecol. Res. 45, 67–133.

Greenstreet, S.P.R., Rogers, S.I., Rice, J.C., Piet, G.J., Guirey, E.J., Fraser, H.M., Fryer, R.J., 2011. Development of the EcoQO for the North Sea fish community. ICES J. Mar. Sci. J. du Conseil 68 (1), 1–11.

Hall, S.J., Collie, J.S., Duplisea, D.E., Jennings, S., Bravington, M., Link, J., 2006. A length-based multispecies model for evaluating community responses to fishing. Can. J. Fish. Aquat. Sci. 63 (6), 1344–1359.

Hartvig, M., Andersen, K.H., Beyer, J.E., 2011. Food web framework for size-structured populations. J. Theor. Biol. 272 (1), 113–122.

Hindmarsh, A.C., Brown, P.N., Grant, K.E., Lee, S.L., Serban, R., Shumaker, D.E., Woodward, C.S., 2005. SUNDIALS: suite of nonlinear and differential/algebraic equation solvers. ACM Trans. Math. Softw. 31 (3), 363–396.

Houde, E.D., 2009. Recruitment variability. In: Jakobsen, T., Fogarty, M.J., Megrey, B.A., Moksness, E. (Eds.), Fish Reproductive Biology: implications for assessment and management. Wiley-Blackwell, Oxford, pp. 91–171.

Hubbell, S.P., 2001. The Unified Neutral Theory of Biodiversity and Biogeography. Princeton University Press, Princeton, NJ.

Hui, A.K., Armstrong, B.H., Wray, A.A., 1978. Rapid computation of the Voigt and complex error functions. J. Quant. Spectrosc. Radiat. Transf. 19, 509–516.

ICES, 2010. Report of the Working Group on the Ecosystem Effects of Fishing Activities (WGECO). ICES Document CM 2010/ACOM: 23, Copenhagen.

Jackson, J.D., 1962. Classical Electrodynamics. John Wiley & Sons, New York.

Jacob, U., Thierry, A., Brose, U., Arntz, W.E., Berg, S., Brey, T., Fetzer, I., Jonsson, T., Mintenbeck, K., Möllmann, C., Petchey, O.L., Riede, J.O., Dunne, J.A., 2011. The role of body size in complex food webs: a cold case. Adv. Ecol. Res. 45, 181–223.

Jennings, S., Blanchard, J.L., 2004. Fish abundance with no fishing: predictions based on macroecological theory. J. Anim. Ecol. 73 (4), 632–642.

Jeppesen, E., Lauridsen, T.L., Mitchell, S.F., Christoffersen, K., Burns, C.W., 2000. Trophic structure in the pelagial of 25 shallow New Zealand lakes: changes along nutrient and fish gradients. J. Plankton Res. 22 (5), 951.

Johnson, R.S., 1997. A modern introduction to the mathematical theory of water waves. Cambridge University Press, Cambridge.
Keitt, T., 1997. Stability and complexity on a lattice: coexistence of species in an individual-based food web model. Ecol. Model. 102 (2–3), 243–258.
Kerr, S., 1974. Theory of size distribution in ecological communities. J. Fish. Res. Board Can. 31, 1859–1862.
Kerr, S., Dickie, L.M., 2001. The biomass spectrum. Columbia University Press, New York.
Kevorkian, J., Cole, J.D., 1996. Multiple Scale and Singular Perturbation Methods. Springer-Verlag, New York.
Koyama, H., Kira, T., 1956. Intraspecific competition among higher plants. VIII. Frequency distribution of individual plant weight as affected by the interaction between plants. Journal of the Institute of Polytechnics, Osaka City University, Series D 7, 73–94.
Lassen, H., Medley, P., 2001. Virtual population analysis: a practical manual for stock assessment. FAO Fisheries Technical Paper 400. Food and Agriculture Organization of the United Nations, Rome.
Law, R., Plank, M.J., James, A., Blanchard, J.L., 2009. Size-spectra dynamics from stochastic predation and growth of individuals. Ecology 90 (3), 802–811.
Marquet, P.A., Quiñones, R.A., Abades, S., Labra, F., Tognelli, M., 2005. Scaling and power-laws in ecological systems. J. Exp. Biol. 208, 1749–1769.
Maury, O., Faugeras, B., Shin, Y.J., Poggiale, J.C., Ari, T.B., Marsac, F., 2007a. Modeling environmental effects on the size-structured energy flow through marine ecosystems. Part 1: the model. Prog. Oceanogr. 4, 479–499.
Maury, O., Shin, Y.-J., Faugeras, B., Ari, T.B., Marsac, F., 2007b. Modeling environmental effects on the size-structured energy flow through marine ecosystems. Part 2: simulations. Prog. Oceanogr. 4, 500–514.
McKendrick, A.G., 1926. Application of mathematics to medical problems. Proc. Edinburgh Math. Soc. 44, 98–130.
Melian, C.J., Vilas, C., Baldo, F., Gonzalez-Ortegon, E., Drake, P., Williams, R.J., 2011. Eco-evolutionary dynamics of individual-based food webs. Adv. Ecol. Res. 45, 225–268.
Millennium Ecosystem Assessment, 2005. Ecosystems and Human Well-being: Synthesis. Island Press, Washington, DC.
Mintenbeck, K., Barrera-Oro, E.R., Brey, T., Jacob, U., Knust, R., Mark, F.C., Moreira, E., Strobel, A., Arntz, W.E., 2012. Impact of Climate Change on Fishes in Complex Antarctic Ecosystems. Adv. Ecol. Res. 46, 351–426.
Möllmann, C., Diekmann, R., 2012. Marine ecosystem regime shifts induced by 1387 climate and overfishing – a review for the Northern hemisphere. Adv. Ecol. Res. 47. In press.
Mulder, C., Elser, J.J., 2009. Soil acidity, ecological stoichiometry and allometric scaling in grassland food webs. Glob. Chang. Biol. 15 (11), 2730–2738.
Mulder, C., Den Hollander, H.A., Hendriks, A.J., 2008. Aboveground herbivory shapes the biomass distribution and flux of soil invertebrates. PLoS One 3 (10), e3573.
Mulder, C., Hollander, H.A.D., Vonk, J.A., Rossberg, A.G., Jagers op Akkerhuis, G.A.J.M., Yeates, G.W., 2009. Soil resource supply influences faunal size-specific distributions in natural food webs. Naturwissenschaften 96 (7), 813–826.
Mulder, C., Boit, A., Bonkowski, M., Ruiter, P.C.D., Mancinelli, G., van Der Heijden, M.G.A., van Wijnen, H.J., Vonk, J.A., Rutgers, M., 2011. A below-ground perspective on dutch agroecosystems: how soil organisms interact to support ecosystem services. Adv. Ecol. Res. 44, 277–358.
Naisbit, R.E., Rohr, R.P., Rossberg, A.G., Kehrli, P., Bersier, L.-F., 2012. Phylogeny vs. body size as determinants of food-web structure. Proc. R. Soc. B 279, 3291–3297.
Nakazawa, T., Ushio, M., Kondoh, M., 2011. Scale dependence of predator–prey mass ratio: determinants and applications. Adv. Ecol. Res. 45, 269–302.

Neubert, M., Blumenshine, S., Duplisea, D., Jonsson, T., Rashlei, B., 2000. Body size and food web structure: testing the equiprobability assumption of the cascade model. Oecologia 123, 241–251.

Newell, A.C., Whitehead, J.A., 1969. Finite bandwidth, finit amplitude convection. J. Fluid Mech. 38, 279.

O'Dwyer, J.P., Lake, J.K., Ostling, A., Savage, V.M., Green, J.L., 2009. An integrative framework for stochastic, size-structured community assembly. Proc. Natl. Acad. Sci. U.S.A. 106 (15), 6170–6175.

O'Gorman, E., Pichler, D.E., Adams, G., Benstead, J.P., Craig, N., Cross, W.F., Demars, B.O.L., Friberg, N., Gislason, G.M., Gudmundsdottier, R., Hawczak, A., Hood, J.M., Hudson, L.N., Johansson, L., Johansson, M., Junker, J.R., Laurila, A., Manson, J.R., Mavromati, E., Nelson, D., Olafsson, J.S., Perkins, D.M., Petchey, O.L., Plebani, M., Reuman, D.C., Rall, B.C., Stewart, R., Thompson, M.S.A., Woodward, G., 2012. Impacts of warming on the structure and function of aquatic communities: individual- to ecosystem-level responses. Adv. Ecol. Res. 47. In press.

OSPAR, 2006. Report on North Sea Pilot Project on Ecological Quality Objectives. Tech. Rep. 2006/239, OSPAR.

Pace, M.L., 1986. An empirical analysis of zooplankton community size structure across lake trophic gradients. Limnol. Oceanogr. 31 (1), 45–55.

Pauly, D., Christensen, V., Walters, C., 2000. Ecopath, Ecosim and Ecospace as tools for evaluating ecosystem impact of fisheries. ICES J. Mar. Sci. 57, 697–706.

Perry, G.L.W., Enright, N.J., 2006. Spatial modelling of vegetation change in dynamic landscapes: a review of methods and applications. Progr. Phys. Geogr. 30 (1), 47.

Peters, R.H., 1983. The ecological implications of body size. Cambridge University Press, Cambridge.

Pigolotti, S., Lopez, C., Hernandez-Garcia, E., 2007. Species clustering in competitive Lotka-Volterra models. Phys. Rev. Lett. 98, 258101.

Platt, T., Denman, K., 1977. Organization in the pelagic ecosystem. Helgol. Wiss. Meeresunters. 30, 575–581.

Platt, T., Denman, K., 1978. The structure of pelagic ecosystems. Rapports et Procès-Verbaux des Réunions du Conseil International pour l'Exploration de la Mer 173, 60–65.

Pope, J.G., Rice, J.C., Daan, N., Jennings, S., Gislason, H., 2006. Modelling an exploited marine fish community with 15 parameters—results from a simple size-based model. ICES J. Mar. Sci. J. du Conseil 63 (6), 1029–1044.

Pratap, A., Govind, Tripathi, R.S., 1999. Magnetic dynamics of bilayer cuprate superconductors. Phys. Rev. B 60, 6775–6780.

Quiñones, R.A., Platt, T., Rodríguez, J., 2003. Patterns of biomass-size spectra from oligotrophic waters of the Northwest Atlantic. Prog. Oceanogr. 57, 405–427.

Reiss, J., Forster, J., Cássio, F., Pascoal, C., Stewart, R., Hirst, A.G., 2010. When microscopic organisms inform general ecological theory. Adv. Ecol. Res. 43 (10), 45–85.

Reuman, D.C., Mulder, C., Raffaelli, D., Cohen, J.E., 2008. Three allometric relations of population density to body mass: theoretical integration and empirical tests in 149 food webs. Ecol. Lett. 11 (11), 1216–1228.

Rice, J., Arvanitidis, C., Borja, A., Frid, C., Hiddink, J.G., Krause, J., Lorance, P., Ragnarsson, S., Sköld, M., Trabucco, B., 2011. Indicators for sea-floor integrity under the European Marine Strategy Framework Directive. Ecological Indicators 12, 174-184.

Riede, J.O., Rall, B.C., Banasek-Richter, C., Navarrete, S.A., Wieters, E.A., Brose, U., 2010. Scaling of food web properties with diversity and complexity across ecosystems. Adv. Ecol. Res. 42, 139–170.

Rodriguez, J., Mullin, M., 1986a. Relation between biomass and body weight of plankton in a steady state oceanic ecosystem. Limnol. Oceanogr. 31, 361–370.
Rodriguez, J., Mullin, M.M., 1986b. Diel and interannual variation of size distribution of oceanic zooplanktonic biomass. Ecology 67 (1), 215–222.
Rodriguez, J., Jiménez, F., Bautista, B., Rodriguez, V., 1987. Planktonic biomass spectra dynamics during a winter production pulse in mediterranean coastal waters. J. Plankton Res. 9 (6), 1183–1194.
Rossberg, A.G., 2007. Some first principles of complex systems theory. Publ. RIMS 1551, 129–136.
Rossberg, A.G., Farnsworth, K.D., 2011. Simplification of structured population dynamics in complex ecological communities. Theor. Ecol. 4 (4), 449–465.
Rossberg, A.G., Ishii, R., Amemiya, T., Itoh, K., 2008. The top-down mechanism for body-mass–abundance scaling. Ecology 89 (2), 567–580.
Rossberg, A.G., Farnsworth, K.D., Satoh, K., Pinnegar, J.K., 2011. Universal power-law diet partitioning by marine fish and squid with surprising stability-diversity implications. Proc. R. Soc. B 278 (1712), 1617–1625.
Schwinghammer, P., 1981. Characteristic size distributions of integral benthic communities. Can. J. Fish. Aquat. Sci. 38, 1255–1263.
Sheldon, R.W., Prakash, A., Sutcliffe Jr., W.H., 1972. The size distribution of particles in the ocean. Limnol. Oceanogr. 17, 327–340.
Sheldon, R., Sutcliffe, W.H.J., Paranjape, M., 1977. Structure of pelagic food chain and relationship between plankton and fish production. J. Fish. Res. Board Can. 34, 2344–2355.
Shephard, S., Fung, T., Houle, J.E., Farnsworth, K.D., Reid, D.G., Rossberg, A.G., 2012. Size-selective fishing drives species composition in the Celtic Sea. ICES J. Mar. Sci. 69 (2), 223–234.
Shin, Y.J., Cury, P., 2004. Using an individual-based model of fish assemblages to study the response of size spectra to changes in fishing. Can. J. Fish. Aquat. Sci. 61 (3), 414–431.
Silvert, W., Platt, T., 1978. Energy flux in the pelagic ecosystem: a time-dependent equation. Limnol. Oceanogr. 23 (4), 813–816.
Silvert, W., Platt, T., 1980. Dynamic energy-flow model of the particle size distribution in pelagic ecosystems. In: Kerfoot, W.C. (Ed.), Evolution and Ecology of Zooplankton Communities. University Press of New England, Hanover, New Hampshire and London, England, pp. 754–763.
Solomon, S., Qin, D., Manning, M., Marquis, M., Averyt, K., Tignor, M.M.B., Miller Jr., H.L., Zhenlin, C. (Eds.), 2007. Climate Change 2007: The Physical Science Basis. Cambridge University Press, Cambridge, UK.
Speirs, D.C., Guirey, E.J., Gurney, W.S.C., Heath, M.R., 2010. A length-structured partial ecosystem model for cod in the North Sea. Fish. Res. 106 (3), 474–494.
Sprules, W.G., Goyke, A.P., 1994. Size-based structure and production in the pelagia of Lakes Ontario and Michigan. Can. J. Fish. Aquat. Sci. 51, 2603–2611.
Sprules, W.G., Munawar, M., 1986. Plankton size spectra in relation to ecosystem productivity, size, and perturbation. Can. J. Fish. Aquat. Sci. 43, 1789–1794.
Sprules, W.G., Casselman, J.M., Shuter, B.J., 1983. Size distributions of pelagic particles in lakes. Can. J. Fish. Aquat. Sci. 40, 1761–1769.
Thibault, K.M., White, E.P., Hurlbert, A.H., Ernest, S., 2011. Multimodality in the individual size distributions of bird communities. Glob. Ecol. Biogeogr. 20 (1), 145–153.
Thiebaux, M.L., Dickie, L.M., 1993. Structure of the body-size spectrum of the biomass in aquatic ecosystems: a consequence of allometry in predator-prey interactions. Can. J. Fish. Aquat. Sci. 50, 1308–1317.

Twomey, M., Jacob, U., Emmerson, M.E., 2012. Perturbing a marine food web-consequences for food web structure and trivariate patterns. Adv. Ecol. Res. 47. In press.

Vasseur, D.A., Gaedke, U., 2007. Spectral analysis unmasks synchronous and compensatory dynamics in plankton communities. Ecology 88 (8), 2058–2071.

von Foerster, H., 1959. Some remarks on changing populations. In: Stohlman, F. (Ed.), The Kinetics of Cellular Proliferation. Grune & Stratton, New York, pp. 382–407.

Wilson, W., Lundberg, P., Vázquez, D., Shurin, J., Smith, M., Langford, W., Gross, K., Mittelbach, G., 2003. Biodiversity and species interactions: extending Lotka–Volterra community theory. Ecol. Lett. 6 (10), 944–952.

Woodward, G., Warren, P.H., 2007. Body size and predatory interactions in freshwaters: scaling from individuals to communities. In: Hildrew, A.G., Raffaelli, D., Edmonds-Brown, R. (Eds.), Body Size: The Structure and Function of Aquatic Ecosystems. Cambridge University Press, Cambridge, pp. 98–117.

Woodward, G., Benstead, J.P., Beveridge, O.S., Blanchard, J., Brey, T., Brown, L.E., Cross, W.F., Friberg, N., Ings, T.C., Jacob, U., Jennings, S., Ledger, M.E., Milner, A.M., Montoya, J.M., O'Gorman, E., Olesen, J.M., Petchey, O.L., Pichler, D.E., Reuman, D.C., Thompson, M.S.A., van Veen, F.J.F., Yvon-Durocher, G., 2010a. Ecological networks in a changing climate. Adv. Ecol. Res. 42, 72–138.

Woodward, G., Blanchard, J., Lauridsen, R.B., Edwards, F.K., Jones, J.I., Figueroa, D., Warren, P.H., Petchey, O.L., 2010b. Individual-based food webs: species identity, body size and sampling effects. Adv. Ecol. Res. 43, 211–266.

Yodzis, P., 1998. Local trophodynamics and the interaction of marine mammals and fisheries in the Benguela ecosystem. J. Anim. Ecol. 67 (4), 635–658.

Yvon-Durocher, G., Montoya, J.M., Trimmer, M., Woodward, G., 2011. Warming alters the size spectrum and shifts the distribution of biomass in freshwater ecosystems. Glob. Chang. Biol. 17 (4), 1681–1694.

Zhou, M., Huntley, M.E., 1997. Population dynamics theory of plankton based on biomass spectra. Mar. Ecol. Prog. Ser. 159, 61–73.